

TECHNICAL UNIVERSITY OF CRETE

Simulation of Fractured Wells

by

Nikoleta N. Dimopoulou

A THESIS

SUBMITTED TO THE FACULTY OF GRADUATE STUDIES
IN PARTIAL FULFILMENT OF THE REQUIREMENTS FOR THE
DEGREE OF MASTER OF SCIENCE
GRADUATE PROGRAM IN PETROLEUM ENGINEERING

SCHOOL OF MINERAL RESOURCES ENGINEERING
GREECE, CHANIA
JANUARY, 2019

The MSc Program in Petroleum Engineering of the Technical University of Crete was attended and completed by Mrs. Dimopoulou Nikoleta due to the Hellenic Petroleum Group Scholarship award.

Table of contents

List of Diagrams	4
List of Figures.....	5
List of Tables.....	7
Acknowledgements	9
Abstract.....	13
Chapter 1: Introduction.....	15
1.1. Problem Statement	18
Chapter 2: Revision.....	20
2.1. Unconventional reservoir features.....	20
2.1.1. Tight gas reservoirs	20
2.1.2. Shale gas reservoirs.....	22
2.1.3. Tight/shale oil reservoirs.....	33
2.2. Common Drilling and Completion Practices	34
2.3. Analytical Models	36
2.3.1. Type curves.....	42
2.3.2. Flowing Material Balance (FMB).....	43
2.3.3. Specialized plots	46
2.4. Capacitance-resistance method for production data analysis.....	47
Chapter 3: Capacitance-Resistance Model	51
3.1. Equivalence between Electrical and Petroleum Engineering.....	51
3.2. Basic Model	53
3.3. Depletion during Transient and BDF-Liquid Reservoirs.....	54
3.4. Continuous Succession of Pseudo-Steady States (SPSS).....	58
Chapter 4: CRM Model.....	60
4.1. Implementation of the CRM	60
4.1.1. Liquid reservoirs	60
4.2. Validation of CRM.....	62
4.2.1. Liquid reservoirs	62
Chapter 5: Description of equations in ECLIPSE	69

Chapter 6: Comparison of all the methods	70
Chapter 7: Grid sensitivity	78
Chapter 8: Conclusions and Summary	81
References.....	83
APPENDIX.....	87

List of Diagrams

Diagram 4.1: Comparison of the CRM and the analytical solution for constant rate production; in a Cartesian of p_{wf} versus time.	66
Diagram 4.2: Comparison of the CRM and the analytical solution for constant rate production; in a log-log plot of $p_i - p_{wf}$ versus time.....	66
Diagram 4.3: Comparison of the CRM (with smaller timesteps) and the Analytical solution for constant rate production of p_{wf} vs time in a Cartesian plot.	67
Diagram 4.4: Comparison of the CRM (with smaller timesteps) and the Analytical solution for constant rate production of $p_i - p_{wf}$ in a log-log plot.	67
Diagram 4.5: Comparison of the CRM and the analytical solution for constant p_{wf} production; in a Cartesian plot of q versus time.	68
Diagram 4.6: Comparison of the CRM and the analytical solution for constant p_{wf} production; in a loglog plot of q versus time.....	68
Diagram 6.1: Comparison of the CRM, ECLIPSE, IMEX and the analytical solution for constant rate production; in a Cartesian plot of p_{wf} versus time.	70
Diagram 6.2: Comparison of the CRM, ECLIPSE, IMEX and the analytical solution for constant rate production; in a loglog plot of $p_i - p_{wf}$ versus time.....	70
Diagram 6.3: Comparison of the CRM, ECLIPSE, IMEX and the analytical solution for constant p_{wf} production; Cartesian plot of q versus time.....	71
Diagram 6.4: Comparison of the CRM, ECLIPSE, IMEX and the analytical solution for constant p_{wf} production; log-log plot of q versus time.	71
Diagram 6.5 Comparison of the CRM, ECLIPSE, IMEX and the analytical solution for constant p_{wf} production; Cartesian plot of q versus time.....	72
Diagram 6.6: Comparison of the CRM, ECLIPSE, IMEX and the analytical solution for constant rate production; log-log plot of $p_i - p_{wf}$ versus time.	72
Diagram 6.7: Comparison of the CRM, ECLIPSE, IMEX and the analytical solution for constant p_{wf} production; cartesian plot of q versus time.	73
Diagram 6.8: Comparison of the CRM, ECLIPSE, IMEX and the analytical solution for constant p_{wf} production; log-log plot of q versus time.	73

Diagram 6.9: Plot of BHP vs time for constant rate production for different permeabilities and vertical traverse fracture (1000mD, 2000m D, 3000mD).	74
Diagram 6.10: Plot of BHP vs time for constant rate production for different permeabilities and vertical traverse fracture (1000mD-5000mD).	74
Diagram 6.11: Figure . Plot of oil rate vs time for constant pressure production for different permeabilities and vertical traverse fracture (1000mD-4000mD).	75
Diagram 6.12: Plot of oil rate vs time for constant pressure production for different permeabilities and vertical traverse fracture (1000mD, 4000mD).	75
Diagram 6.13: Plot of BHP vs time for constant rate production for different permeabilities and horizontal traverse fracture (1000mD-5000mD).	76
Diagram 6.14: Plot of BHP vs time for constant rate production for different permeabilities and horizontal traverse fracture (5000mD, 6000mD).	76
Diagram 6.15: Plot of oil rate vs time for constant pressure production for different permeabilities and horizontal traverse fracture (1000mD - 5000mD).	77
Diagram 6.16: Plot of oil rate vs time for constant pressure production for different permeabilities and horizontal traverse fracture (5000mD, 6000mD).	77
Diagram 7.1: Plot of BHP vs time for constant rate production for traverse fracture oriented in the horizontal direction and different grid sizes.	78
Diagram 7.2: Plot of oil rate vs time for constant pressure production for traverse fracture oriented in the horizontal direction and different grid sizes.	79
Diagram 7.3: Plot of BHP vs time for constant rate production for traverse fracture oriented in the vertical direction and different grid sizes.	79
Diagram 7.4: Plot of oil rate vs time for constant pressure production for traverse fracture oriented in the vertical direction and different grid sizes.....	80

List of Figures

Figure 1.1: Resource triangles of oil and gas endowment (Aguilera, 2013).	15
Figure 1.2: World oil and gas resource pyramid (Ben E. Law).	16
Figure 1.3: Comparison of the methods used for reservoir characterization and production prediction.	18
Figure 2.1: Conventional and unconventional reservoirs.	20
Figure 2.2: Basin Centered Gas Accumulation Model.	21
Figure 2.3: Diagram of dual transmissivity nature of Deep Basin clastic reservoirs. Higher permeability conglomerate (sweet spot) encased in lower permeability tight sandstone reservoir (Zaitlin and Moslow 2006)	22

Figure 2.4: Increases in production and well count in the Barnett shale from 1990 to 2010 (Newell 2010).	23
Figure 2.5: Hydrocarbon generation window and organic maturation with respect to the value of the vitrinite reflectance. Modified from Steyl and Van Tonder (2013).	26
Figure 2.6: An example of sonic resistivity overlay in different situations.	28
Figure 2.7: Plot of Langmuir (model) isotherm versus pressure.	29
Figure 2.8: Graph of a sorption curve from gas shale.	30
Figure 2.9: Ternary diagrams of Barnett mineralogy (Loucks and Ruppel 2007).	31
Figure 2.10: Mineralogy ternary diagram showing analysis by well (Loucks et al., 2012).	31
Figure 2.11: Biogenic and Thermogenic Gases.	32
Figure 2.12: Oil shale composed of clayey and silty laminae saturated with kerogen and naphthenes (black), Slavonia crude oil and gas field, Croatia.	33
Figure 2.13: Comparison of possible fracture geometries created in tight and shale reservoirs (Warpinski et al. 2009).	35
Figure 2.14: Importance of horizontal well placement strategy on SRV coverage, modified from Mayerhofer et al. (2010).	36
Figure 2.15: Hydraulically fractured well in a rectangular reservoir (Wattenbarger et al., 1998).	37
Figure 2.16: Schematic representation of the trilinear-flow model representing three contiguous flow regions for a multiple-fractured horizontal well (Brown et al., 2011).	38
Figure 2.17: Display of (a) a horizontal well with multiple branch fractures and (b) its representation by a model ($k_1 > k_2$) (Stalgorova and Mattar 2013).	39
Figure 2.18: Schematic and dimensions of the five region model for one quarter of a fracture (Stalgorova and Mattar, 2013).	40
Figure 2.19: Plot of p/Z versus cumulative production.	43
Figure 2.20: Plot of reservoir pressure at constant rate and pseudosteady state conditions (Fekete).	44
Figure 2.21: Plot of oil flowing material balance with normalized rate and cumulative production (Fekete RTA poster).	44
Figure 2.22: Plot of normalized pseudo-pressure vs material balance pseudo-time, for gas FMB (Fekete RTA poster).	45
Figure 2.23: Gas flowing material balance (Fekete RTA poster).	46
Figure 2.24: Characteristic P/Z curve depicting the dual- or tri-transmissivity nature of a Deep Basin reservoir as observed in the 10-33-67-7w6 well (Adapted from Moslow, 2005).	49

Figure 2.25: Typical plot of p/Z vs. cumulative gas production. (Source: Shahamat and Aguilera, 2010).....	49
Figure 2.26: Plot of rate vs. cumulative gas production, showing Shahamat and Aguilera (2010). Blue squares are real gas rate data, brown dashed line is theoretical performance (including an excellent history match), and green dashed line is the calculated contribution from the tight or ultra-tight formation to the producing reservoir.....	50
Figure 4.1: Process for applying CRM for constant rate production of liquid reservoirs (Shahamat, 2014).....	61
Figure 4.2: Process for applying CRM for constant pressure production of a liquid reservoir.....	61
Figure 4.3: Comparison of the CRM and the complete solution for constant rate production; (a) Cartesian plot of p_{wf} versus time, (b) Loglog plot of $(p_i - p_{wf})$ versus time.....	64
Figure 4.4: Comparison of the CRM and the analytical solution for constant p_{wf} production; (a) Cartesian and (b) loglog plot of q versus time.....	65

List of Tables

Table 3.1: Summary of analogy between flow of fluid in a porous medium and flow of electricity in an electrical conductor.....	52
Table 4.1: Reservoir geometry and properties used for generating the analytical solutions.....	63
Table 4.2: Parameters used in CRM for constant rate and constant pressure production of the liquid reservoir with specified properties in Table 4.1.	64

Acknowledgements

At this point, I would like to take this opportunity to thank all the people who helped me through this road.

First and foremost, my supervisor, Dr. Christos Chatzichristos, has my total respect and gratitude for the support and scientific guidance that he provided throughout the development of this study. I want to also thank warmly all the professors for their motivation and enthusiasm. The knowledge I have acquired is not limited to the technical point of view but I have also learnt a lot from a personal point of view, the way to cope with problems and life.

In addition, I want to express my appreciation to my family and my close friends, who, with their love and psychological support, helped me overcome any obstacle that occurred in my path. Finally, I would also like to thank HELPE for the scholarship and for giving me the opportunity to achieve my goals, and NCSR Demokritos for accepting me as a guest in order to conduct my thesis in the institution.

My parents gave me the best thing anyone could give me,

they believed in me!!!

Dedicated to them

Abstract

Since the world is in constant need of energy sources and even if the renewable source energy plays and will play a key role in the increasing energy demands, the world will continue to be insufficient in sustainable energy. Thus unconventional reservoirs (tight/shale gas, tight oil, oil sands) will play an important part in satisfying the ever-increasing future energy demands, a fact that has drawn the attention of the petroleum industry. The declining oil and gas supply from conventional reservoirs combined with the drastic increase in unconventional oil and gas contribution has led us to the conclusion that unconvensionals will hold a leading role in the global energy mix in the future. The difficult part is estimating the reserves and predicting future oil or gas well production of these types of reservoirs. An easy and relatively quick way of evaluating a well performance based on past production history data is the decline curve analysis. But when it is implemented in tight or shale reservoirs, the outcome might be unacceptable and unsatisfying probably due probably to ultra-low permeabilities and heterogeneities of the reservoir. All of the aforementioned led to the development of this thesis.

In the first part some of the basic features of gas and oil shales and tight-gas sands reservoirs are presented, simultaneously with the assertive recovery solutions. Then a Capacitance-Resistance Model is used that was proposed firstly by Shahamat (2014) in order to show the equivalence between electrical and petroleum engineering. The continuous succession of pseudo-steady states is introduced to entitle the application of depletion equations through a step-by-step process to analyze the behavior of the reservoir during transient and boundary dominated flow.

In the second part, the produced CRM model is compared with an analytical solution in order to verify the results and examine the reliability of the model which was proposed, for forecasting production rates during transient flow and BDF. Then both of these solutions are compared with results of two different reservoir numerical simulators, ECLIPSE 100 and IMEX-CMG. The conclusions that were made from this study are presented in the last section.

Chapter 1: Introduction

Energy demands are constantly growing through the years which create a need for more and more advanced and increased energy supplies in the world, so hydrocarbon resources will play a key role in the next decades. They can be categorized, according to their reservoir quality, abundance and the technologies utilized for their recovery, into different groups in a triangle (Masters 1979, Holditch 2006). This categorization was first used by Masters (1979) who proposed the resource triangle. According to Holditch (2006) the natural resources, just like any other resource, follow a log-normal distribution in nature. This means that best grade (best quality) resources are smaller than the lower quality reservoirs and are easier to exploit, but the lower quality reservoirs, are usually larger in size, but more difficult to extract. Figure 1.1 depicts a gas-resource triangle (on the left) and the closer to the base you go, the lower the quality of the reservoir and instead of quality one could use the term permeability. The numbers on the left side represent the ordinary values of each group of reservoir that is the reason why the higher quality reservoirs are on the top and the lower quality at the bottom. Unconventional reservoirs require assertive operating practices such as steam injection stimulation treatment or even advanced technologies which will help recover oil and natural gas, economically. Tight-gas sands, gas and oil shales, coalbed methane, gas-hydrate deposits and shale oil and gas reservoirs, heavy and extra-heavy oil and tar sands reservoirs are the most common unconventional reservoirs.

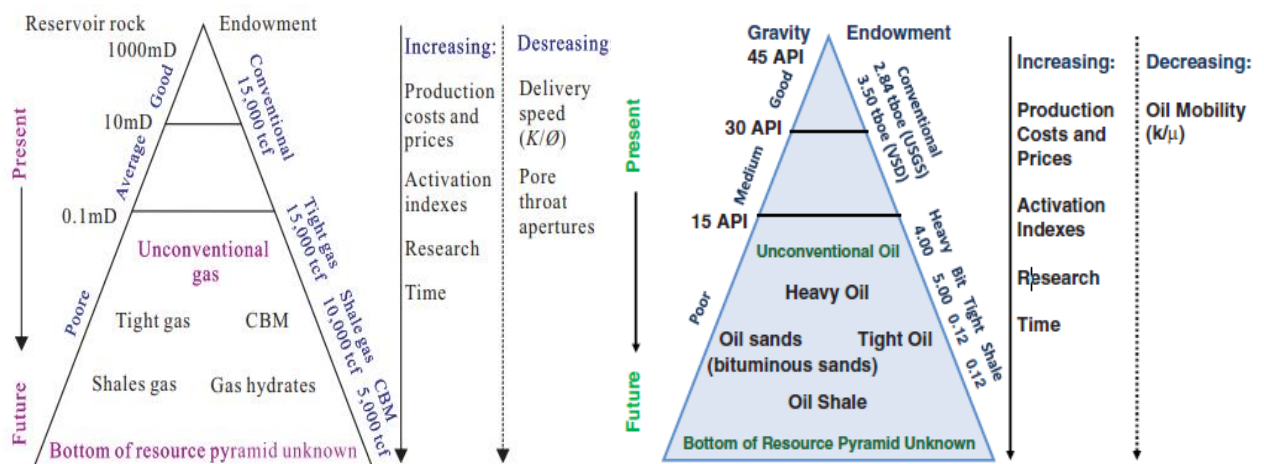


Figure 1.1: Resource triangles of oil and gas endowment (Aguilera, 2013).

In the figure above, two resource triangles for oil and gas world's estimates are illustrated, which comprise global endowment and activation indexes. USGS defined the term endowment as the sum of hydrocarbon volumes, which is the accumulative

production together with the reserves, and undiscovered hydrocarbons (Aguilera 2010). Activation index refers to the evaluation of the total investment needed in order to gain access or “activate” new oil or gas fields and it is expressed in dollars per volume per day (\$/barrel/day) of stabilized production (Economides and Oligney, 2000). From figure 1.1, it is obvious that conventional reservoirs are the reservoirs with high API, low viscosity, high permeability and small size which means small endowment and require less production cost, hence lower activation index. As mentioned before, the bottom of the triangles belongs to the unconventional reservoirs which are characterized by big volumes of hydrocarbons, hence high endowment. It is very difficult though to extract their resources, thus advanced methods and technologies are required for this case. As a consequence this increases the activation indexes and the price of oil or gas.

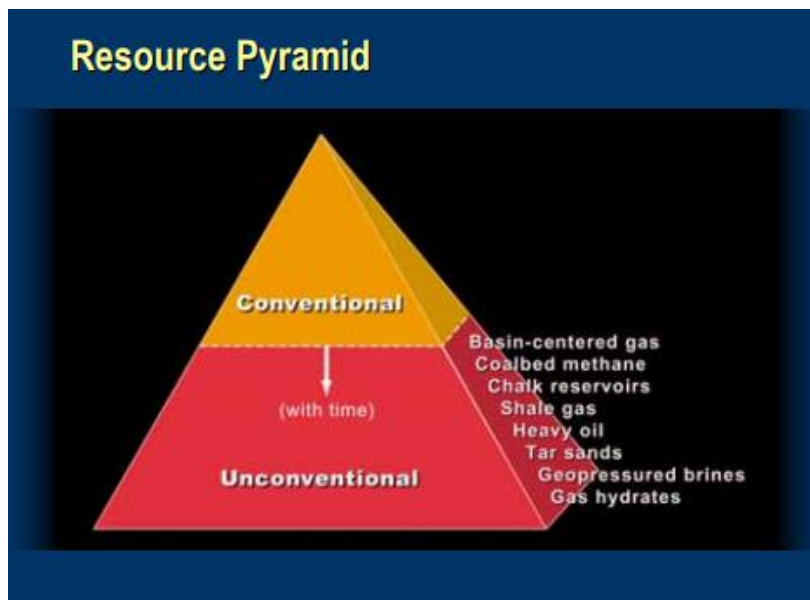


Figure 1.2: World oil and gas resource pyramid (Ben E. Law).

In the world oil and gas resource pyramid, in figure 1.2, the closer you go to the base of the pyramid, the larger the volume of hydrocarbons. The fact that the bottom of the pyramid is unexplored is a reality which commands a new prospect for the future for unconventional reservoirs. According to the Wall Street Journal (Yergin D. and Ineson R., 2009), the unconventional gas plays are “the biggest energy innovation of the decade.”

Tight and shale oil and gas reservoirs have gained the attention of the people in the petroleum industry due to their size and the advanced technologies and

methodologies which provided the knowledge to exploit them. Mostly USA and Canada have targeted these kinds of reservoirs, and they mainly started applying multi-stage hydraulic fracturing treatments and horizontal wells. Tight gas provides almost 6.6 TCF, which is 56% of the United States unconventional gas yield. On the contrary in 2009, when the total gas production in the United States was 22.5 TCF, shale gas contributed 3.3 TCF, which is approximately 16% of the total gas production according to the Energy Information Administration (EIA). In 2010 the total gas production in the United States raised to 24.1 TC and shale gas went up by 7% and reached the 23%. Moreover it is expected that for the next decades, the shale gas recovery will continue to grow and until 2035 it is expected that it will increase to 50% of the total produced gas volume of the US. Correspondingly in 2010, the the Canadian Society for Unconventional Gas (CSUG) reported that the produced amount of shale gas was over 1100 TCF, which mainly came from the Western Canada Sedimentary Basin (Shahamat, 2014).

Taking into account all the aforementioned it is pointed out that in North America, unconventional resources play an important part in satisfying energy demands, although internationally, they are not of the same importance to world energy supply but due to the rising demands, the unconventional resources must also be explored and developed. As a result this continuous urge for production leads to the need of developing new methodologies in order to produce and predict the estimated reserves of unconventional oil and gas wells. In the next part of this study, recent processes and models will be proposed and analyzed to estimate the reserves and predict the future production.

1.1. Problem Statement

The most difficult and most challenging task reservoir engineers have to deal with is the future production performance of a reservoir and the evaluation of its characteristics. Different methods can be proposed and utilized depending on the required amount of input data, their reliability and the desired accuracy of the results, as well as the availability of time and resources. Although there are cases where a simple estimation of expected ultimate recovery (EUR) and prediction of rate decline might be desired, there are also cases, besides this, where the mathematical models and maybe an integrated reservoir simulation can be utilized in order to evaluate the procedures that take place. So according to the objectives and the amount of time, data and resources figure 1.3 illustrates the three different accessible methods for performance prediction and reservoir behaviour.

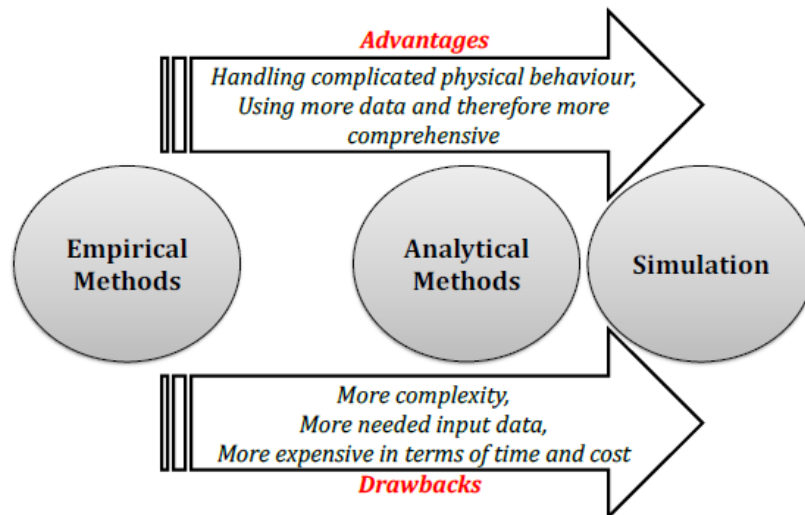


Figure 1.3: Comparison of the methods used for reservoir characterization and production prediction.

Since the integrated reservoir simulation evaluates more complicated reservoir processes, it requires a larger amount of data and therefore it is a time-consuming process. On the other hand, the analytical methods are less comprehensive but less data are needed and as a consequence they are faster, less expensive and easier to handle. Furthermore, empirical methods can be used for production prediction, and they have the advantage of being simpler and require minimal data, so they are easier to use. Arps method (1945) apart from being an easy to use method with the minimal data required, can also be used in different types of formations with

significantly different permeabilities, a fact which has resulted in becoming one of the most common industry applications.

In tight and shale reservoirs, geological along with fracture geometry complexities make forecasting their behaviour a difficult task to deal with. In such reservoirs, commingling different layers is a common practice so the amount of contribution by each layer to the total well's production, the types of flow regimes in each layer, and the collective combination of the layers can remarkably change the Arps parameters obtained based on a single layer assumption. Moreover, in such reservoirs their very low permeability causes an extended transient flow period which can last for years, and as a consequence the b-values in Arp's equation can be greater than unity (Shahamat, 2014).

Furthermore, these low permeability reservoirs usually result in using hydraulic fracturing treatments, a fact which further complicates their flow behaviour. Especially in shale reservoirs, fractures produce an enormous contact surface area with very high permeability, which causes the development of the Stimulated Reservoir Volume (SRV). This huge surface area causes the creation of an extensive linear flow period (Anderson et al. 2010), and fracture dominated flow (Duong 2011). These can be translated into the need for accommodation of transient flow in the traditional decline analysis in a manner consistent with reservoir engineering concepts (Shahamat, 2014).

Chapter 2: Revision

As it is common knowledge that unconventional resources are hydrocarbon reservoirs which are ultralow-permeable and have endowed significantly to oil and gas production worldwide. These types of reservoirs are difficult to produce and require special recovery operations and more sensitive technologies to be implemented and thus fundamental parameters and processes are much more difficult to be conceived in order to conduct performance analysis and achieve commercial production. In this chapter we will discuss some of the basic features of tight-gas sands, gas and oil shales reservoirs, simultaneously with the assertive recovery solutions and practices that contribute in production, by making these type of reservoirs, economically viable.

2.1. Unconventional reservoir features

2.1.1. Tight gas reservoirs

According to the U.S. Gas Policy Act of 1978, the required in situ gas permeability should be equal to or less than 0.1 mD for the reservoir to qualify as a tight gas formation. Nowadays, this is probably the most commonly accepted definition (Spencer 1989). If we look back to the 80's, the tight gas reservoir systems, according to Spencer (1989) and the table that he provided, were considered as the reservoirs having permeabilities less than 0.1 mD, while nowadays those reservoirs are characterized by a much smaller permeability of the order of 0.001 mD (Blasingame 2008).

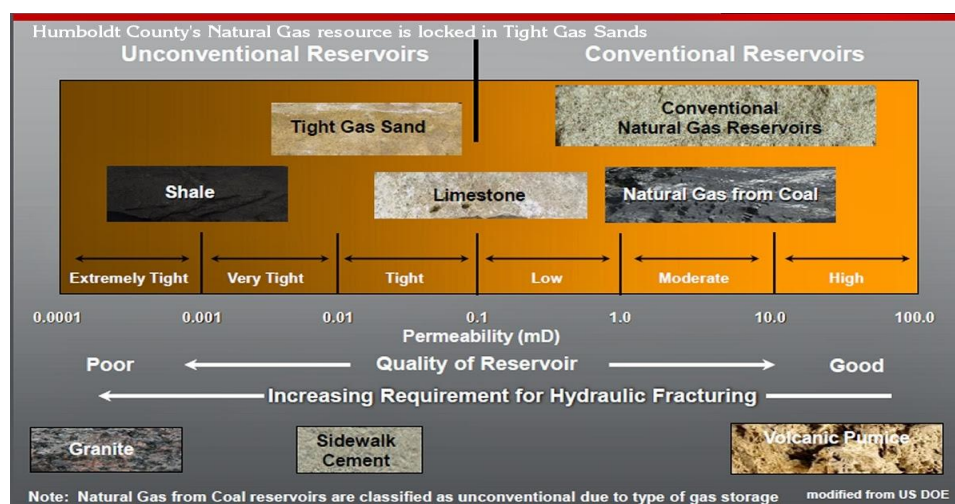


Figure 2.1: Conventional and unconventional reservoirs.

The best definition of tight gas reservoir is given by Holditch (2006): “a reservoir cannot be produced at economic flow rates or recover economic volumes of natural

gas unless the well is stimulated by a large hydraulic fracture treatment or produced by using a horizontal wellbore or multilateral wellbores.”

Two different opinions exist over the nature and the geological setting of these type of reservoirs (tight gas reservoirs). The first one classifies these reservoirs as basin-centered gas accumulations, a type of continuous accumulation, with spatial dimensions which exceed those of conventional oil and gas accumulations, and exist independently of the water column, without owing their existence to the buoyancy of gas in water. On the contrary, the second maintains the idea that gas fields encounter in poor-quality reservoir rocks with low permeability in conventional structural, stratigraphic, or combination traps. In tight gas systems, production depends on finding the location of the enigmatic sweet spots. Sweet spots in pervasive tight gas reservoirs are outlined by source-rock richness or thickness, by natural fractures, higher pressure and reservoir quality (i.e. better permeability and porosity), and by other factors such as conventional traps within penetrative gas accumulations. The Deep Basin reservoir in the Elmworth-Wapiti field, in the western edge of the Western Canada Sedimentary Basin (WCSB), is a characteristic sweet spot (Figure 2.2). It is the targeted aggradationally stacked Lower Cretaceous high permeability conglomeratic shoreface that can be depicted by a greater reservoir quality which has porosities higher than 12% and permeabilities that start from 1mD and may exceed the 1000mD within successions of lower reservoir quality tight sandstones, siltstones, organic shales and coals. In figure 2.3 there is a representation of the dual-transmissivity reservoir, which delineates that the position of the less permeable rocks can be near (above, below, or lateral) the reservoir connected to the wellbore.

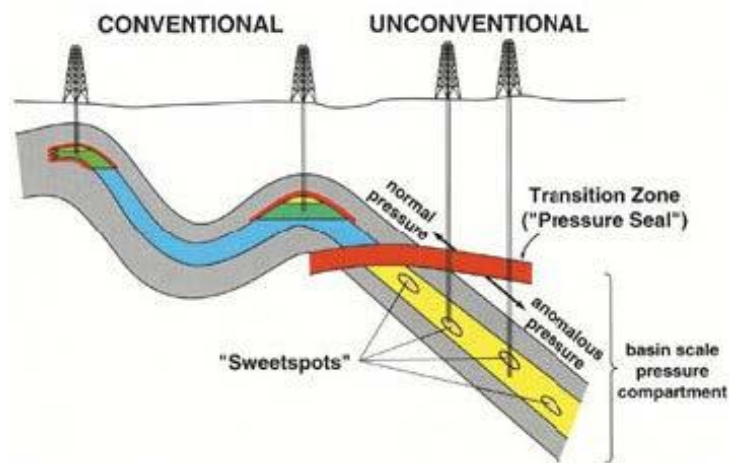


Figure 2.2: Basin Centered Gas Accumulation Model.

Usually the natural gas (in tight formations) before it migrates to the tight reservoir where it can be trapped and stored, it is created in shale. But in order to produce it and benefit economically from tight reservoirs, it is of great importance to be naturally fractured.

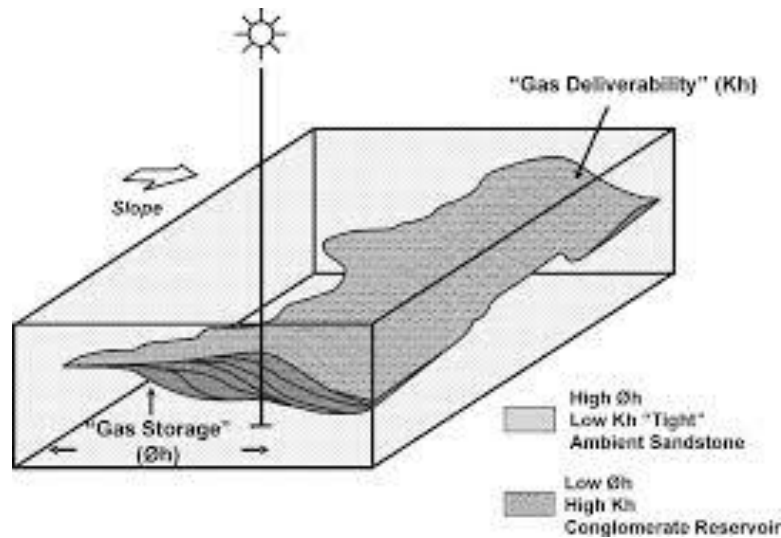


Figure 2.3: Diagram of dual transmissivity nature of Deep Basin clastic reservoirs. Higher permeability conglomerate (sweet spot) encased in lower permeability tight sandstone reservoir (Zaitlin and Moslow 2006)

2.1.2. Shale gas reservoirs

Shale gas reservoirs contain natural gas which is formed and trapped inside shale¹ formations and are often referred to as “unconventional gas reservoirs”. Shale gas has been a substantial natural gas resource in the United States since the early 1900s (first produced in 1821) from the Devonian shales of eastern North America, an idea that was gradually transmitted to the rest of the world. The end of the 1990’s, constituted the beginning of production leap, where the application of horizontal drilling made its appearance.

Although, in 2000 it supplied only 1% of the total U.S. natural gas production, ten years later this percentage rose up to 20% and as it is predicted from the U.S. government's EIA (Energy Information Administration) by the year 2035, shale gas will provide almost 50% of the total U.S. natural gas. Despite the fact that shale is the

¹ Shale: fine-grained, clastic sedimentary rock composed of mud that is a mix of flakes of clay minerals and tiny fragments of other minerals, especially quartz and calcite. It is the most common sedimentary rock. Shales and mudrocks contain roughly 95 percent of the organic matter in all sedimentary rocks.

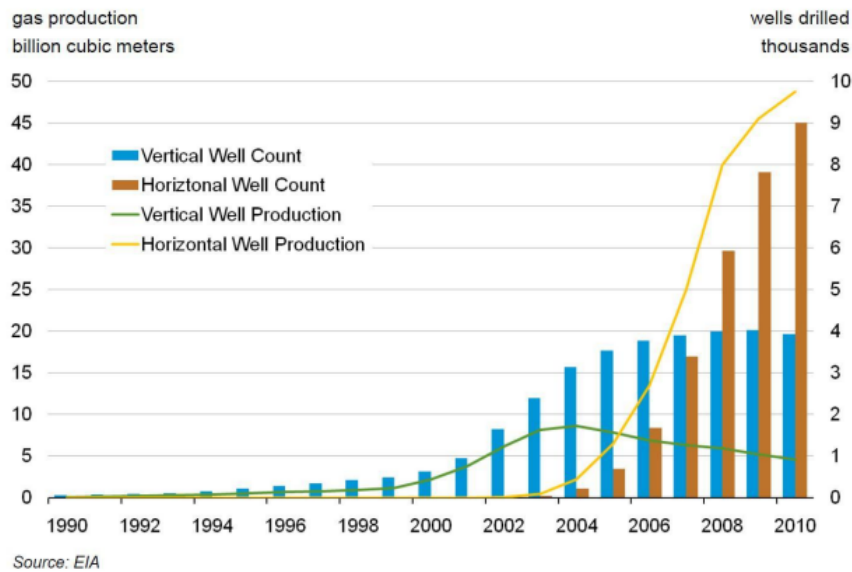


Figure 2.4: Increases in production and well count in the Barnett shale from 1990 to 2010 (Newell 2010).

most widespread sedimentary rock on earth, there has been a lack of attention regarding wide research on shale rock, compared to sandstone or limestone until recently, when technological developments and advances in operation mechanisms, led to the gradual development of several shale projects. Due to the absence of interest for an extensive period of time, unreliability and vagueness was generated concerning the struggle to yield accurate measurements of key properties such as (matrix) permeability and porosity. An additional problem that sometimes created confusion was that of the homonymous term “shale”.

Shale is defined by ERCB in Section 1.020(2) 27.1 of the Oil and Gas Conservation Regulations (OGCR) as a “lithostratigraphic unit having less than 50% by weight organic matter, with: less than 10% of the sedimentary clasts having a grain size greater than 62.5 micrometers; and more than 10% of the sedimentary clasts having a grain size less than 4 micrometers”. According to M.E. Tucker (2001) shales have the meaning of “laminated clayey rock”, but also the meaning of the “general class of fine-grained rocks”.

Some geologists (Potter et al., 1980) use shale to classify all fine-grained rocks, while others (Spears, 1980; Stow and Piper, 1984) disagree with this option because they prefer to call “mudrocks” the fine-grained sedimentary rocks and “shales” the fissile fine-grained rocks. What really predominates is the general classification of fine-grained rocks, using the term “mudstone” and the term “shale” for fissile varieties. The mutual characteristic and meaning though of the term ‘shale’ among the geologists is that grains and pores in these types of rock are smaller than tight

and conventional formations. Another problem that has come to light through the years is the inability to define shale porosity, permeability and fluid saturation in the lab. Due to the complexity of the attributes of the shale reservoirs and rocks (complex nano-metric scale pores and microstructure), it is very challenging to analyze processes and conditions that constitute a key part in production.

Shale is not only a source rock, but a reservoir rock and seal simultaneously, since gas is generated and trapped in shale. It constitutes an exceptional source rock when it comes to commercial shale reservoirs, which occur in extensive areas, just like tight gas reservoirs, composing like these continuous accumulations. According to Aguilera (2010) gas can be entrapped and held in shale in five different ways. Firstly, as adsorbed gas into the kerogen material, secondly as free gas trapped in nonorganic interparticle (matrix) porosity, and third as free gas trapped in microfracture porosity. Another way is as free gas stored in hydraulic fractures created during the stimulation of the shale reservoir, and the last one, as free gas trapped in a pore network developed within the organic matter or kerogen. As expected, their complexity and specialness has led to the development of hybrid combination of methods, which primarily were demonstrated for coals or conventional reservoirs, in order to determine pore systems, flow characteristics or other shale properties (Bustin et al. 2008).

Moreover, most of the commercial laboratories resist in revealing their methodologies; hence it is unfeasible to assess the validity of the outcome or the methods. Thus, since there is no standard method of measurement from the American Petroleum Institute (API) for shale systems, operators have established internal rules, traits and specifications in order to categorize gas shale systems. The following table depicts a partial list of common sources for major reservoir and rock properties for shale gas reservoirs.

Some of the most influential petrophysical properties mentioned in the table are: rock composition, porosity, total organic carbon (TOC) content, saturation, permeability and mechanical properties. Shale reservoirs are defined as organic-rich and fine grained (Bustin 2006), but the size of microfractures, the clay content and type, the mineral and organic matter type, and content, as well as the thermal maturity of shale may have an impact on shale properties and affect their behaviour. The presence of organic matter and mineral composition play a key role in governing shale properties by affecting the allocation of pores and fluid saturation.

Table 2.1: Common sources for significant shale reservoir and rock properties (Shahamat, 2014).

Reservoir Property	Data Source
Porosity	Helium gas expansion, high-pressure mercury injection (MICP), nuclear magnetic resonance (NMR), log analysis (calibrated to core)
Permeability	Core Analysis: Steady-state and unsteady state (pressure- and pulse-decay), micro and nano CT scanning Well-test Analysis: (pre- and post-fracture) Injection / falloff (IFOT), diagnostic fracture injection test (DFIT), post-fracture flow and buildup Production Analysis: Rate-transient analysis, simulation history-matching
Water saturation	Core extraction (Dean Stark, Retort), capillary pressure, log analysis (using lab-based electrical property measurements)
Free and sorbed gas	Desorption canister testing and adsorption isotherms, calibrated log analysis
Total organic carbon	Leco TOC and RockEval (calculated), Log analysis
Thermal maturity	Vitrinite reflectance (Ro), RockEval (calculated)
Rock composition	X-Ray Diffraction, Fourier-Transform Infrared visual point count (for optically resolvable grains), Inductively Coupled Plasma Mass Spectrometry (ICP-MS) and Scanning Electron Microscopy with Energy Dispersive Analytical System (SEM-EDAS)

Grains and pores of gas shale reservoirs are of a very small size, while pore throat diameters are, usually, sub-micron in size. Such reservoir rocks can be described by a high stress-sensitivity, an attribute which may be held responsible for the occurrence of microfractures, due to the fluctuation of permeability with time and effective pressure during production (and pressure drop). Although there is a serious difficulty in measuring such low matrix permeabilities, several attempts of determining their value, led to values of the order of few to a couple nanoDarcies. Concerning water saturation, commercial labs usually apply two different methods for fluid extraction. The first is the Dean Stark method and the second is the retort method. Furthermore, special processes are necessary to define capillary pressure, so as to assess water saturation, which sometimes may take moderate to high values, while others can be extremely low.

Another parameter which has played a key role to the designation of potential existence of shale gas accumulations is the level of the thermal maturity. Thermal maturity points out the heat driven reactions that are needed in order to break down organic matter into hydrocarbons. So, a source rock can be characterized as immature, mature or post-mature, regarding its ability to generate hydrocarbons, by measuring vitrinite reflectance or by pyrolysis. The reflectance of vitrinite was first

used to predict the thermal maturity of coal beds and later for the metamorphism from kerogens to hydrocarbons. The reason why vitrinite macerals were chosen for this assessment, is their sensitivity to temperatures (60 - 120 °C), which are consistent with the formation of hydrocarbons.

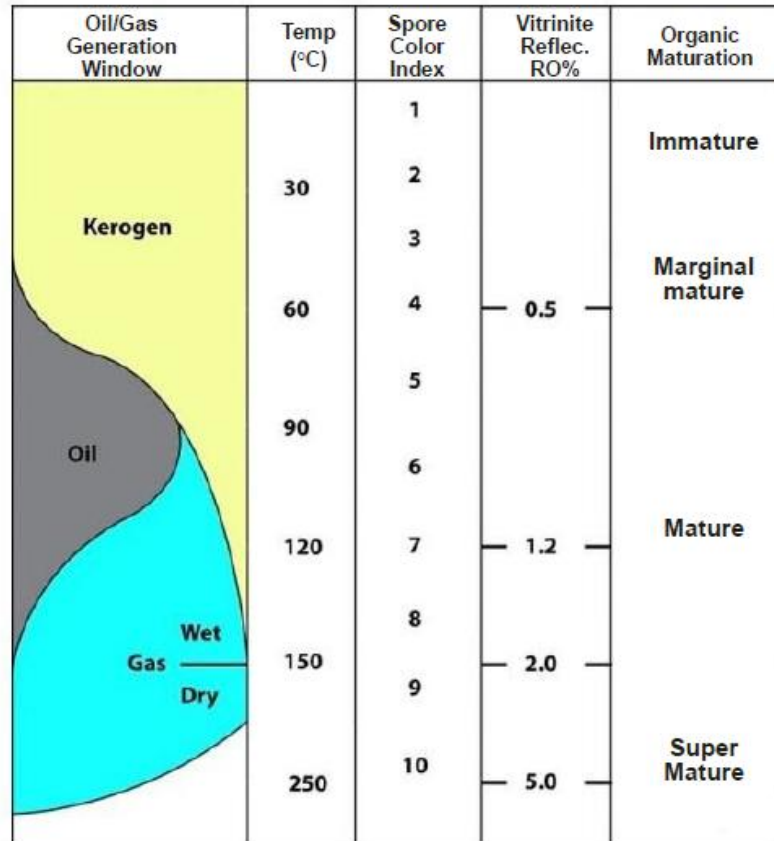


Figure 2.5: Hydrocarbon generation window and organic maturation with respect to the value of the vitrinite reflectance. Modified from Steyl and Van Tonder (2013).

A reflectance of 0.5 to 0.6% marks the beginning of organic matter transforming into oil, while reflectance of 0.85 to 1.1% points out the termination of this transformation into oil production. Figure 2.5, depicts a reflectance range between 1.0% and 1.3% for wet gas and condensate, while for dry this value is greater than 1.3%. At the picture above, the value of the vitrinite reflectance is illustrated as function of oil or gas generation window, organic maturity and temperature.

Another significant criterion, which should be examined for the classification of shales is the total organic carbon (TOC). A quantity which measures the amount of organic carbon found in a rock and is directly related to rock's capability to yield hydrocarbons, hence, it is a very critical determinant of the potential productivity of

shale gas reservoirs and not only. Adsorbed gas is gas adsorbed on the surface of organics and clays, so it is strongly correlated to the total organic carbon quantity.

Using log analysis models TOC values can be calculated in order to determine gas shales quality and predict gas content, G_c . Many alternative methods can be used for calculating the organic content from logs such as Passey's "DlogR" method, basic analysis and visual analysis. Visual analysis from logs is used for displaying potent hydrocarbons in conventional reservoirs but also it can be used in organic rich shales, if this process is applied in radioactive zones. This method uses, as a base, the porosity-resistivity overlay technique so as to verify the existence of possible oil and gas shales, as well as source rocks. Sonic logs or density logs are used as porosity index, thus, sonic logs are lined up and set above the resistivity logs in order the sonic curve to be precisely above the resistivity curve in the low resistivity shales. There are also baselines which are the outcome of the absolute value of the sonic and resistivity curve (in the low resistivity shales) and are affected by depth and geological age.

Low resistivity shales are considered to be non-source rocks and are unlikely to be gas shales. Shales or silts with source rock potential will show considerable crossover between the sonic and resistivity curves. Considering the fact that shales, which can be thought as potential source rock, display remarkable crossing between the two curves, the low-resistivity shales are unlikely to be gas shales because they cannot be characterized as source rocks (Passey et al. 1990).

As it is already mentioned it is of major importance to measure the quantity of stored gas basically for two reasons: 1) in order to determine the potential existence of stored gas in shales and 2) to conceive the rates and also the mechanisms through which gas will be transported and produced. Shale gas reservoirs differentiate from conventional gas reservoirs as the adsorbed gas ranges between 20% and 85% of the total gas storage (Yang et al., 2015).

Although there are many studies concerning gas desorption in coalbed methane reservoirs, the sorption properties of coal cannot be entirely matched to shale gas but to some extent, it can be used to shale reservoirs (Shahamat, 2014). In order to predict desorbed gas volumes and the content of organic material, while producing, coalbed gas adsorption curves are used. Usually pure methane is used so as to create and define these isotherms but the result is unreliable for estimating multicomponent gas desorption volumes. Sorption curves are formed with the assistance of various analytic and semi-analytic processes such as multicomponent interactions and transient responses (Shahamat, 2014).

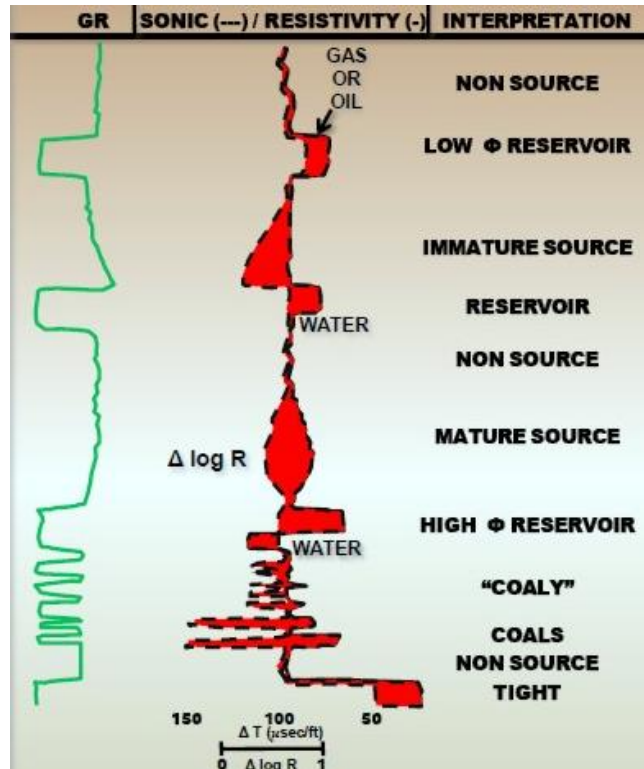


Figure 2.6: An example of sonic resistivity overlay in different situations.

The most regular empirical mathematical model that is employed, in order to measure the quantity of desorbed gas, is the Langmuir model. This method is based on a non-linear relationship between the volume of gas which might be sorbed onto a surface and pore pressure. As Langmuir sorption isotherms indicate, this process is done under constant temperature, and the equation that describes the aforementioned relationship is given below:

$$\theta = \frac{V_L P}{P + P_L} \quad (1)$$

where,

θ is the total volume of gas adsorbed per unit volume of the reservoir in equilibrium at pressure P in scf/ton,

P is pore pressure (assumed to be the average reservoir pressure) in psi,

V_L (Langmuir volume), the maximum sorption capacity of the coal or shale in scf/ton

and P_L (Langmuir pressure), at which the total gas volume adsorbed, θ , is equal to one-half the Langmuir volume in psi.

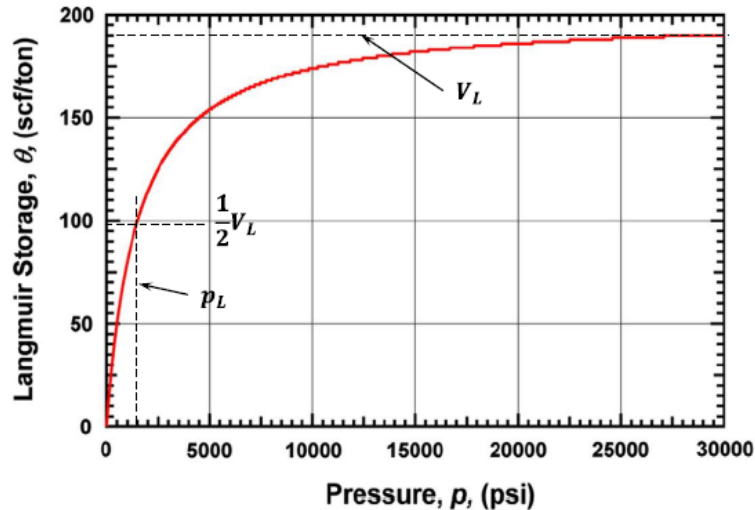


Figure 2.7: Plot of Langmuir (model) isotherm versus pressure.

Langmuir volume and Langmuir pressure are determined from core samples. More specific, Langmuir pressure (P_L) is the pressure at which half of the volume of gas is desorbed, while Langmuir volume (V_L) stands for the total volume of gas at infinite pressure, symbolizing the utmost capacity of gas that can be stored (Shahamat, 2014). In figure 2.7 a typical Langmuir curve is illustrated as a function of pressure. It is distinct and undoubtful, that as the Langmuir pressure increases to infinity, the volume of potential desorbed-gas content from the organic shale material approaches the Langmuir volume (Liang Wang et al, 2015). Langmuir's theory uses as a basis a kinetic principle, according to which, the rate of adsorption (or else the accommodation coefficient) counterbalances the rate of desorption, a principle that Gao et al. (1994) supports and explains that this happens because of the ultra-low permeable shale medium and consequently the flow is low through the kerogenic media.

Sorption curves demonstrate the largest amount of volume of gas that shale can store, under equilibrium conditions at a given pressure and temperature, and there are two different ways to determine them: the direct and the indirect method. The first method in order to estimate the sorption curves suggests that the core must be cut, during drilling and should be set straight away into a metallic can. Afterwards the volume of gas, from the shale the way it will evolve gradually with time, should be measured (Crain 2011) and when gas from the sample stops evolving, it is crushed and then the residual gas should be measured (Figure 2.8). The other method utilizes the core or cuttings which are collected but the difference is that the core does not need to be fresh, in this way this method is more economical. These isotherms are the outcome of experimental measurements, where a powdered coal sample is used and six different pressure points, at constant temperature, are used,

in order to measure the saturated methane content of this sample (Mavor and others, 1990). At this point the greatest amount of gas storage capacity of the reservoir is estimated, as well as the pressure at equilibria, by utilizing Langmuir's equation (equation 1).

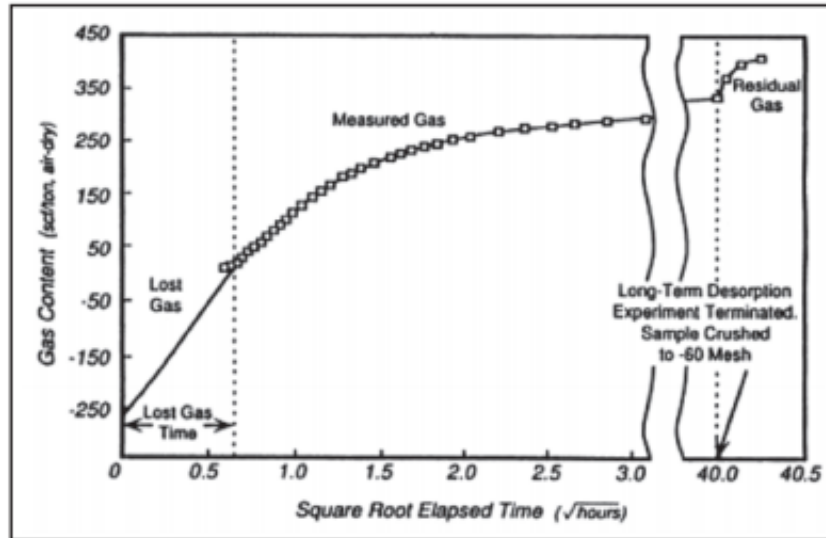


Figure 2.8: Graph of a sorption curve from gas shale.

As it is already been stated, shale is a fine-grained sedimentary rock, formed from mud which mostly consists of clay minerals and tiny fragments of other minerals, especially quartz and calcite. Although shales are mostly composed of clays, many rocks that are composed of other minerals are also called shales, which they really are silts or silty shales or shaly silts with very small values of porosity and permeability (Crain 2011). As a result, some shales might not be shales at all, but they could be siltstones. From time to time, there are rocks that look like shales while conducting a log analysis. For example the existence of radioactive zones due to uranium (and little kerogen), the large density-neutron separation, the low resistivity and the high PE values act together and plot against the proper identification of the rock, leading to a misguided conclusion. Accordingly, it would be very beneficial to verify the rock composition of the shales, so as to avoid misinterpretation and attain a much more improved completion, production and development planning.

An approach is to use a ternary graph of a shale displaying its mineralogical constituents. The three apexes of the equilateral triangle, that it is used for the ternary plot, illustrate the ratios of three different variables, which in this case will represent three group of minerals that appear akin properties. Each point of the barycentric plot stands for a different composition of the three minerals, so according to the position of the point, an appropriate interpretation of the behavior of the sample can be made. Loucks and Ruppel (2007) created a ternary graph of Barnett

mineralogy which displays that the clay group of minerals presents a smaller value from the quartz (also feldspar, pyrite and phosphate) group. Taking also into account the ternary diagram in figure 2.10, which relates mechanical and chemical stability to mineral composition, we can conclude that samples, which consist of greater than 40% clay minerals (dashed line), tend to have low fragility and brittleness (rocks higher in brittle mineral content are higher in brittleness, J. Tuo, C. Wu, M. Zhang, 2014). Thus, judging from the Barnett ternary diagram, samples appear to have less than 40% of the clay group of minerals, so the reservoir can be described as more brittle and suitable to a hydraulic fracturing production.

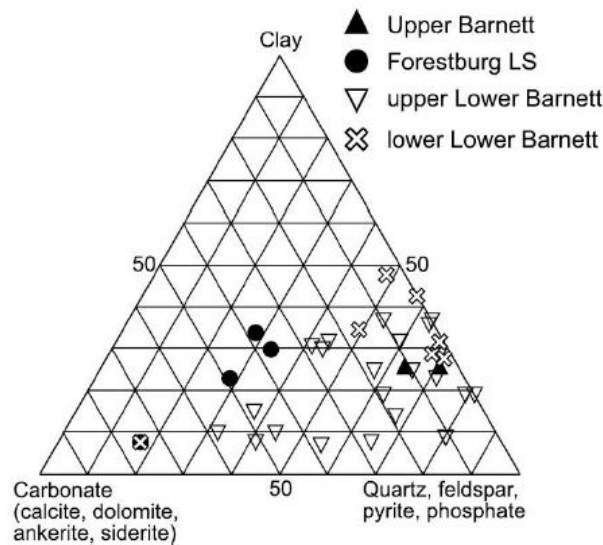


Figure 2.9: Ternary diagrams of Barnett mineralogy (Loucks and Ruppel 2007).

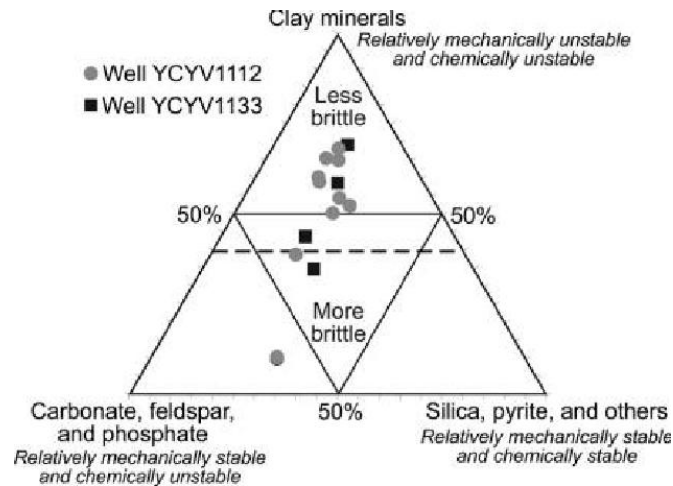


Figure 2.10: Mineralogy ternary diagram showing analysis by well (Loucks et al., 2012).

There are two principal processes which generate methane and by which the shale gas reservoirs can be categorized: (i) biogenic (methane generated from methanogenic archae) and (ii) thermogenic (methane generated from chemical reactions, without the existence of microorganisms).

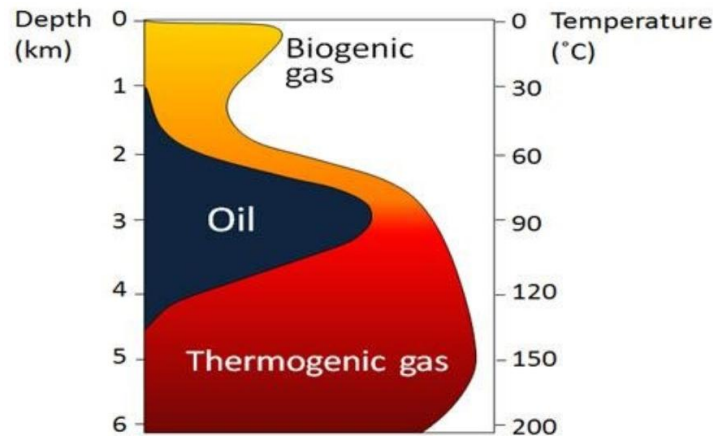


Figure 2.11: Biogenic and Thermogenic Gases.

In biogenic shale gas reservoirs, gas is produced by methanogenic organisms, so it is a direct consequence of bacterial activity. Methanogens are microorganisms found in shallow sediments that chemically break down organic matter to produce methane. This process usually takes place close to the earth's surface, so biogenic shales are being formed at shallower depths (500 – 4000 ft). Moreover, they are mostly composed of pure methane, they can be found in bodies of fine-grained sediment mainly because of its higher initial organic content (TOC often > 10 wt%), and they are thermally immature. This last property has as a result, the smectitic clay contents not to be entirely converted to illite, so they have higher swelling clays proportions. It is worth mentioning, that biogenic shales are more sensitive in case of damage from reactions between swelling clays and fluids containing water. As typical clay-rich rocks, they tend to be less consolidated, hence they depend on the presence of open natural fractures, which are able to provide a channel that will support water and gas production. After fracking biogenic shales, water must be first removed from fractures (natural or not), before production of the sorbed gas begins, which means that large volumes of water can be produced in these types of shales.

On the other side, thermogenic shales often are found at (subbottom) depths exceeding 3000 ft and have relatively lower values of TOC (> 2 wt%) than the biogenic shales, probably because most of the TOC has been converted to hydrocarbons. In biogenic shales the organic matter is not usually being buried deep enough to generate hydrocarbons. Thermogenic shales are generated under conditions of high temperature and great pressure from kerogens. As a consequence the organic matter, in these type of reservoirs, has been considerably prepared to form gas which is stored in the pore space and sorbed to the organic matter. Thermogenic shale gas reservoirs typically accommodate great amounts of Silica or Carbonate and “healed” natural fractures (Chan et al., 2011), a feature that shows brittleness and hence thermogenic shales can be mentioned as “fracturable” instead

of “fractured” shales. Therefore, their initial gas rates from fractured horizontal wells are generally greater than those of the biogenic shales.

2.1.3. Tight/shale oil reservoirs

Tight oil is light crude oil contained in relatively impermeable shale, siltstone, sandstone and carbonate rock deposits, which are closely linked to oil-source shales (X. Zhang, 2016). According to public opinion generally the term “tight oil” is used as an alternative of the term “shale oil”. But sometimes it might be confused with oil shale, which is a sedimentary rock rich in organic matter, or shale oil, which is oil produced from oil shales. Therefore, shale oil is a subset of tight oil. The term "light tight oil" is used from the I.E.A. (International Energy Agency) and terms like "tight oil" and "shale-hosted oil" are used from the World Energy Resources (2013), for oil produced from shales (or generally from low permeability formations).

Furthermore, as it is already mentioned, “shale oil” should not be mistaken with “oil shale”. Oil shale is an ancestor of oil, known as kerogen that is trapped and held in rocks with considerably low porosity and permeability. This fact makes the release of kerogen extremely difficult. Oil shale is a source rock consisted mainly of kerogen type I, in contrast to coal bed methane reservoirs which on average accommodate kerogen type III. Their color ranges from dark gray to black due to high proportions of naphthenes or other kerogen.

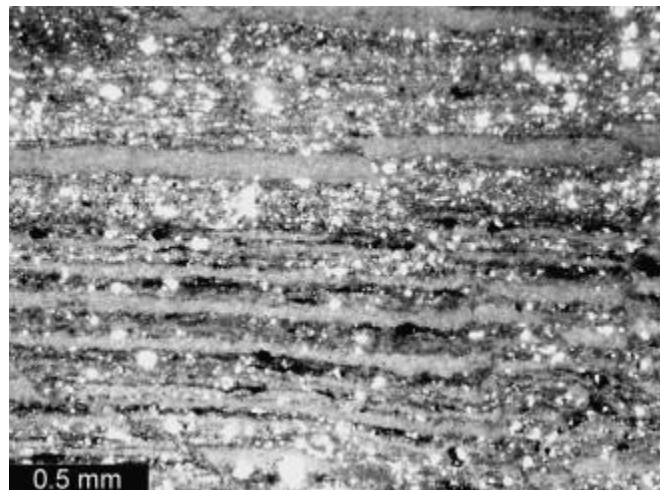


Figure 2.12: Oil shale composed of clayey and silty laminae saturated with kerogen and naphthenes (black), Slavonia crude oil and gas field, Croatia.

Apart from shale gas reservoirs, shale oil reservoirs are highly fissile and rich with clay, which means they are divided into layers where the existence of clay stone is enormous. These horizontal layers, illustrated in figure 2.12, can be stretched for

hundreds and thousands of miles. Shale oil formations are found in higher depths than oil shales, which sometimes may exceed the 15000 feet.

2.2. Common Drilling and Completion Practices

Developments in drilling and production technologies, especially in horizontal drilling and high volume hydraulic fracturing, gave access to previously unapproachable oil or gas fields, situated in several areas around the world.

As mentioned before, the permeabilities of tight/shale oil/gas reservoirs are ultra-low and because of this phenomenon, the only way to produce hydrocarbons, from an economic point of view, are by generating a huge surface area with high conductivity and which is in close proximity to the wellbore and create a fracture “network”.

With fracturing treatment the contact area of the wellbore with the reservoir is increased. Fracking or hydrofracturing is the shorthand for hydraulic fracturing which is a stimulation technique of a well by safely tapping tight rocks or shales, with the assistance of a pressurized liquid. This liquid could be water or water mixed with sand or proppants pumped at high-pressure in order to generate cracks that due to grains of sand stay open and allow fluids (gas, oil and brine) to flow easier. The additives are used to reduce friction and therefore decrease the pumping pressure needed but also prevent pipe corrosion and assist the efficiency of the well. It is mainly implemented to boost the oil or gas recovery in unconventional reservoirs. A further examination of this procedure led to the conclusion that in tight and shale reservoirs it was found that the most advantageous choice of fracturing fluid is slickwater.

Slickwater is a fluid which consists of very few additives combined with proppant, such as sand added into water in order to increase the fluid flow (therefore a very low viscosity). The process involves also injecting friction reducers, and friction reducers speed up the mixture. Thus, slickwater with its low viscosity is pumped into the reservoir, leaks into the microfractures and increases the contacted surface area with minimum formation damage. It was first used in the Barnett shale, where 800,000 gal. of water and 200,000 lbs. of sand were utilized as proppant. So, fluid volumes and sand tonnages together with pump-rates, are obviously factors that affect slickwater’s successful outcome (King 2010). It can produce a complex network of fractures and these geometries were illustrated by Fisher et al. (2005) and Warpinski et al. (2009), Figure 2.13. They mentioned that the bi-wing planar fracture is a simplification of this operation and in essence a very complex network is created around the wellbore.

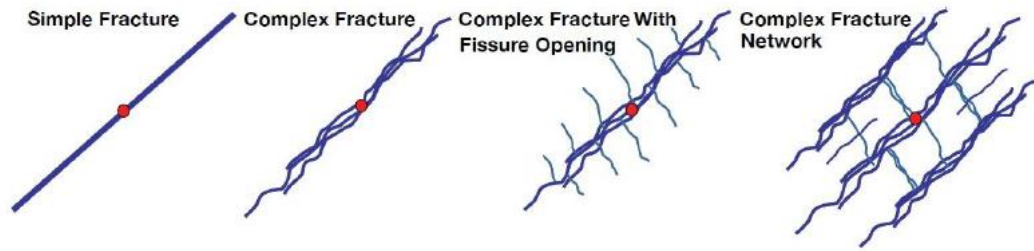


Figure 2.13: Comparison of possible fracture geometries created in tight and shale reservoirs (Warpinski et al. 2009).

Another way to maximize the contact area with a single wellbore is by drilling a horizontal well in a direction to assist transverse fracturing. Multi-stage hydraulic fracturing can be applied to open-hole and cased-hole wells. Although open holes were thought to be out-of-date, the fact that they provide higher productivity and lower cost, has extended the interest of the operator. The open hole completions are simple but each completion step should be handled properly and in the appropriate sequence otherwise the completion and simultaneously the well performance will be badly affected. On the other hand, a cased hole will not be so affected if the operations are not so carefully completed. Even if the well is damaged when production begins, at least there will not be any complications or problems with the completion equipment, and it can usually be run and operated. However this does not occur in many open hole completions.

In open-holes, packers are typically used to isolate stages, while in cased-holes, effective isolation of stages requires a good cement job. Usually cased and cemented completions are used because they give better control of number and location of fracture initiation (at perforation clusters). According to King (2010), the more perforation clusters and stages in cased and cemented completions the higher the possibility of dense fracturing. This way, due to fracture complexity an enhanced permeability region called stimulated reservoir volume (SRV), is developed. Although slickwater fracturing improves productivity, the SRV of an individual well is often small. Hence, multiple wells, massively fractured, with closer well spacing in order to create overlapping SRVs would result an enhanced recovery (Figure 2.14). Small changes of this approach such as, fracturing of multiple parallel laterals simultaneously (simul-frac) or in short alternating sequences (zipper-frac) are depicted in figure 2.14 (Shahamat, 2014).

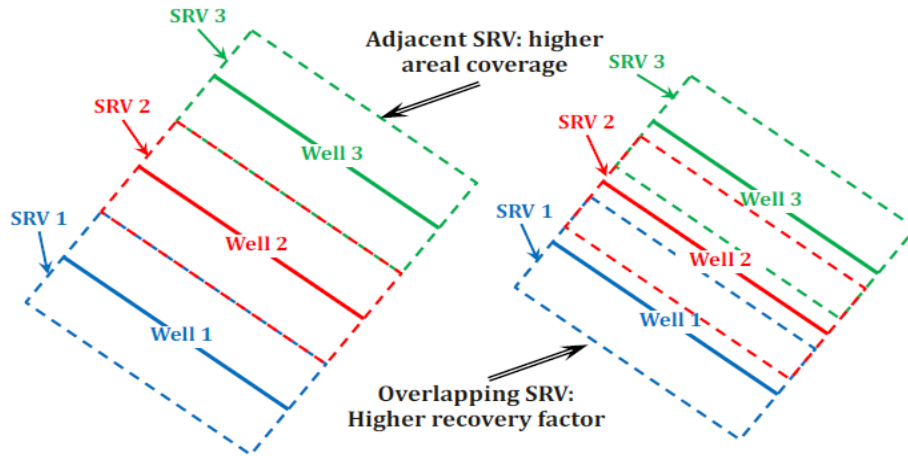


Figure 2.14: Importance of horizontal well placement strategy on SRV coverage, modified from Mayerhofer et al. (2010).

2.3. Analytical Models

A big variety of models are available, depending on the diversity of the well and reservoir conformations, which have an analytical solution. On a case-by-case basis the model that is chosen to be used can modify entirely the result of a prediction. In any case, the choice of the most suitable model demands thoughtful examination of numerous features and aspects, such as log and seismic data, geology, but also data that arose from neighboring wells drilled into the same area. This section is basically a short overview of a few analytical models which are regularly utilized for production data analysis.

When Gringarten and Ramey (1973) were modeling a vertically fractured horizontal well in a rectangular, homogeneous, isotropic reservoir with no-flow outer boundaries and constant pressure (initially), they presented the analytical solutions by applying Green's function. Thereafter, they used again Green's function and product solution method, in order to create an analytical expression for the pressure distribution acquired by a fractured well in a homogeneous reservoir. The producing pressure is uniform along the fracture (infinite fracture conductivity) and the analytical solutions which were used are for a uniform flow distribution in the fracture.

According to Clonts' and Ramey's (1986) study, analytical solutions for pressure response of a horizontal well within a finite anisotropic orthogonal reservoir was demonstrated, using as a basis again the Green's function. Thompson et al. (1991) were based on Green's function, to address the issue of the solution to be evaluated with accuracy over all time ranges offering as little computational effort as possible.

In addition, they presented a practical approach of alternating solutions at different times. For example, by using cylindrical source solution during early times and Green's function solution during late times. This method can be proved useful in plenty of situations. From horizontal wells and fractured wells, to wells and reservoirs dealing with any flow problem which requires Green's function solutions.

Wattenbarger et al. (1998) used the reservoir configuration shown in Figure 2.8 and provided analytical constant rate and constant wellbore pressure solutions from infinite conductivity fractured wells in such reservoirs. They also provided simple and practically useful early-time and late-time approximations for these solutions.

In figure 2.15 the top view of the reservoir geometry is depicted. The well is in the center of a rectangular reservoir and it has fractures, with infinite conductivity, which extend all the way to the lateral boundaries of the drainage area. The distance from the center of the reservoir to the outer boundary, in the direction that is perpendicular to the hydraulic fracture is y_e . Taking into account the aforementioned, the flow is linear, as it is delineated in figure 2.15, and it is vertical to the hydraulic fracture.

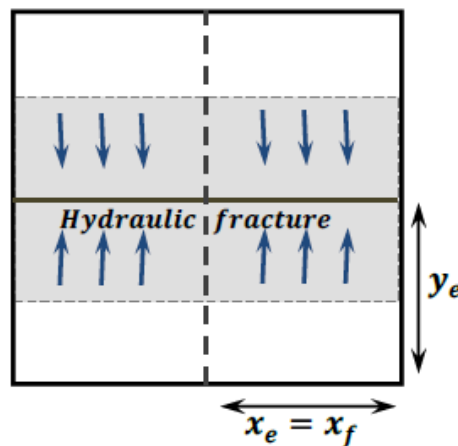


Figure 2.15: Hydraulically fractured well in a rectangular reservoir (Wattenbarger et al., 1998).

For the same reservoir geometry with multistage fractures, El-Banbi (1998) introduced a new method using as basis linear dual porosity analytical solutions. Afterwards, this model was used by Bello and Wattenbarger (2010) as a basis to examine the skin effect. They tried to history match production of shale gas wells from five flow different regions stating that most of the shale gas wells, display a linear flow from the matrix to the fractures presenting considerable skin. The outcome was a new analytical equation and the skin on linear flow behaviour was modeled by asymptotic solutions. Desorption was not taken into account in their work, that was

one of the assumptions they made, as well as there was no drainage from the outer reservoir (M. Shahamat, 2014).

Brown et al. (2011) suggested modeling the pressure-transient and production behavior of hydraulically fractured horizontal wells in low permeability shale reservoirs, with an analytical tri-linear flow solution. Figure 2.16 delineates a schematic representation of their simulation, where there is a naturally fractured medium in the Stimulated Reservoir Volume (SRV) surrounded by an outer reservoir region of lower permeability. The outer-reservoir is assumed not to be contributing to production considerably, but if it does it feeds the inner-reservoir via linear flow.

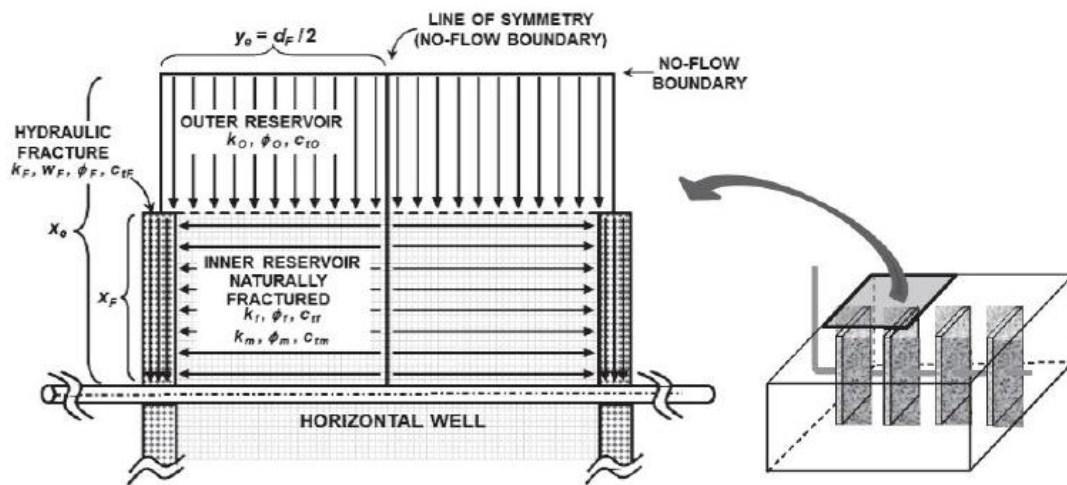


Figure 2.16: Schematic representation of the trilinear-flow model representing three contiguous flow regions for a multiple-fractured horizontal well (Brown et al., 2011).

The inner-reservoir supplies the fractures via linear flow, and the fluid in the fractures travels linearly till it reaches the wellbore. The radial convergence of flow toward the horizontal well within the hydraulic fracture is taken into account through the skin factor (flow choking in fractures), hence the trilinear model becomes more realistic after the termination of the early-time radial flow. The (trilinear-flow) solution is more suitable to be acquired in the Laplace-transform domain due to the probability of presence of natural fractures to the inner reservoir. So, with the application of Stehfest algorithm (1970), the Laplace-transform domain is numerically inverted into the time domain. Their model was verified by using the semi-analytical solution, developed by Medeiros et al. (2008), which simulates fractures as porous media.

In order to produce from multiple fractured horizontal wells, Brohi et al. (2011) suggested a linear composite model where the solution for the inner reservoir differs from the one for the outer reservoir. More specifically, for the inner reservoir a linear dual porosity flow solution is used and for the outer reservoir a linear single porosity solution is used respectively, combined (for both) with continuity of pressure and flux

at their interface. Their solution to the problem was acquired in Laplace domain, and this model is the same as the one that Brown et al. (2011) used, with a difference in coupling of the three regions. Brohi et al. (2011) actually used a numerical simulator so as to validate some of the assumptions they made in the progress of their work.

Brown et al. (2011) and Brohi et al. (2011) presented models and solutions concerning the pressure distribution for a system in which the SRV region occupies the whole area between hydraulic fractures. The model is divided in three regions: high-permeability region, low-permeability region, and fracture. Stalgorova and Mattar (2013) extended this trilinear solution into their model, with the difference that they splitted the reservoir into five different regions and not three like in the previous model.

The solution Brown proposed, concerned the pressure distribution for a system, in which the SRV region occupies the whole area between hydraulic fractures, whereas Stalgorova and Mattar (2012) proposed a solution for a system in which the stimulated region occupies only part of the area between the fractures. Thus, the five region model includes a rectangular reservoir with fractures which create a stimulated constricted region, while the rest of the reservoir is non-stimulated. This model uses as a basis the fact that fractures do not follow a simple straight path, but in reality they spread with a more complex pattern, possibly by creating a branch (fracture branching), which in its turn, develops regions of higher permeability around each fracture. As it is illustrated in figure 2.17, all the aforementioned can be modeled by a lower permeability region surrounding the stimulated regions (high permeability regions), which is formed around each fracture.

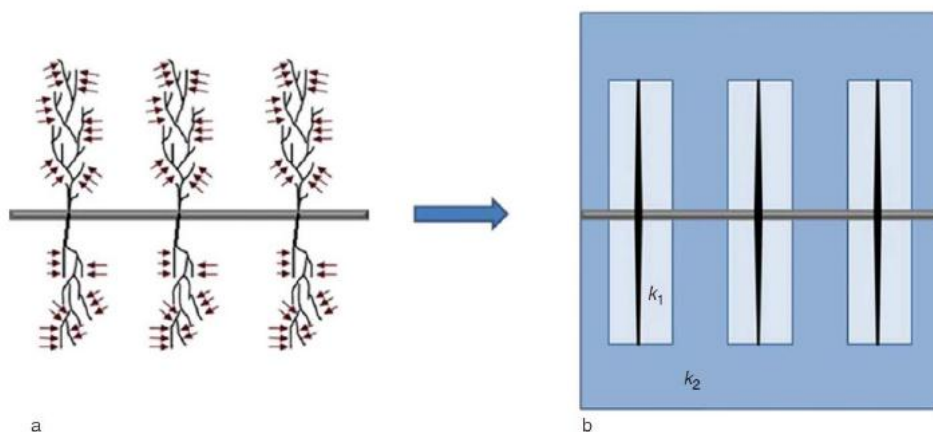


Figure 2.17: Display of (a) a horizontal well with multiple branch fractures and (b) its representation by a model ($k_1 > k_2$) (Stalgorova and Mattar 2013).

The region of higher permeability covers the area around the fracture in order to depict the branching of the fracture. Moreover, the system is symmetric and that is

the reason why in figure 2.18 only one-quarter of the space between the fractures is used. As can be seen, there is a combination of five linear flows between the neighboring zones, and arrows are used to delineate the direction of the flow in every region. Obviously, the non-stimulated zones are the regions 2,3,4 representing the original reservoir rock and region 1 represents the enhanced permeability zone. Linear flow travels from the non-stimulated zones (region 2, 3 and 4) to the enhanced permeability zone (region 1), then from region one to the hydraulic fracture and finally from hydraulic fracture towards wellbore.

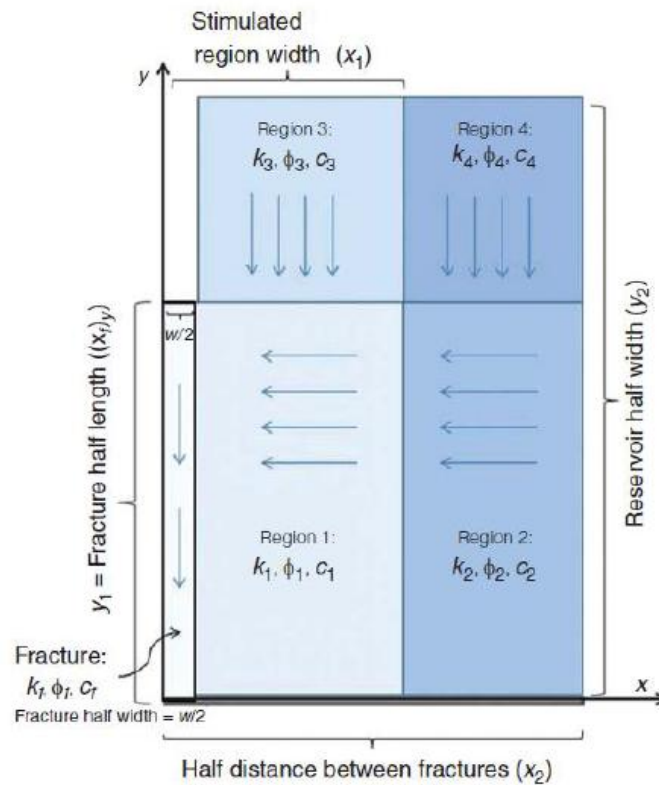


Figure 2.18: Schematic and dimensions of the five region model for one quarter of a fracture (Stalgorova and Mattar, 2013).

The way Brown et al. (2011) developed the solutions was adopted by Stalgorova and Mattar (2013), who used Stehfest algorithm (1970) to invert numerically the Laplace-transform domain into the time domain. They also reached to the conclusion that results from numerical simulation and five-region model, concurred only when the geometry of the system follows certain constraints.

There are also assumptions that were made for liquid flow problems in order to establish a linear partial differential equation within the systems of interest. For instance, the solutions of the models were derived by assuming that viscosity (μ) and compressibility (c) remained constant. On the other hand, gas is far more

compressible than liquid and a change in pressure implies a change not only in compressibility but also in viscosity and the deviation factor (z-factor).

Thereafter, when deriving the solutions of analytical models for gas, the result gives a nonlinear partial differential equation but there is no available analytical solution in the literature for that. Many scientists, engineers and researchers over the years tried to remove the nonlinearity out of the partial differential equation by using pseudo-time and pseudo-pressure. The latter was originally defined by Al-Hussainy and Ramey in 1966, which was later abtly redefined by Meunier et al. (1987), Eq. 2, to maintain the unit of pressure and avoid dealing with the units of pseudo-pressure (psia²/cp). Pseudo-pressure is given from the equation below:

$$p_p = \frac{\mu_{gi} z_i}{p_i} \int_{p_b}^p \frac{p}{\mu_g(p)z(p)} dp \quad (2)$$

As it was already discussed, the integrand in the equation above is a function of pressure, while the variable of integration is simultaneously pressure, so the value of pseudo-pressure can be accurately computed. However, this does not apply for gas pseudo-time. The definition of pseudo-time (Agarwal, 1979) concerns a transformation which is able to explain changes in gas compressibility and viscosity; it alludes to the definition of pseudo-pressure. Another similarity between them is that when normalizing pseudo-time, a useful variation is acquired (Fraim and Wattenbarger 1987, Meunier et al. 1987):

$$t_a = \mu_{gi} c_{ti} \int_0^t \frac{1}{\mu_g(p)c_t(p)} dt \quad (3)$$

Although pseudo-pressure can be rigorously computed, pseudo-time is not so accurate transformation, due to the fact that the integrand is a function of pressure while the variable of integration is time.

Many syggestions over the years were made by different researchers for calculating pseudo-time. More specifically, Agarwal (1979) determined a new function for pseudo-time in which viscosity and compressibility were evaluated at the wellbore pressure. Also, Fraim and Wattenbarger (1987) proposed calculating a normalized time at the average reservoir pressure (instead of wellbore pressure), for transient and boundary dominated flow analysis transient. Afterwards, Anderson and Mattar (2007) explained that if the production is in the transient flow period, using the average reservoir pressure for pseudo-time calculation can cause abnormal model responses. Thus, they proposed calculating pseudo-time, by getting the values of gas properties at the average pressure within the region of influence and not of the total pore volume. In order to find the region of influence they used the concept of

radius of investigation and as a result the volume which was supposed to be used for the average pressure calculation. Recently, Tabatabaie et al. (2013) suggested in their study the idea of using the liquid type curve in order to find the volume of investigation and the material balance equation for calculating the average pressure within the region of influence, and all these at constant rate production. They used an iterative procedure and expressed their concern of extending this method to cases where the rate fluctuates. They also pointed out that the application of superposition is still not valid and the suggested technique cannot be used.

It should be noted that the partial linearization of the governing differential equation, by transforming pressure and time to pseudo-pressure and pseudo-time respectively, allows the use of liquid solutions to gas flow cases.

2.3.1. Type curves

Type curves are preplotted solutions to analytical models, which are usually demonstrated in a dimensionless form and by using the type curve matching process, a proximate reservoir characterization method can be attained. This way the solution is presented simpler than the direct use of the equation. There are several kinds of type curves which are used to interpret well tests and they first appeared in oil industry during the seventies. Fetkovich (1980) is the most known well test engineer and the one who blazed a trail in using type curves for production data analysis. He placed liquid analytical infinite and finite reservoir solutions, at constant bottomhole pressure production of a well located at the center of a closed circular reservoir, in the same type curve (using dimensionless variables) with the empirical decline curve equations proposed by Arps. This way he showed a set of type curves used to estimate parameters and predict production. It worths mentioning that apart from the steady bottomhole flowing pressure (p_{wf}) in gas wells, Fetkovich also considered that there are no alterations in the PVT properties with reservoir pressure. Fetkovich type curves were used from Carter (1985), for finite radial and linear flow systems, with small changes in order to take into account variations in gas properties which depend on pressure and evaluate reservoir size. Blasingame and Lee (1986) presented a new method of estimating drainage area size and also used a superposition plotting function. Some years later, Palacio and Blasingame (1993), presented a solution which was based on material balance pseudo-time, so as to transform data for cases of fluctuating pressure into an equivalent system, which is producing liquid under constant rate. When they used the material balance time function, the analytical exponential stem of the Fetkovich type curve became a unit-slope straight line in a log-log plot (Shahamat, 2014). The aforementioned details and

the fact that integral functions have the ability to smoothen data, hence improve matching of data and type curves, led Blasingame and his colleagues to present new plotting functions so as to create new sets of type curves.

Palacio and Blasingame (1993), concerning the fluctuating rate and pressure production data, gave more attention on the analysis of gas wells. Others like Doublet et al. (1994) worked on analysing of oil wells and Pratikno et al. (2003) focused on fractured wells. But the common base of all these models was the assumption of a circular outer boundary. Araya and Ozkan (2002) dealt with different aspects on the use of decline curve analysis for horizontal, vertical and fractured wells. Wattenbarger et al. (1998), worked mostly on linear flow in tight and shale reservoirs, therefore they suggested a rectangular reservoir which was fractured while fracture was extended till the boundaries of the reservoir.

2.3.2. Flowing Material Balance (FMB)

Material balance analysis is a principal concept in reservoir engineering, considering it is a tool which is utilized to compute the original hydrocarbons-in-place in a reservoir. According to the general material balance equation, production volumes and pressure conditions are correlated to the original oil, gas, and water in the reservoir. In static material balance the well must be shutted-in at several points during its depletion so as to get the average reservoir pressure and compute the original hydrocarbons in place.

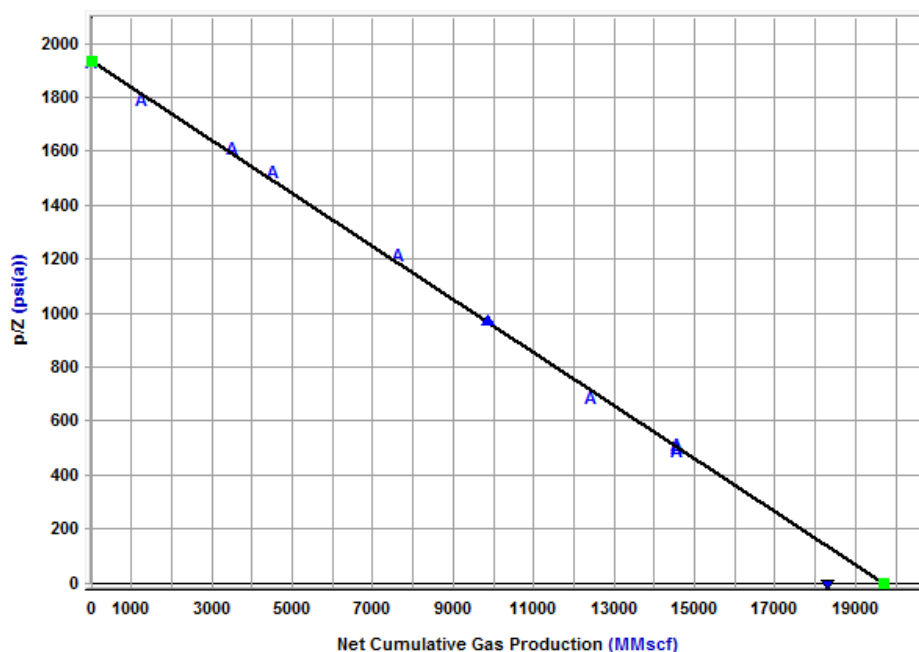


Figure 2.19: Plot of p/Z versus cumulative production.

For instance, in gas wells through the plot of $(p/Z)_{avg}$ versus cumulative production, a straight line is obtained. This means that the equation can be analyzed as a linear relationship. It should be pointed out that shutting in the well is impractical or not an option sometimes. Therefore, when shutting in the well is not an option; the flowing material balance is the alternative, which is based on a boundary-dominated flow (or pseudo-steady state flow), but also the flowing pressures and rates are used instead of the average.

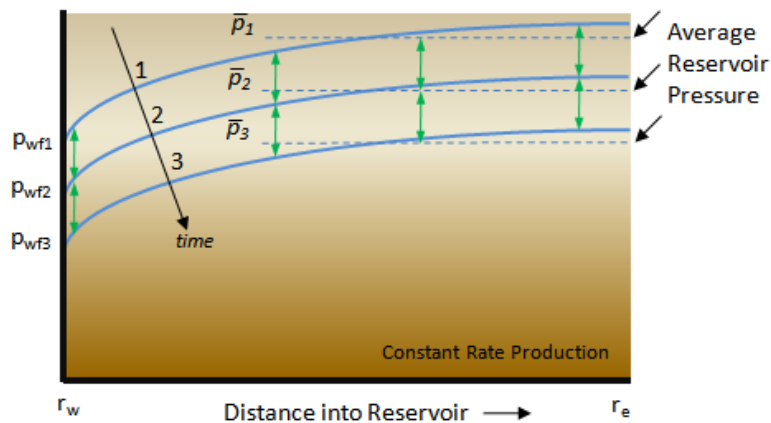


Figure 2.20: Plot of reservoir pressure at constant rate and pseudosteady state conditions (Fekete).

During depletion under constant rate and stabilized (pseudo-steady state) conditions, the pressures of every point inside the reservoir are connected to the average reservoir pressure. More specific, the pressure decay at the wellbore and the pressure decay at any location in the reservoir, as well as the reduction of the pressure at the point which depicts the average reservoir pressure, while the well is flowing, is the same.

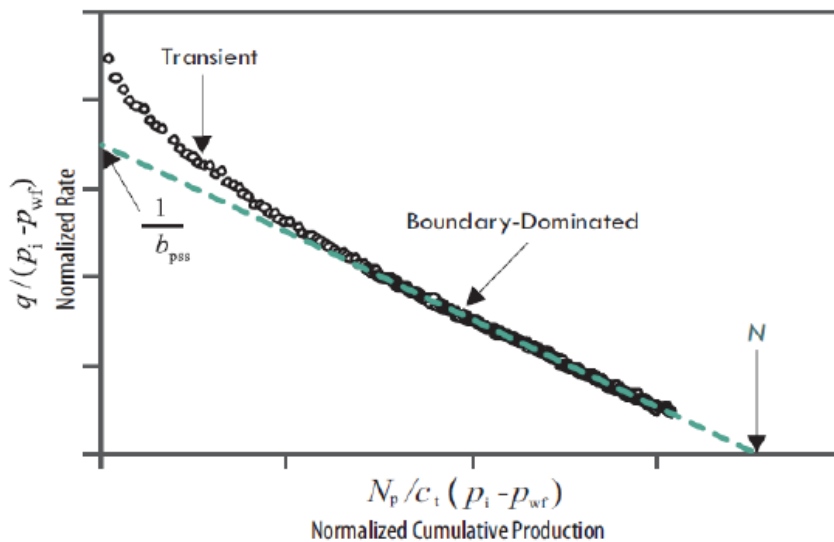


Figure 2.21: Plot of oil flowing material balance with normalized rate and cumulative production (Fekete RTA poster).

One can take advantage of this condition and present the equation in a way, that its plot would be illustrated by a straight line which could be used to compute the original hydrocarbons in place. For instance, when using the normalized rate $\left(\frac{q}{p_i - p_{wf}}\right)$ and the normalized cumulative production $\left(\frac{N_p}{c_t(p_i - p_{wf})}\right)$ of a liquid reservoir, their plot displays a straight line and the original hydrocarbons in place (N) can be calculated from the x-intercept (figure 2.21). As far as it concerns the gas production from a reservoir, a graph of normalized pseudo-pressure $\left(\frac{p_{pi} - p_{pwf}}{q}\right)$ vs. material balance pseudo-time $\left(\frac{G_{pa}}{q}\right)$, requires the calculation of pseudo-pressure and pseudo-time (figure 2.22). G_{pa} is the cumulative production which is computed based on pseudo-time, where $G_{pa} = \int_0^{t_a} q dt_a$. As it is already known, pseudo-time (t_a) is used to deal with the changing of gas properties (viscosity, compressibility), as the pressure changes. The product of gas viscosity and compressibility is a function of the reservoir size, which itself is the objective of the flowing material balance process and thus the gas flowing material balance requires an iterative approach.

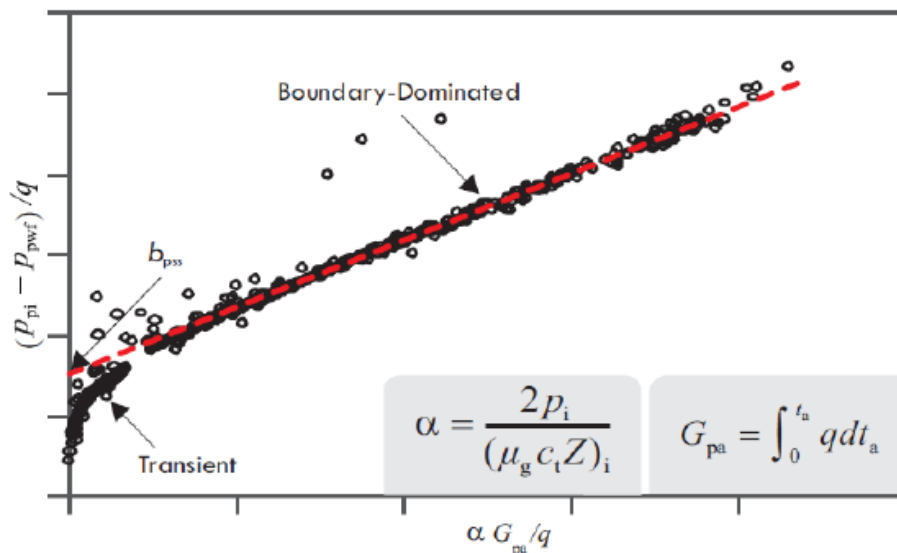


Figure 2.22: Plot of normalized pseudo-pressure vs material balance pseudo-time, for gas FMB (Fekete RTA poster).

The pseudosteady-state flow constant, b_{pss} , indicates the pressure loss corresponding to pseudo pressure due to pseudo steady-state inflow (Fekete Associates). A valid estimation of b_{pss} may be acquired by plotting the normalized pseudo-pressure against the material balance pseudo-time data. The straight line portion of this graph (figure 2.22) represents the boundary dominated flow, and the y-

intercept is the b_{pss} . The pseudosteady-state flow constant can be used to plot p/Z against G_p . If the straight line of the late times is extrapolated to zero p/Z (till y-axis) (figure 2.23), it gives the original gas in place (G).

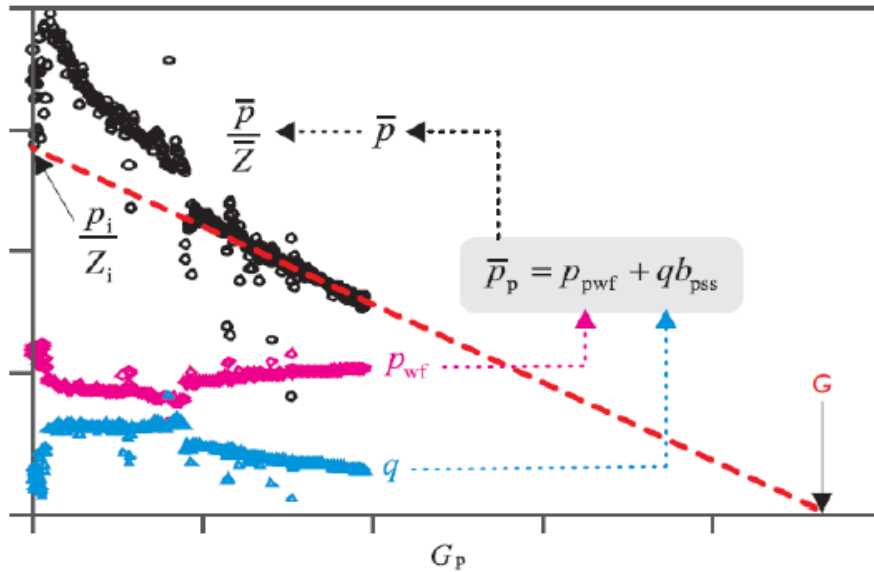


Figure 2.23: Gas flowing material balance (Fekete RTA poster).

The fact that flowing material balance has simplicity at its graphical representation, has made it widespread and acclaimed. At first this method was developed for a volumetric gas reservoir. Although it did not take into account some drive mechanisms, Moghadam et al. (2011) extended it to include all the sources of energy. These drive mechanisms are: effects of the formation compressibility, residual fluids expansion, aquifer support, connected reservoirs, or even adsorption in coal/shale. The only difference between the old and the new method is that it uses p/Z^{**} instead of p/Z (Moghadam et al. 2011).

2.3.3. Specialized plots

Some of the easiest and effortless methods which can assist in analyzing production data are the specialized plots. The common characteristic between these plots is that they are hiding a straight line which is normally used for evaluating the reservoir behaviour during a specific flow regime. Usually in unconventional reservoirs (tight and shale) specialized plots are of great significance, due to the fact that linear flow is the governing flow regime for long periods of time. According to Anderson et al. (2010) one of the most important plots is the square root-time plot, $\frac{p_{pi} - p_{pwf}}{q}$ against \sqrt{t} . It is a specialized plot and it is useful for examining linear flow and describing the (shale gas) well performance. Fractured shale gas reservoirs are particularly dominated by linear flow, but also linear flow appears straight line behaviour on the

square-root-of-time plot. From the slope fracture half-length and permeability can be computed. This way, some of the reservoir properties can be determined, just from a simple diagnostic plot. There are many applications of this method, especially for unconventional reservoirs, and this is the reason why plenty of studies and researchers are using it in their work (Ibrahim and Wattenbarger 2006, Nobakht and Clarkson 2012a, Nobakht and Mattar 2012). Each study emphasises on different details and issues. Some of them deal with the effect of skin under constant rate and constant production and its repercussions on other reservoir parameters and others with changes in reservoir properties during production. It should be also noted that another matter of special attention in these studies, is the use of pseudo-time (Shahamat, 2014).

2.4. Capacitance-resistance method for production data analysis

There are plenty of methods that can be used to analyze the reservoir behavior from a mathematical point of view. Over the years, researchers thought of approximating the flow of a fluid in a reservoir with the flow of electricity, through the electrical units. This kind of connection between petroleum engineering and electrical engineering has been used a lot for simulating and modeling the production data of reservoirs. Bruce (1943) was the pioneer of this effort when he used the terms electrical capacitance and resistance, and constructed an electrical network to simulate the fluid flow. Also, he presented functions in order to make the analogy accurate, thus he proposed the current to be equivalent to the flow of the fluid and pressure to electrical potential. Later Wahl et al. (1962) used this idea to a much larger in size resistor-capacitor network and the associated control equipment and depicted an electrical model and its application to analyze and simulate four of the most fruitful reservoirs in Saudi Arabia. They applied a trial-and-error process in which they were modifying the values of resistance and rarely of the capacitance, until the point the voltage history of each controller would match the pressure history of the well(s) it would stand for. After a lot of resistance adjustments and less in capacitance, the final model emerged, and was then used to model predictions of future reservoir and individual well performance.

Lately this method has obtained an extraordinary predilection/preference from engineers who work in the petroleum industry, due to its ability to be used for predictions by utilizing production and injection rate data to calibrate a model. The newer capacitance-resistance models are developed mostly to evaluate and predict

the performance of a waterflood (or a gas flood) and improve it, or even examine communication between wells (Sayarpour et al., 2009). To cut a long story short, CRM is based on signal-analysis methods in which the injection rates are employed as the input signals and production rates are the output signals, whereas they assumed a constant productivity index. Then they used a nonlinear multivariate regression process with connectivity indices and time constants to demonstrate reservoir and fluid properties between injectors and producers.

Moreover, there is a variety of ways that this model (CRM) could be developed. Shahamat and Aguilera (2010) proposed a new methodology which can be used in tight gas formations for the assessment of production decline analysis and material balance calculations of a single well. It is utilized in low and ultra-low permeability formations (tight/shale gas reservoirs), by solving the continuity and flow equations for these reservoirs. It consists of two separate sections. The first one is a reservoir production domain which victuals the wellbore and the second is a source segment which supplies the reservoir that communicates with the wellbore . The target is to equilibrate the rates of the two compartments, the ultra-low permeability source segment and the reservoir production domain which supplies the wellbore.

In cases of very low permeability and complex geology, such as in tight gas reservoirs, the material balance plot (p/Z vs G_p) does not provide the regular, standard single straight line trend for the determination of the original gas in place (OGIP). Instead, as the plot illustrates, in figure 2.24, there is a divergence from the ordinary straight line, resulting an unceasing increase of OGIP, maybe by two, three times or more. According to Zaitlin and Moslow (2006), this outcome is due to the dual or triple transmissivity of the system. Shahamat and Aguilera (2010) explained through the methodology (used by Pulle, 1982) they developed, by utilizing tanks, the nonlinear behaviour of the material balance plot, and created an identical material balance signature as it is depicted in figure 2.25.

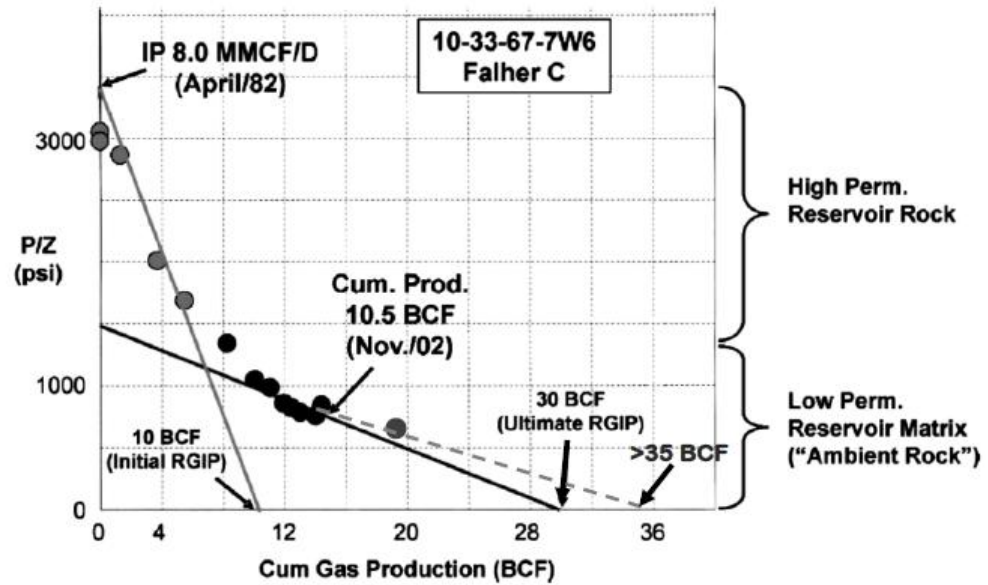


Figure 2.24: Characteristic P/Z curve depicting the dual- or tri-transmissivity nature of a Deep Basin reservoir as observed in the 10-33-67-7w6 well (Adapted from Moslow, 2005).

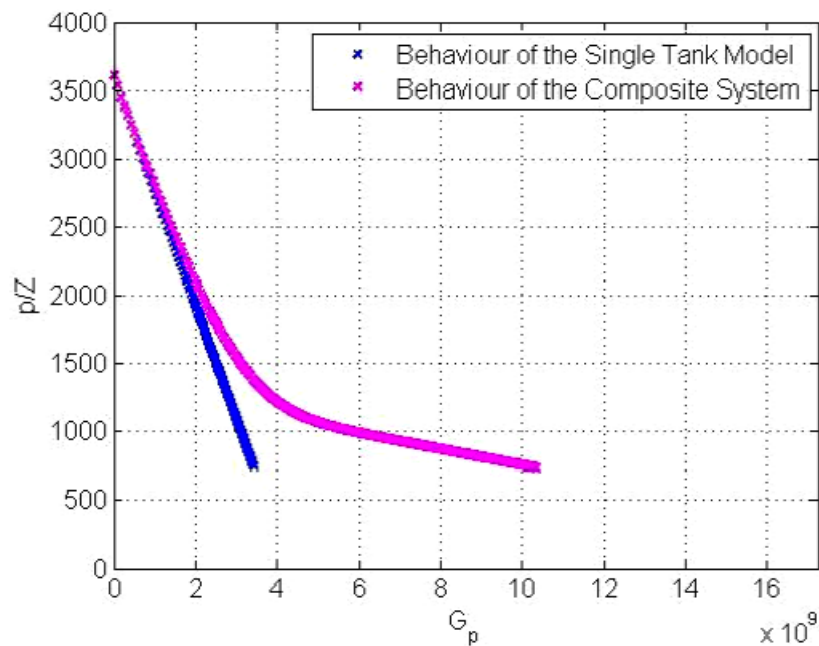


Figure 2.25: Typical plot of p/Z vs. cumulative gas production. (Source: Shahamat and Aguilera, 2010).

The methodology that Shahamat and Aguilera (2010) developed was applied to field data, which were introduced by Kupchenko et al. (2008). Gas production rate is plotted against cumulative gas production, as it is demonstrated in figure 2.25. Figure 2.26 includes data from the prediction model of Shahamat and Aguilera, which is in accordance with the real production data from the work of Kupchenko et al (2008). The gas contribution from the tight source is also displayed in the same figure.

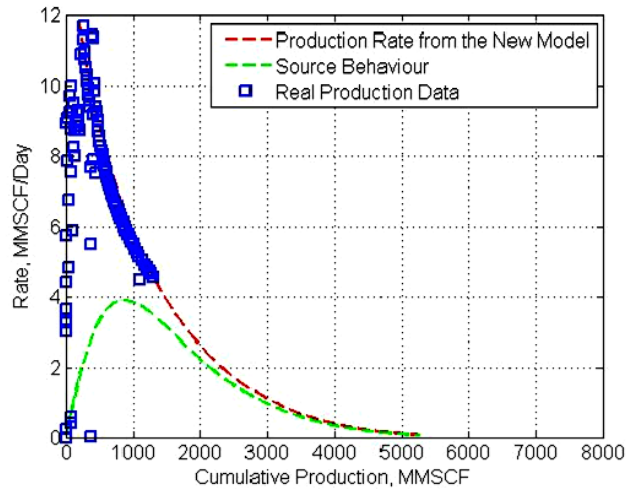


Figure 2.26: Plot of rate vs. cumulative gas production, showing Shahamat and Aguilera (2010). Blue squares are real gas rate data, brown dashed line is theoretical performance (including an excellent history match), and green dashed line is the calculated contribution from the tight or ultra-tight formation to the producing reservoir.

The correlation between flow of fluid and electricity and therefore the capacitance-resistance models (CRM) has been used for developing original methodologies in this thesis to forecast pressure and rate in fractured reservoirs with dominant transient linear flow regime and compare it with other commercial simulators. This is the subject of the next chapters in this thesis.

Chapter 3: Capacitance-Resistance Model

3.1. Equivalence between Electrical and Petroleum Engineering

Flow of fluids in a porous medium can be correlated to the flow of current through a conduit. Electric current is the movement of electric charge. According to Ohm the current (I) which travels through a conductor between two different points depends on the potential difference (ΔE) across their distance. The conventional mathematical equation which describes this relationship and it is called the Ohm's Law, $I = \Delta E/R$, and the constant of proportionality, is introduced, the electrical resistance, R . Resistance is inversely proportional to the cross-sectional area of the conductor, proportional to its length and the intrinsic properties of the conductor (resistivity).

Correspondingly, Darcy's Law, which is also known as fluid flow equation, correlates the pressure difference to the flowrate during production, in the petroleum industry. In essence, it indicates the pressure difference between average reservoir pressure (p_{avg}) and wellbore pressure (p_{wf}) to produce the so-called deliverability equation $q = \Delta P/R$, where $\Delta P = P_{avg} - P_{wf}$. It is of great importance the fact that fluid-flow equation exploits the term of average pressure. This term and its variations with time, during depletion, are very valuable for the determination of rock and fluid properties and as a result for the prediction of the reservoir performance, the economic efficiency and management. Resistance (R), by means of analogy, is a function of the properties of the reservoir, cross-sectional area (A_c) and length (L) over which the flow takes place. On the contrary, resistivity cannot be matched with another term in the petroleum field but conductivity can with the mobility ratio (k/μ). Conductivity is analogous to mobility, because as conductivity denotes the easiness of flow of current, the mobility declares the easiness of fluids flowing in the reservoir.

Apart from the resistance term, there is also the term capacitance, which is the ability of storing electric charge (store energy) at a given voltage. It is described as the ratio of the change in an electric charge (stored energy) to the potential difference (voltage, ΔE). The mathematical relationship between the current "through" a capacitance of a conductor and the rate of change of voltage over time is $I = C \frac{dE}{dt}$.

Correspondingly capacitance (or Storage Capacity) in petroleum engineering is the capability of a reservoir to provide energy (pressure). It is actually defined as the ratio

of the cumulative production of fluid to the pressure difference due to depletion. From a mathematical point of view, the product of the total compressibility ($c = -\frac{1}{V} \frac{dV}{dP}$) and the volume of the reservoir whence the production is taking place ($C = \frac{c \times V}{B}$) demonstrates the term capacitance (C). It is akin, in form of definition to the wellbore storage constant the way it was defined by van Everdingen and Hurst (1949), with the difference that the volume and compressibility of the reservoir are used instead of the volume and compressibility of the wellbore. The summation of the equivalence between the electrical and petroleum systems is delineated in table 3.1. In petroleum engineering capacitance and resistance depend on the length through V (the reservoir volume) and L, respectively. It should be stressed that f_1 and f_2 in table 3.1 are two different functions operating on the arguments inside the parentheses.

Table 3.1: Summary of analogy between flow of fluid in a porous medium and flow of electricity in an electrical conductor.

	Electrical Engineering	Petroleum Engineering
Driving force	Voltage Difference, ΔE	Pressure difference, ΔP
Flow equation	Ohm's Law, $I = \frac{\Delta E}{R}$	Fluid flow equation, $q = \Delta P / R$
Storage equation	Faraday equation	Compressibility equation
Resistance, R	$R = f_1(\text{material property}, A_c, L)$	$R = f_1(\text{fluid and rock property}, A_c, L)$
Capacitance, C	$C = I \frac{dt}{dE}$	$C = - \frac{q dt}{dp}$

This equivalence between electrical and petroleum engineering can describe production behaviour of any reservoir, during both transient flow and boundary-dominated flow (BDF) conditions. The behaviour of a liquid reservoir during BDF is simple. The reservoir has been thoroughly analyzed, the fluid properties are considered to be constant, and hence values of capacitance and resistance are fixed. On the contrary, as simple as it is to analyze the behavior of a liquid reservoir during BDF, so difficult and complicated it is to explain its behaviour during transient flow period. This happens because the signal propagates with time, so the distance of investigation changes as well. As a result variations in capacitance and resistance are produced. Assuming that the flow regime is known, during the transient flow

period the concept of continuous succession of pseudo-steady states can be used for applying the tank-type production (Shahamat, 2014).

3.2. Basic Model

Figure 3.1(a) displays the model that has been chosen to be used in this study which is the same basic reservoir model as that of Wattenbarger et al. (1998) and Nobakht et al. (2012). In this picture the top view of a rectangular reservoir is depicted, with a hydraulic fracture in the center which extends all the way to the lateral boundaries of the reservoir. The spot where the fracture is located, completely traverses the reservoir, thus at first the performance of the reservoir displays transient linear flow (perpendicular to the fracture) until the point the distance of investigation (y_{inv}) reaches the outer boundary of the reservoir in the y -direction (y_e); thenceforth, the reservoir exhibits a boundary dominated flow regime. Tight and shale reservoirs of low or ultra-low permeability usually exhibit linear flow regime for long periods of time due to production, so this geometry is possibly the most suitable for this occasion. Figure 3.1(b) also demonstrates the tank representation of the model of Figure 3.1(a). The tank representation of the model of this study that is mentioned above is illustrated in figure 3.1(b). Pressure is considered to be the same at every point inside the production tank because there is no resistance that would create a pressure difference. On the other hand, there are barriers to fluid flow from the production tank to the wellbore which are represented by the form of resistance, while the skin effect at the wellbore is supposed to be zero.

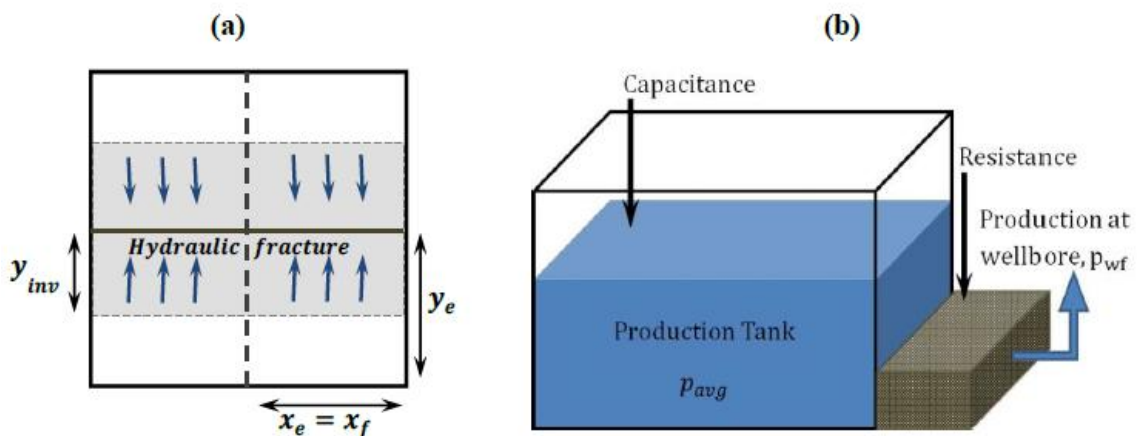


Figure 3.1: Top view of a hydraulically fractured well in a rectangular reservoir (a) and its tank representation (b).

The propagation of the pressure shock into the reservoir is represented by the area that is investigated each time and it could be calculated from the equation of distance of investigation (y_{inv}), Eq. 4. According to this equation there is an area that has been substantially disturbed by the production at the wellbore (and thus has particularly contributed), which depends on the properties of the rock, the fluids and the period of time that the flow occurred and its form is given below:

$$y_{inv} = \alpha_1 \sqrt{\frac{\beta_2 kt}{\phi \mu c}} \quad (4)$$

In this equation, k stands for the permeability in md, c is the compressibility in psia^{-1} , ϕ is the porosity, μ is the viscosity in cp and time t is in days. $\beta_2=0,00633$ and α_1 is a constant which relies not only on the criterion used for determining the distance of investigation, but also depends on the type of production at the wellbore. So Wattenbarger et al. (1998) suggested two different values for each type of production: $\alpha_1=1.42$ for constant rate and $\alpha_1=2$ for constant pressure. Nobakht and Clarkson (2012a) proposed after some years another value for this constant for constant pressure production, giving $\alpha_1=2.55$.

In this work and based on simulation studies, we use $\alpha_1=1.76$ for constant rate and $\alpha_1=2.23$ for constant pressure production. It should be noted that time t used in the equation, (4), of distance of investigation is realistic and useful only for $t < t_{BDF}$, where t_{BDF} is the time it takes the signal to arrive at the boundary. When applying this limit to the equation above, it establishes and secures that the computed distance of investigation y_{inv} in the y -direction cannot exceed the boundaries of the reservoir.

3.3. Depletion during Transient and BDF-Liquid Reservoirs

Depletion can be defined as the fall of the average reservoir pressure with time due to fluid production. The mathematical equation used so as to calculate the amount of depletion during production for a specific time interval, is the material balance equation which is written below:

$$\Delta p_{dep} = \frac{q \Delta t}{C} \quad (5)$$

In this function, C stands for the capacitance in Stb/psia and Δp_{dep} is the pressure depletion due to production for the time interval Δt .

As it has already been stated, the fluid-flow equation connects the wellbore pressure and the average reservoir pressure to the flowrate. This equation is given by the formula:

$$q = \frac{1}{R} (p_{avg} - p_{wf}) \quad (6)$$

where R stands for resistance in psia/StbD and is equal to the inverse of the productivity index (PI).

Capacitance (C) and resistance (R) in the above equations depend on the flow geometry and can be obtained analytically for simple reservoir geometries. For flow of a liquid within the reservoir geometry shown in Figure 3.1, C and R can be easily obtained as below:

$$C = \frac{4x_f ch\phi}{5.615B} \times y_{inv} \quad (7)$$

$$R = \frac{\beta_1 B\mu}{2\pi khx_f} \times (\alpha_2 \times y_{inv}) \quad (8)$$

In the equations above, $\beta_1=2\pi \times 141.2$ and α_2 is a constant given from the deliverability equation and is equal to $\frac{\pi}{6}$ for constant rate and $\frac{2}{\pi}$ for constant pressure production (Wattenbarger et al. 1998). According to the equations, both of those terms, are functions of the distance of investigation, y_{inv} , therefore the values of capacitance (C) and resistance (R) change with time. One could claim that it would be more appropriate to determine parameters (C, R) that are only connected to the reservoir characteristics and not to the type of production. Hence, two new terms were introduced capacity (C^*) and resistivity (R^*) which are determined through the equations:

$$C^* = \frac{C}{y_{inv}} \quad (9)$$

$$R^* = R / (\alpha_2 \times y_{inv}) \quad (10)$$

The two new terms that were introduced in the above equations, capacity and resistivity, in the occasion of zero skin effect, has two special benefits for production prediction. First and foremost, hydraulic diffusivity is equal to the product of capacity and resistivity, equation 11, which is a feature that controls the velocity at which the pressure signal moves through the reservoir, and it can be used to determine the distance of investigation, Eq. 4. Second advantage, is the existence of a parameter (CRR, Eq. 12), which comes when dividing the capacity with the resistivity. This

parameter is an attribute of linear flow and can be used for forecasting the performance of the reservoir. The same parameters were used from Clark (1968) and Gringarten et al. (1974) in order to compute the variations of pressure with time, when analyzing a constant rate linear flow.

$$\frac{1}{C^* \times R^*} = \frac{\pi}{2} \left(\frac{\beta_2 k}{\phi \mu c} \right) \quad (11)$$

$$CRR = \frac{C^*}{R^*} = \frac{8\pi}{5.615\beta_1} \frac{k\phi c}{\mu} \left(\frac{x_f h}{B} \right)^2 \quad (12)$$

It should be stressed out that the pressure behaviour during BDF of both types of production (constant terminal rate and constant terminal pressure) can be described by the terms capacitance and resistance. Equation 5 and the fact that both terms remain constant during BDF, leads to the conclusion that constant terminal rate for the same time intervals, causes an equivalent pressure depletion. Furthermore, according to equation 6, during constant rate production any pressure reduction at the well produces the same result (reduction) in the average reservoir pressure by the same quantity. In essence, during BDF and constant rate production wellbore pressure follows the path of the average reservoir pressure. On the contrary, this does not occur when production is under constant terminal pressure, because the stability of pressure value at the wellbore indicates that the flowrate, used for determining the depletion, is continuously dropping.

It should be pointed out that during transient flow regime the above analysis cannot be taken into account because the situation is completely different. In order to explain this flow behavior, the transient solution of the reservoir configuration shown in Figure 3.1, is used. Different equations and dimensionless parameters are used to explain this behaviour. The average pressure p_{avg} within the investigated volume is calculated by the distance of investigation equation (Eq. 4). Afterwards, the location at which the pressure is equal to the average pressure is computed by using the integral method, so Figure 3.2 is acquired. In figure 3.2 (a) it is delineated the pressure profile at three different successive times during transient flow at constant rate production with their average pressure values.

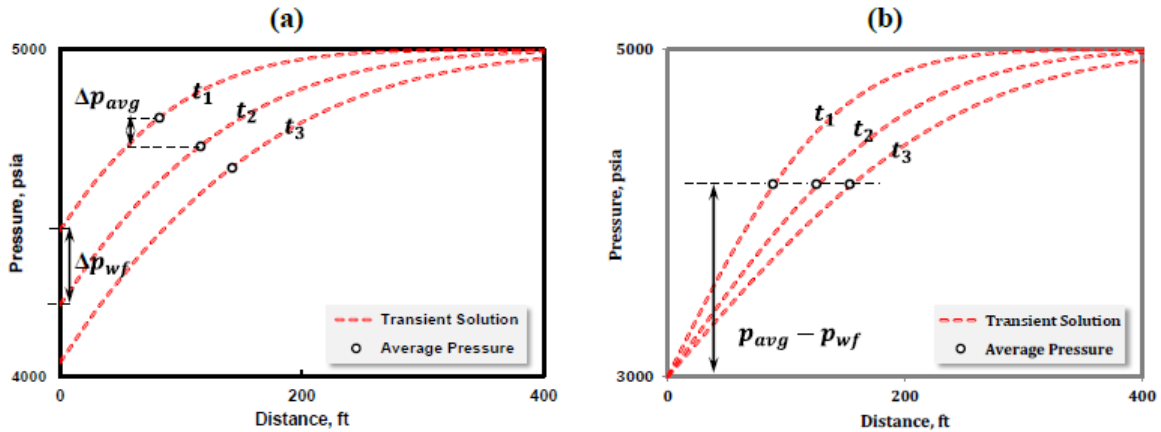


Figure 3.2: Pressure profile during transient linear flow; (a) at constant rate, (b) at constant pressure production, and the average pressure values.

When comparing the wellbore pressure and average pressure values for each time, it is crystal clear that p_{avg} and p_{wf} does not reduce by the same amount and the average pressure drop during any time period is smaller than half the pressure drop at the wellbore. This is because during the transient flow period the distance of investigation changes continuously (i.e. y_{inv}) and so does the reservoir size and it differs a lot from BDF where p_{avg} and p_{wf} follow each other

On the other hand the plot of constant pressure production of the same reservoir is a completely different case. In figure 3.2 (b) it is delineated the pressure profile at three different successive times during transient flow at constant pressure production with their average pressure values. According to the graph, during transient linear flow, the average pressure value remains constant during any time period, and it does not represent the wellbore pressure or the initial one. As a consequence, the pressure difference ($p_{avg} - p_{wf}$) is stable from t_1 to t_3 , but due to the increase of y_{inv} , the resistance raises with time and this causes the rate to fall.

Taking into account all the aforementioned, one can conclude that the distance of investigation in the calculations is important, if someone considers using the depletion equation during transient flow. Therefore, the idea of continuous succession of pseudo-steady states is introduced so as to represent the transient flow period, for both types of production, using simple depletion and resistance equations (Shahamat, 2014).

3.4. Continuous Succession of Pseudo-Steady States

Muskat (1937) suggested continuous succession of (steady) states as a process which permits the application of the simple steady-state equations that deal with time variant systems, where the time transient is of great importance in its behaviour. This process can be helpful for systems where the pressure disturbances that are transmitted through the porous medium are considered as effectively instantaneous. As a result it would be proper for the reservoir to be of a limited size, with high permeability and incompressible or slightly compressible fluids. In 2008 a new method was proposed by Whittle and Gringarten using a deconvolved derivative response in order to determine the minimum tested volume and relied on the assumption of successive pseudo-steady states. More specifically, during the transient period, the system was considered behaving like a continuously growing tank. Later Tabatabaie et al. (2013) used this methodology for determining the volume of the region of influence and utilize it to compute pseudo-time function during transient flow.

Based on this process and the electrical method that has already been mentioned, the thought of successive pseudo-steady states, in a producing reservoir under constant rate or constant pressure (p_{wf}) at transient flow period, is suggested. Thus, the continuous succession of the pseudo-steady state equations can represent the concept provided that:

- The main flow regime (e.g. linear or radial) can be reasonably approximated,
- Distance of investigation equation is used for determining the changes in capacitance and resistance,
- Based on the material balance equation production between two timesteps results in the depletion of the associated capacitance,
- Resistance, hence pressure or flowrate of the next time step are acquired from the fluid-flow equation and the reservoir pressure resulting from depletion of the capacitance at the previous time step.

The procedure consists of the stepwise coupling of the material balance equation for the investigated volume with the fluid-flow equation. It should be noted that regardless of the type of production, the depletion computations between two successive steps (t_j and t_{j+1}) are performed assuming a constant rate of production, and this is where the name pseudo-steady states comes from (Shahamat, 2014).

All the aforementioned, the equations of depletion and fluid-flow used in the CRM model, are applicable for liquid reservoirs with constant fluid properties, such as viscosity and compressibility. This method can be applied for gas if only we take into account the variations in gas properties. Gas compressibility equation is given below, Eq. 13, and is known as gas material balance equation.

$$\Delta \left(\frac{p}{Z} \right)_{dep} = \frac{q_g \Delta t}{c} \quad (13)$$

Moreover, the term of pseudo-pressure can be used for the gas fluid-flow equation as it is written below:

$$q_g = \frac{p_{p,avg} - p_{p,wf}}{R} \quad (14)$$

Where, p_p is the normalized pseudo-pressure. Equations 9 and 10 can be used for gas reservoirs in order to correlate capacitance and resistance with capacity and resistivity, respectively, the same way it is used for liquids. Hydraulic diffusivity as mentioned before is equal to the product of capacity and resistivity, and both of these terms are independent of the type of production.

It should be stressed out that in Eq. 14, pseudo-pressure is required for determining the depletion value, whereas Eq. 13 computes the depletion amount in terms of p/Z . As a result, the table of gas properties is required in order to change pressure to pseudo-pressure and to p/Z and usually linear interpolation between its entries is needed so as to compute p_p and p/Z for any pressure value.

Chapter 4: CRM Model

4.1. Implementation of the CRM

The way CRM works reminds a lot the performance of a numerical simulator. It is composed of a step-by-step depletion determination and combines it with the fluid-flow equation. After the reservoir production has started, usually flowrate and pressure data are acquired. CRM at the first time step utilizes the flowrate and wellbore pressure data, as well as other parameters, related to the properties and features of the reservoir, in order to (history) match pressures and rates and afterwards, use it to obtain the future behavior and the future production. In addition, for linear flow the parameter that is required to be aware of is the ratio of capacity to resistivity (and not both C^* and R^*), because utilization of the initial rate/pressure data, that constantly decrease, constrains the (CRM) results and as a consequence reduces the number of parameters that are needed to history match for the rest of the data. In essence, if the initial rate/pressure data are rational, then any combination of C^* and R^* giving the same CRR value, will produce an equivalent outcome. In this study the distance of investigation (y_{inv}) is considered to be $R^*=1$. This way CRM lumps all the reservoir characteristics into the ratio of capacity to resistivity (CRR). Next section marks out any approach or technique CRM needs, in order to evaluate constant rate and constant pressure production data of liquid and gas reservoirs.

4.1.1. Liquid reservoirs

The plan of action that will be followed for a liquid reservoir, producing under constant flowrate, is given below, in figure 4.1 and we will try to recreate it. To begin with, the first move is to particularize the inputs (q , CRR, t_{BDF} , p_{wf}), as illustrated in figure 4.1. Next move is to use the inverse of the product of capacity and resistivity, $\left(\frac{1}{C^* \times R^*}\right)$, in order to define the hydraulic diffusivity. After calculating the hydraulic diffusivity, the distance of investigation must be determined through Eq. 4, which is applied for each timestep until time reaches the upper limit that is for $t = t_{BDF}$, and y_{inv} takes its highest value, y_e . Fourth step is to use the values of the investigated distance, multiply each one with the capacity, for every step, in order to compute the capacitance and thereon the depletion pressure, Eq. 5. This way the initial pressure at the wellbore and the depletion pressure are known, thus can be used to compute the wellbore pressures at each timestep, in a step-by-step process.

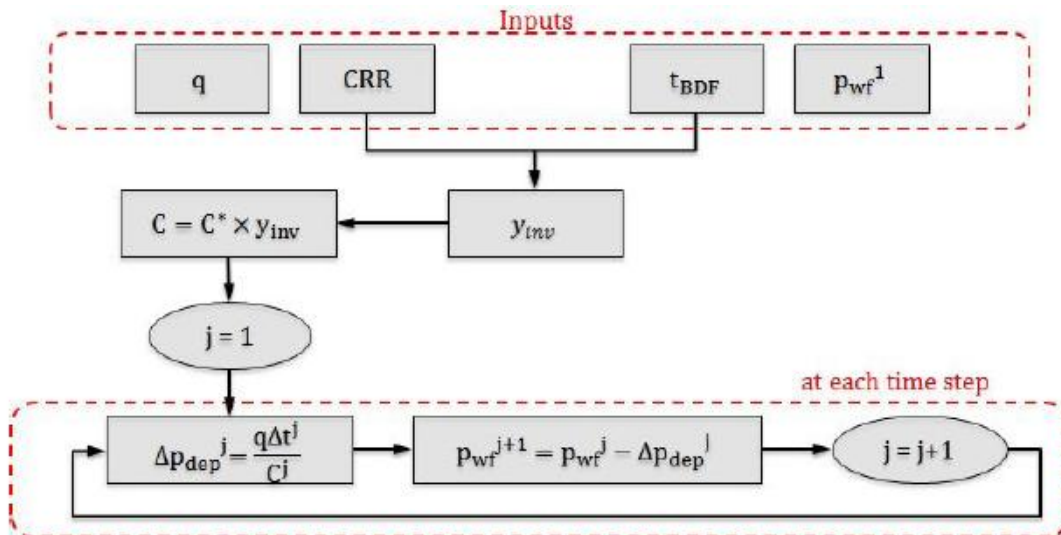


Figure 4.1: Process for applying CRM for constant rate production of liquid reservoirs (Shahamat, 2014).

The process that will be followed for a liquid reservoir, producing under constant pressure, is given below, in figure 4.2 and there is quite a resemblance to the constant rate production situation. The only dissimilarity between these two cases is that the calculated investigated distance as well as capacity and resistivity are utilized to determine the depletion pressure. By replacing the calculated pressure depletion to the material balance equation, Eq. 5, the new average pressure is obtained and subsequently the new production rates, by replacing the new average pressure to the fluid-flow equation, Eq. 6. Hence, the initial production rate is known thus can be used to compute the flowrates at each timestep, in a step-by-step process.

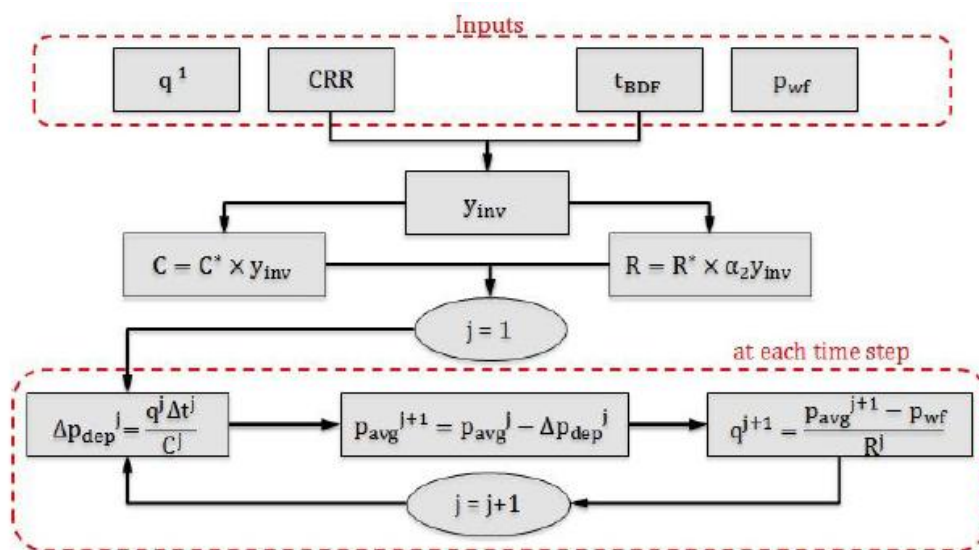


Figure 4.2: Process for applying CRM for constant pressure production of a liquid reservoir.

4.2. Validation of CRM

In this segment, the proper methodology was utilized in order to create algorithmically rate/pressure production data for both liquid and gas reservoirs. In addition, all the aforementioned processes of this chapter were applied to determine the performance of CRM when trying to history match the production data. The aim is to attain acceptable results in comparison with the results of the other proper methodologies, such as numerical and analytical solutions. As a result their agreement verifies the validness of the capacitance-resistance model.

4.2.1. Liquid reservoirs

Analytical solutions were utilized for the verification of CRM processes for liquid production reservoirs under constant flowrate and constant pressure. These solutions implicate the dimensionless diffusivity equation and different initial and boundary conditions for a finite reservoir and afterwards acquire analytically the solutions and express them in real time domain. Since the analytical solutions are valid through the whole time of production and as a consequence they include both transient and boundary-dominated flow (Shahamat, 2014).

Constant rate production of a liquid reservoir with geometry shown in Figure 3.1 gives a declining wellbore pressure whose behavior during both transient and BDF can be described using the analytical complete solution shown in Eq. 3.12. Constant pressure production of the same reservoir, on the other hand, gives a declining rate behavior that can be described using the analytical complete solution in Eq. 3.13.

$$p_D = \frac{\pi}{2} \left(\frac{t_D}{y_{eD}} \right) + \pi y_{eD} \sum_{n=1}^{\infty} \left\{ \frac{1}{(n\pi)^2} \left(1 - e^{-\left(\frac{n\pi}{y_{eD}} \right)^2 t_D} \right) \right\} \quad (15)$$

$$q_D = \frac{4}{\pi y_{eD}} \sum_{n=1}^{\infty} \left\{ e^{-\left(\frac{(2n-1)\pi}{2y_{eD}} \right)^2 t_D} \right\} \quad (16)$$

Where, p_D stands for the dimensionless pressure for producing under constant flowrate and q_D stands for the dimensionless flowrate when producing under constant pressure. Moreover, t_D and y_{eD} represent the dimensionless time and distance, respectively.

The equations 15 and 16 are used in order to provide the proper performance of a liquid reservoir when the flow is linear. As it is expressed in the above equations, with the intention of developing satisfactory results during transient flow, an infinitely

number of quantities are added (minimum 100). On the other hand, concerning boundary-dominated flow, the equations used are less complex and form the widely known equation of pseudo-steady state for constant rate production and exponential decline equation for constant wellbore pressure production.

For the constant rate production situation, the parameters in table 4.1 as well as Eq. 15, were employed to create a group of pressure data. Correspondingly, combining the same values from table 4.1 and Eq. 16 a group of data with decreasing rate can be generated, if the wellbore pressure is stable at 500 psia. Subsequently, the pressure and flowrate production data for each type of production mentioned were used to evaluate the CRM procedure.

The parameters employed in CRM for both types of production (Table 3.2(b)), constant flowrate and constant wellbore pressure, are acquired from Eq. 4 and Eq. 7 – Eq. 12 and reservoir properties defined in Table 4.1. In table 4.2 the two main parameters, capacity (C^*) and resistivity (R^*), of the CRM method are missing, but their ratio is given instead (CRR). This happens only because the analysis signifies that only their ratio parameter (CRR) is adequate for attaining acceptable results. As it is illustrated in figure 4.3, the results from the two methodologies for constant rate production are compared. The CRM results are represented by the continuous red lines and the complete solutions by the black circles.

Table 4.1: Reservoir geometry and properties used for generating the analytical solutions.

Parameters	Values
p_i , psia	5000
k , md	0.01
h , ft	100
y_e , ft	500
x_e , ft	500
x_f , ft	500
μ , cp	0.6
ϕ , fraction	0.1
B , bbl/Stb	1.0
c , psia ⁻¹	7.5×10^{-6}
s , (skin factor)	0
q , MscfD (for constant rate production)	10
p_{wf} , psia (for constant wellbore pressure production)	500

Table 4.2: Parameters used in CRM for constant rate and constant pressure production of the liquid reservoir with specified properties in Table 4.1.

Constant Rate Parameters	Values
p_{wf} , psia	4840.7
q , MscfD	10
CRR, (Mscf/psia) ² /Day	0.158
t_{BDF} , days	574
Constant Pressure Parameters	Values
p_{wf} , psia	500
q , MscfD	180
CRR, (Mscf/psia) ² /Day	0.158
t_{BDF} , days	360

According to figure 4.3 the use of the parameters depicted in Table 4.2, for the constant rate liquid production, and taking into account the plan of action delineated in figure 4.3, an almost identical fit of the analytical solution with the CRM is attained. The Cartesian plot of wellbore pressure, p_{wf} , versus time is illustrated in figure 4.3 (a) while the pressure difference ($p_i - p_{wf}$) against time is outlined in a log-log plot in figure 4.3 (b). It worths mentioning that in figure 4.3(b) there are two different straight lines of half and unity slopes. These half and unity slopes indicate the existence of the dominant flow regimes, which are linear flow and boundary-dominated flow, respectively.

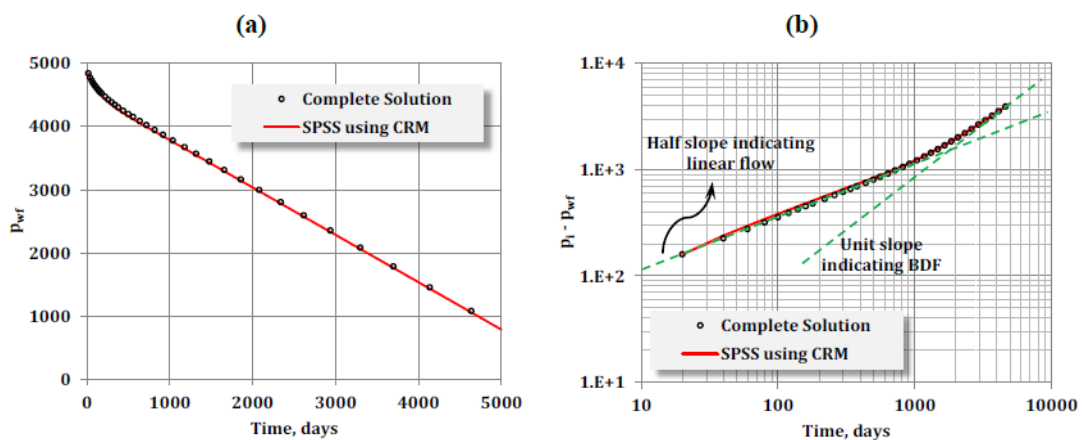


Figure 4.3: Comparison of the CRM and the complete solution for constant rate production; (a) Cartesian plot of p_{wf} versus time, (b) Loglog plot of $(p_i - p_{wf})$ versus time.

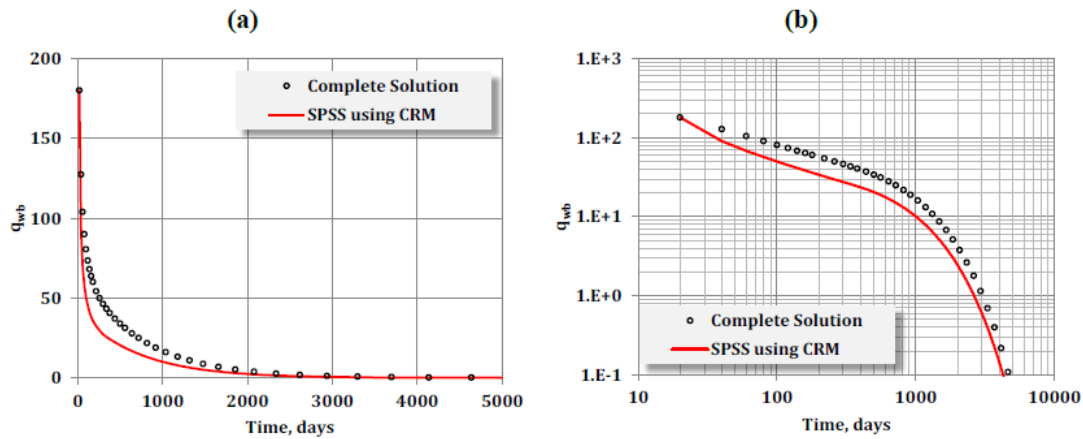


Figure 4.4: Comparison of the CRM and the analytical solution for constant p_{wf} production; (a) Cartesian and (b) loglog plot of q versus time.

As it is illustrated in figure 4.4(a) and 4.4(b), the results from the two methodologies for constant wellbore pressure production are compared. The CRM results are represented by the continuous red lines and these of the complete solution by the black circles. The computed parameters for constant wellbore pressure production used in CRM are demonstrated in table 4.2. It should be pointed out that as a consequence of using greater α_1 value in Eq. 4 for producing under constant wellbore pressure ($\alpha_1=2.23$) than under constant rate production ($\alpha_1=1.76$), the computed t_{BDF} for constant wellbore pressure is smaller than the constant rate production. This deviation shows that the propagation of the pressure shock is different in speed between the two types of production.

The Cartesian plot of the wellbore flowrate, q_{wb} , versus time is illustrated in figure 4.4 (a) and the loglog plot of flowrate versus time is depicted in figure 4.4 (b), as it was presented by Shahamat (2014), and the fit between the two curves, of the two methodologies of each plot, is not adequate. Probably due to assuming a constant rate in the CRM model, affected the production of the reservoir. When production rate is high, especially at early times, then the pressure depletion is high as well and as a consequence, the rate falls more abruptly.

In the figures below the CRM and analytical solution are illustrated the way we recreated the solutions that Shahamat proposed. First, in figure 4.1 is the comparison of the two solutions for constant rate production in a Cartesian and then in a log-log plot where the BHP is illustrated, against time when the fracture is planar to the y -direction. The two solutions do not fit exactly, probably for the same reasons mentioned before. It is possible a better match of the declining rates can be obtained by using smaller time steps for the depletion calculations.

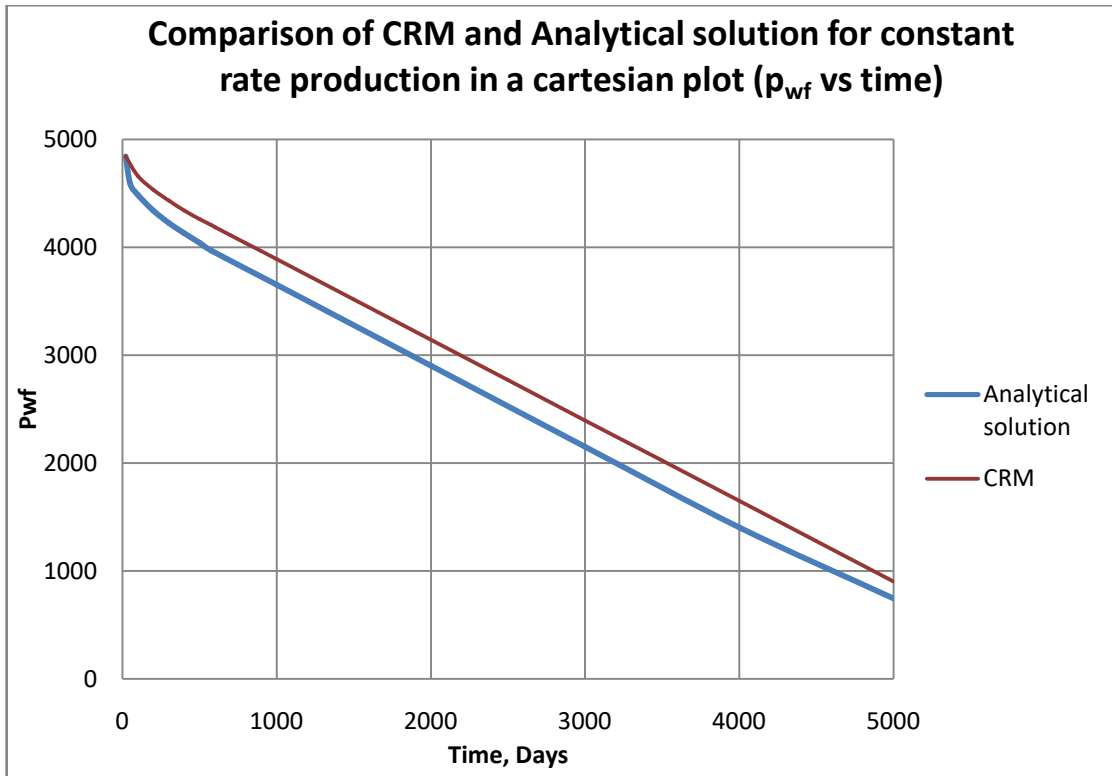


Diagram 4.1: Comparison of the CRM and the analytical solution for constant rate production; in a Cartesian of p_{wf} versus time.

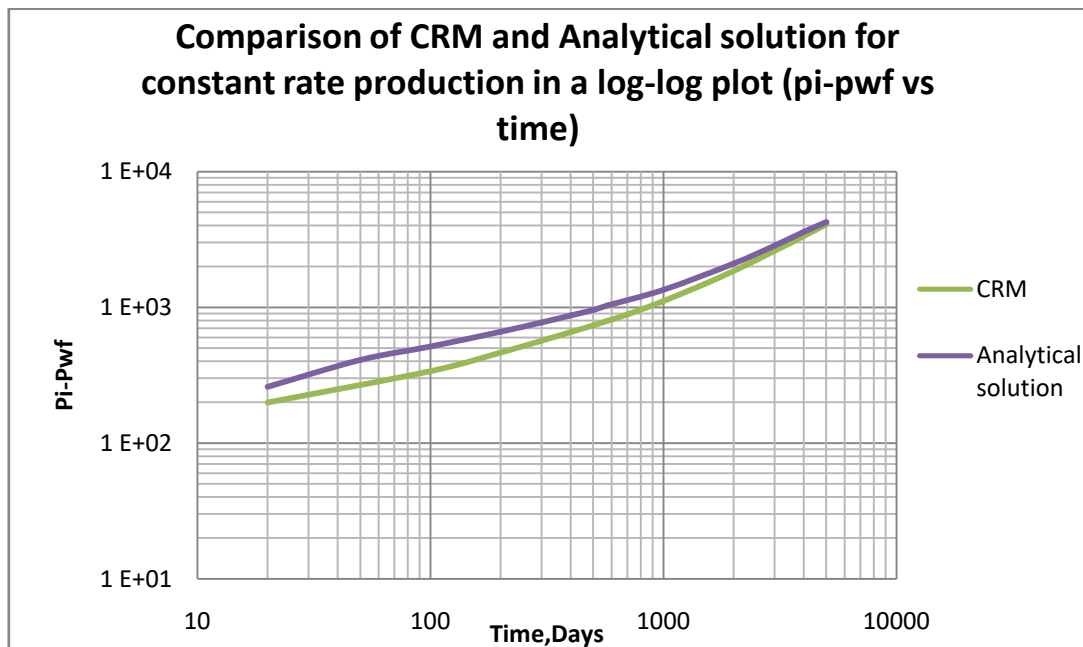


Diagram 4.2: Comparison of the CRM and the analytical solution for constant rate production; in a log-log plot of $p_i - p_{wf}$ versus time.

A better fit for the two solutions can be achieved either by utilizing smaller time steps or by using iteration on the calculated rate for the depletion calculations. In diagram 4.3 a much better match is depicted due to the smaller time steps that were used. A

fact which determines the validity of the approach. Moreover the same result may be obtained when using more iterations on the calculated rate.

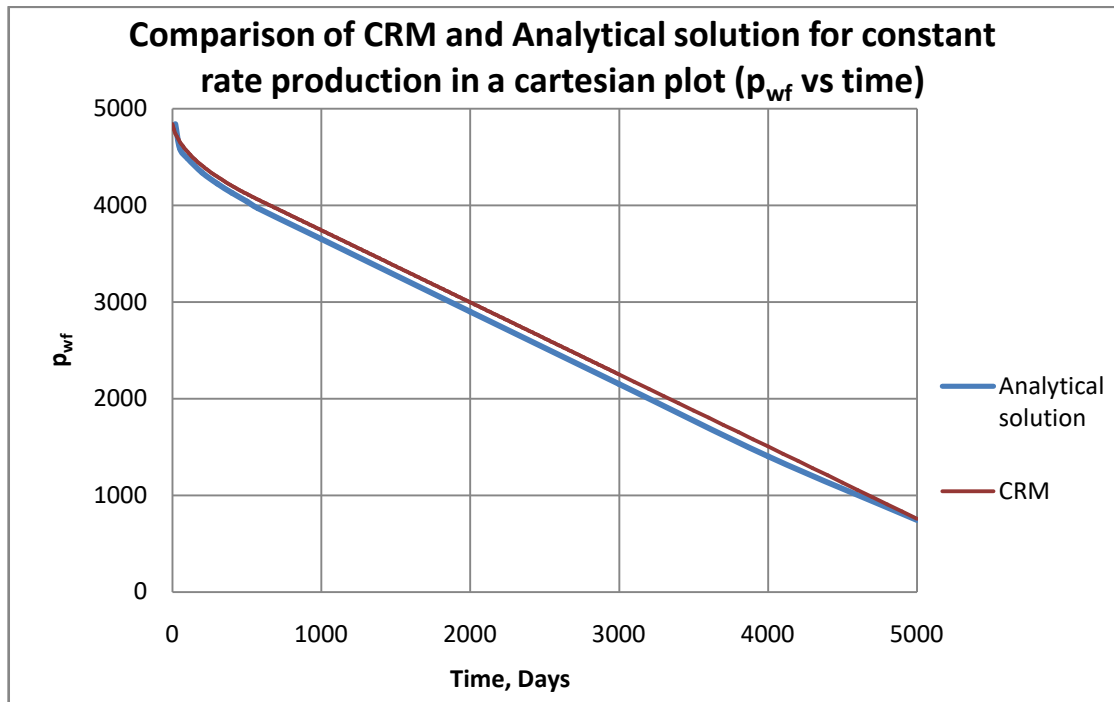


Diagram 4.3: Comparison of the CRM (with smaller timesteps) and the Analytical solution for constant rate production of p_{wf} vs time in a Cartesian plot.

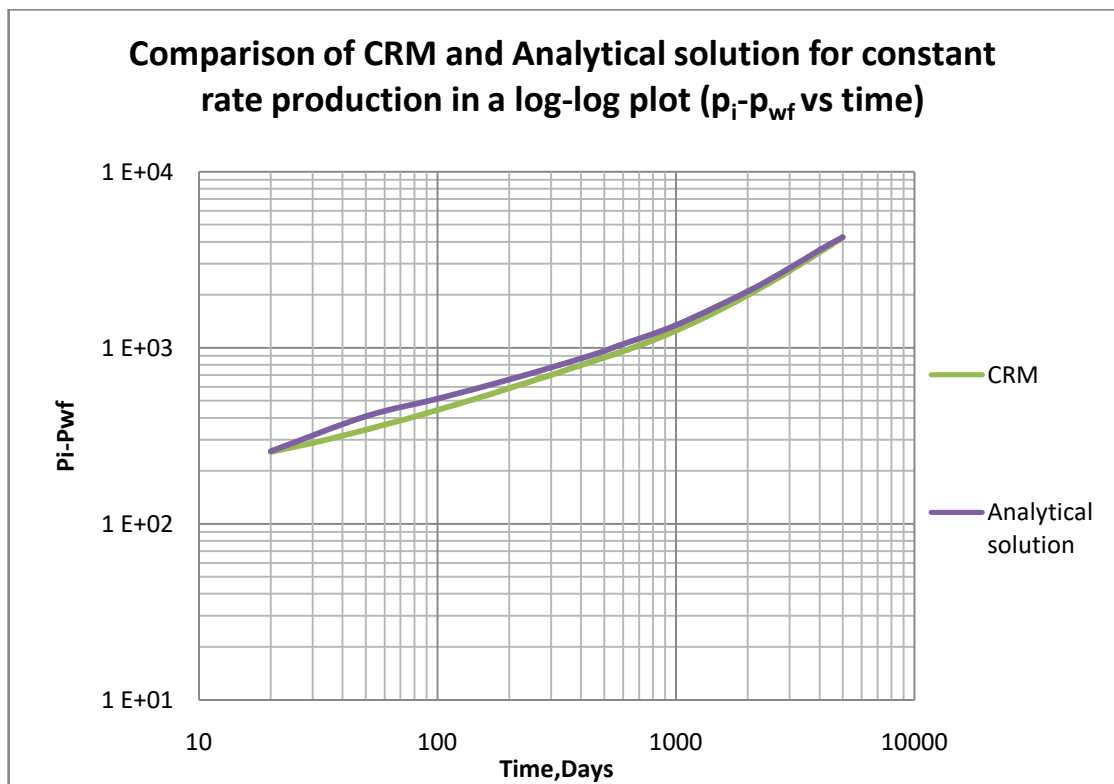


Diagram 4.4: Comparison of the CRM (with smaller timesteps) and the Analytical solution for constant rate production of $p_i - p_{wf}$ in a log-log plot.

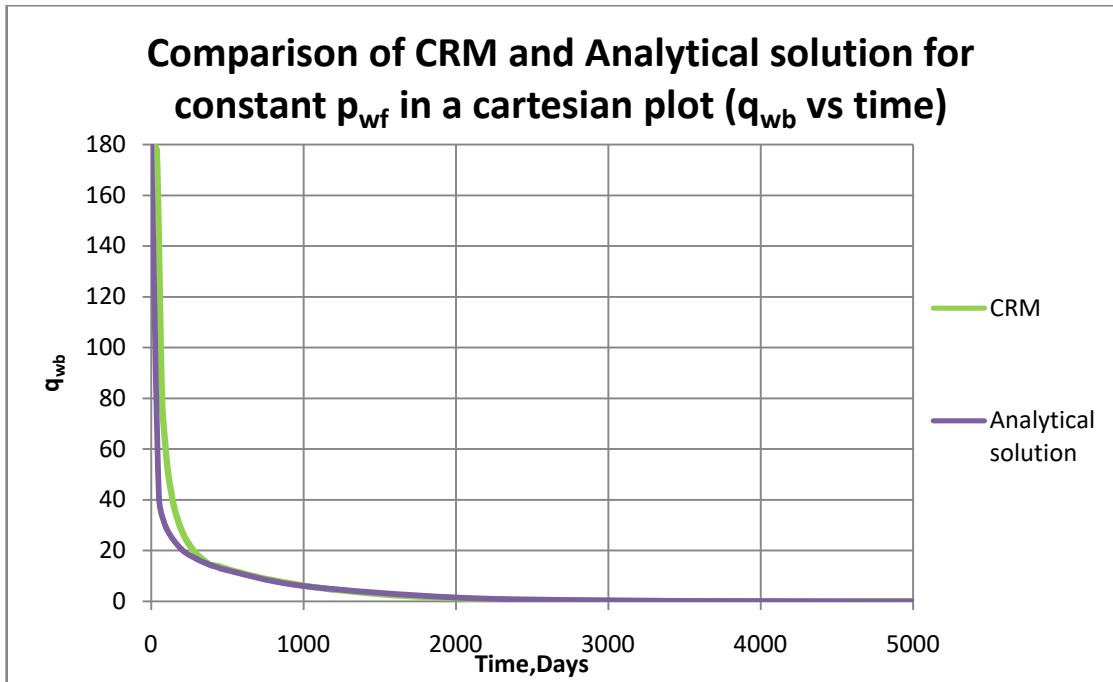


Diagram 4.5: Comparison of the CRM and the analytical solution for constant p_{wf} production; in a Cartesian plot of q versus time.

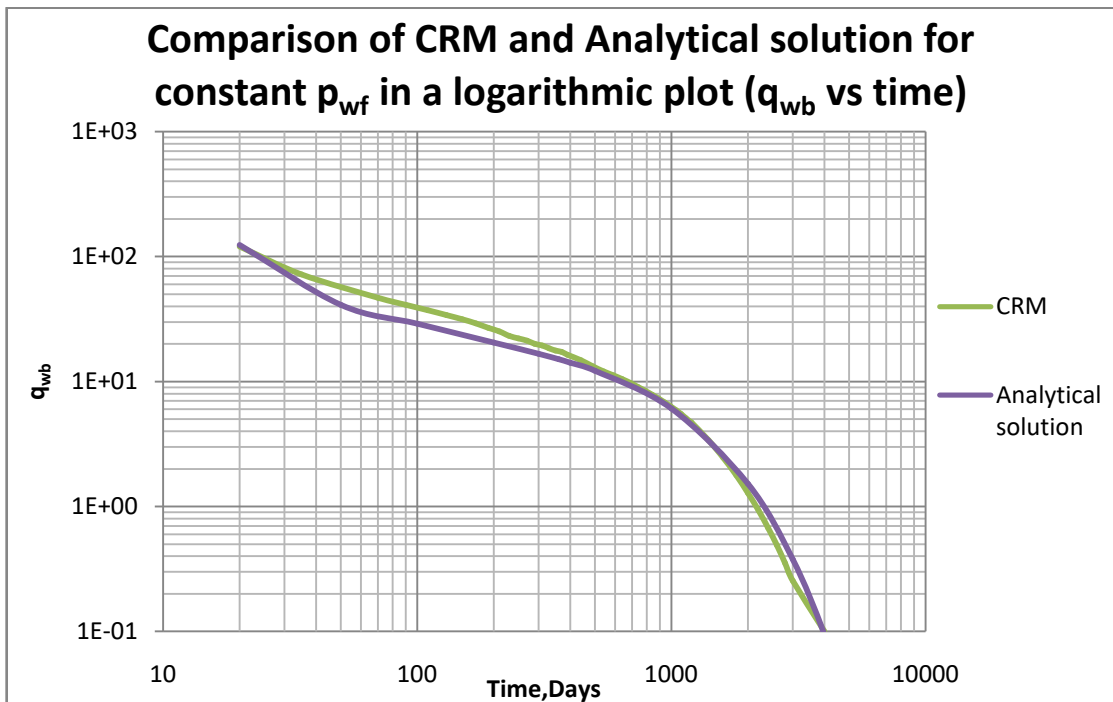


Diagram 4.6: Comparison of the CRM and the analytical solution for constant p_{wf} production; in a loglog plot of q versus time.

Chapter 5: Description of equations in ECLIPSE

The non-linear residual, R_{fl} , for each fluid component, which in our case is oil and water, in each grid block at each time step, is:

$$R_{fl} = \frac{dM}{dt} + F + Q \quad (20)$$

Where,

dM is the mass, per unit surface density, accumulated during the current time step, dt

F is the net flow rate into neighboring grid blocks

Q is the net flow rate into wells during the time step

R_{fl} is defined for each cell and each fluid in the study.

In the black oil case the fluids are oil, water and gas; in the compositional case they are the hydrocarbon components and water.

Chapter 6: Comparison of all the methods

Case 1. Vertical Fracture

The two methods were compared with numerical solutions from two different programs (ECLIPSE and IMEX). The two numerical solutions fit better with each other during the late times whereas during the early times all solutions are very close.

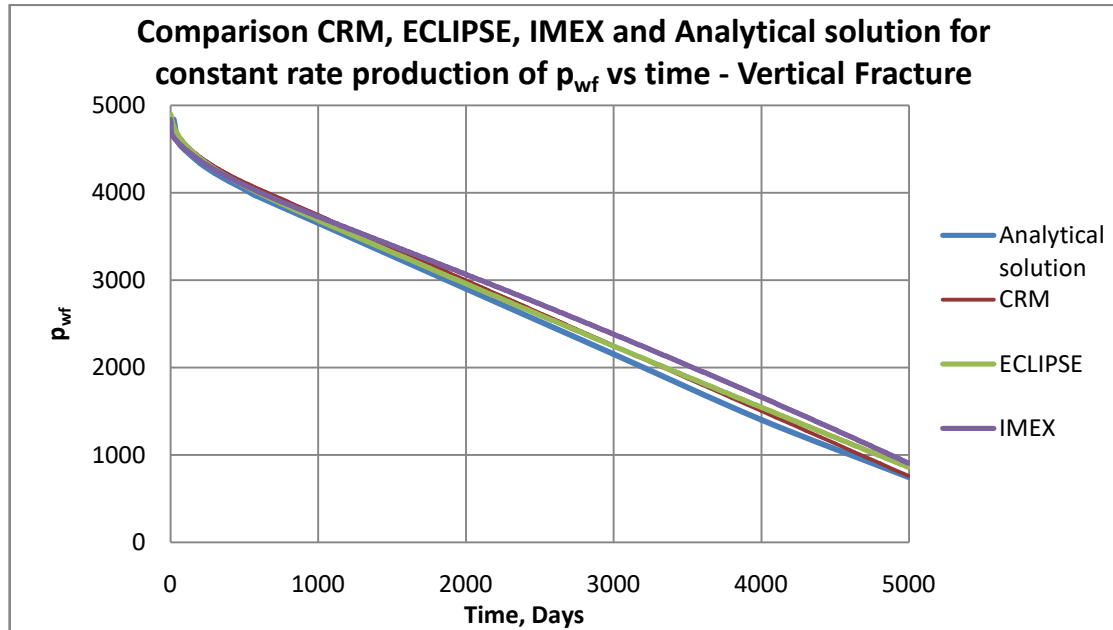


Diagram 6.1: Comparison of the CRM, ECLIPSE, IMEX and the analytical solution for constant rate production; in a Cartesian plot of p_{wf} versus time.

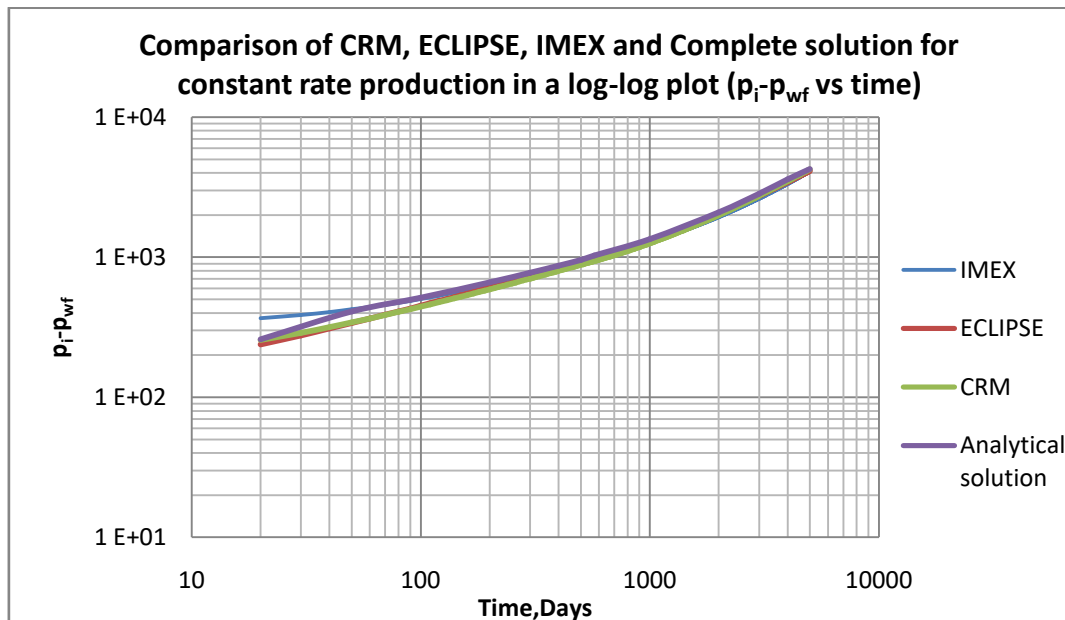


Diagram 6.2: Comparison of the CRM, ECLIPSE, IMEX and the analytical solution for constant rate production; in a loglog plot of $p_i - p_{wf}$ versus time.

In the graph above IMEX curve seems to present the higher differences during the early times.

Later, the same way for constant pressure production and a vertical planar fracture. Again CRM curve matches almost perfectly the analytical solution but they do not fit with the two numerical solutions. A fact that is also depicted in diagram 6.4.

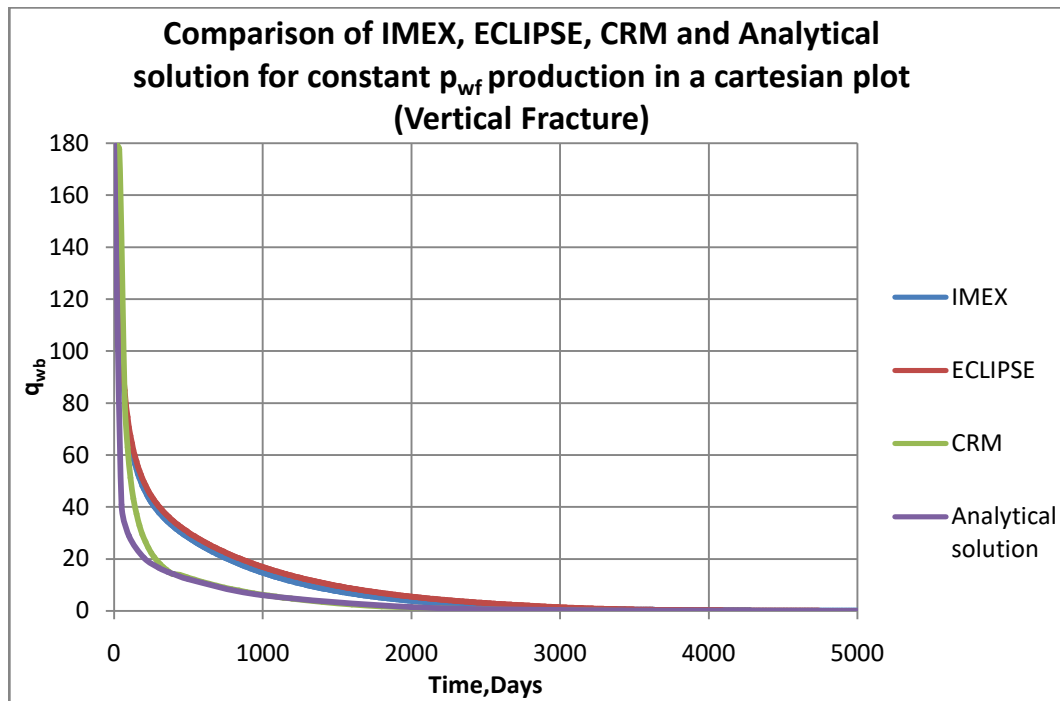


Diagram 6.3: Comparison of the CRM, ECLIPSE, IMEX and the analytical solution for constant p_{wf} production; Cartesian plot of q versus time.

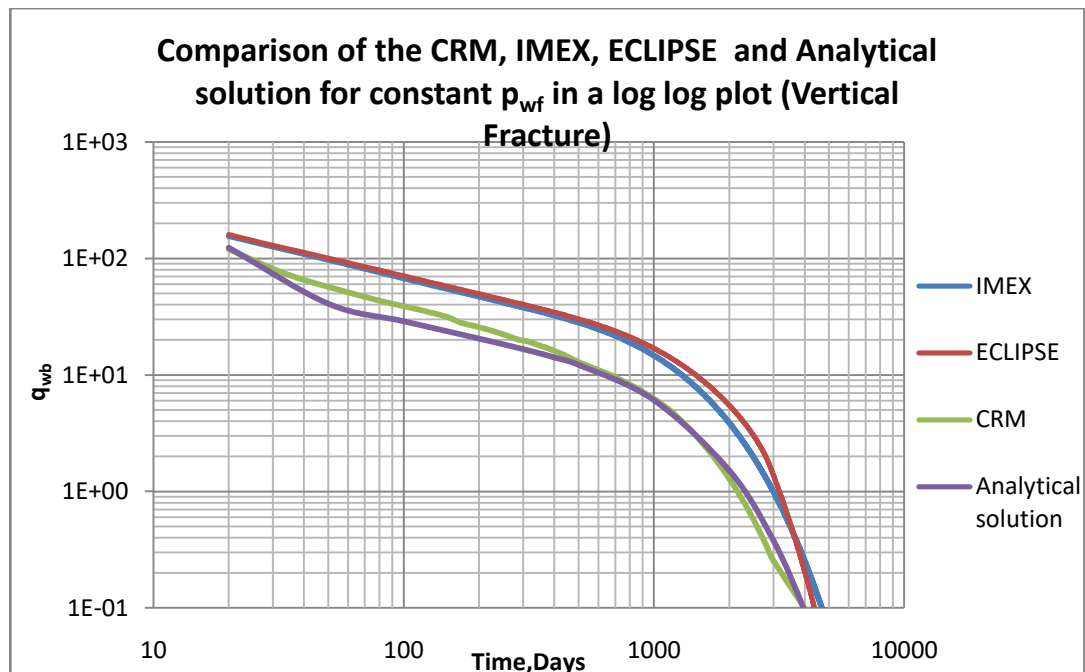


Diagram 6.4: Comparison of the CRM, ECLIPSE, IMEX and the analytical solution for constant p_{wf} production; log-log plot of q versus time.

Case 2. Horizontal Fracture

The next part includes the comparison between the four different solutions for constant rate and constant BHP production but this time the fracture of the reservoir is assumed to be horizontal. Figure 6.5 illustrates the bottomhole pressure against time. All solutions are very close, but the IMEX curve has an abrupt fall at the very beginning, which is also in agreement with the log-log plot.

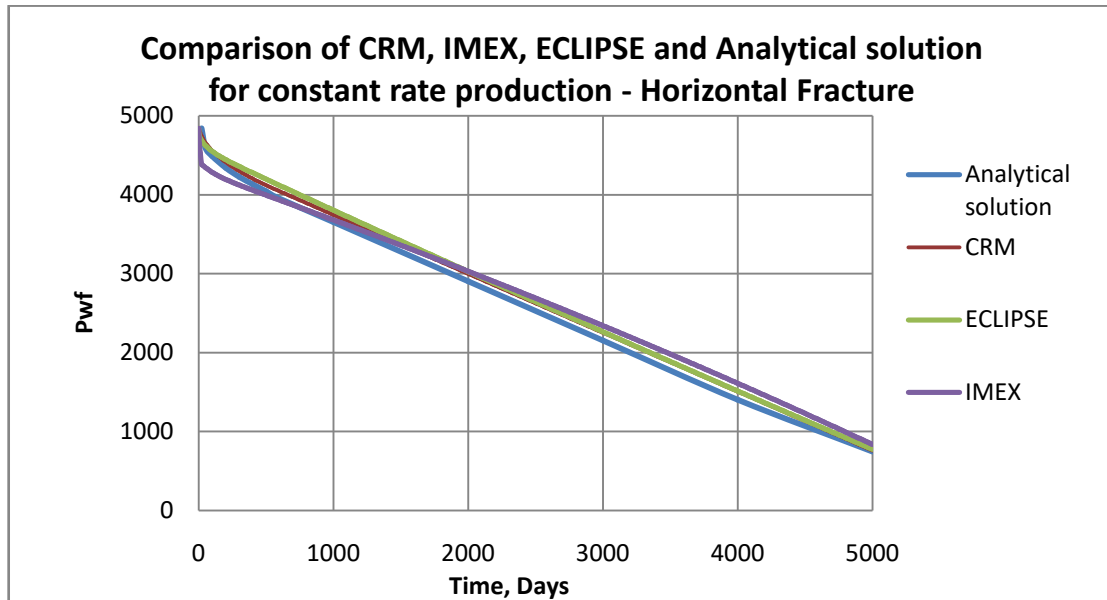


Diagram 6.5 Comparison of the CRM, ECLIPSE, IMEX and the analytical solution for constant p_{wf} production; Cartesian plot of q versus time.

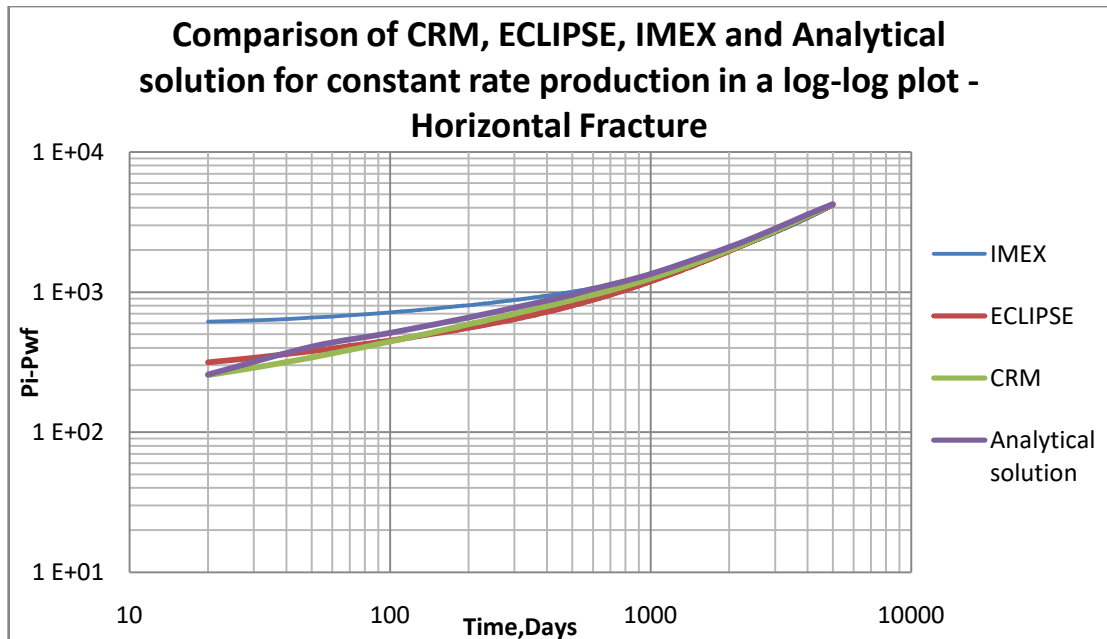


Diagram 6.6: Comparison of the CRM, ECLIPSE, IMEX and the analytical solution for constant rate production; log-log plot of $p_i - p_{wf}$ versus time.

According to diagram 6.7 the capacitance-resistance model is in great agreement with the analytical solution and the IMEX solution is very close to the ECLIPSE one, a fact that is also depicted in diagram 6.8.

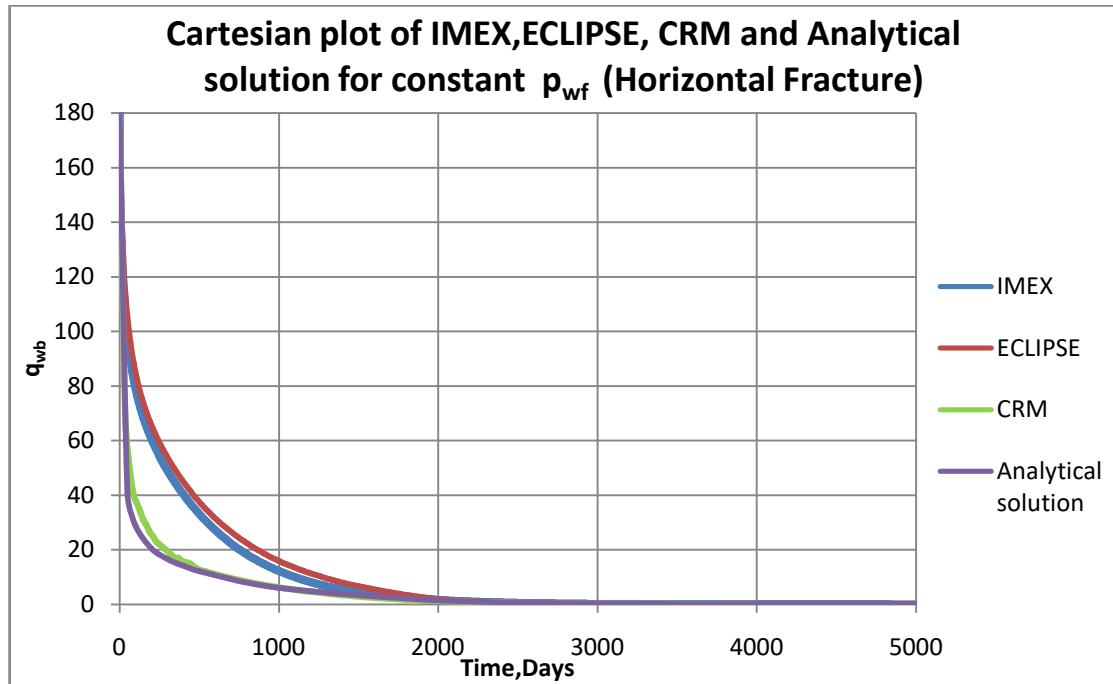


Diagram 6.7: Comparison of the CRM, ECLIPSE, IMEX and the analytical solution for constant p_{wf} production; cartesian plot of q versus time.

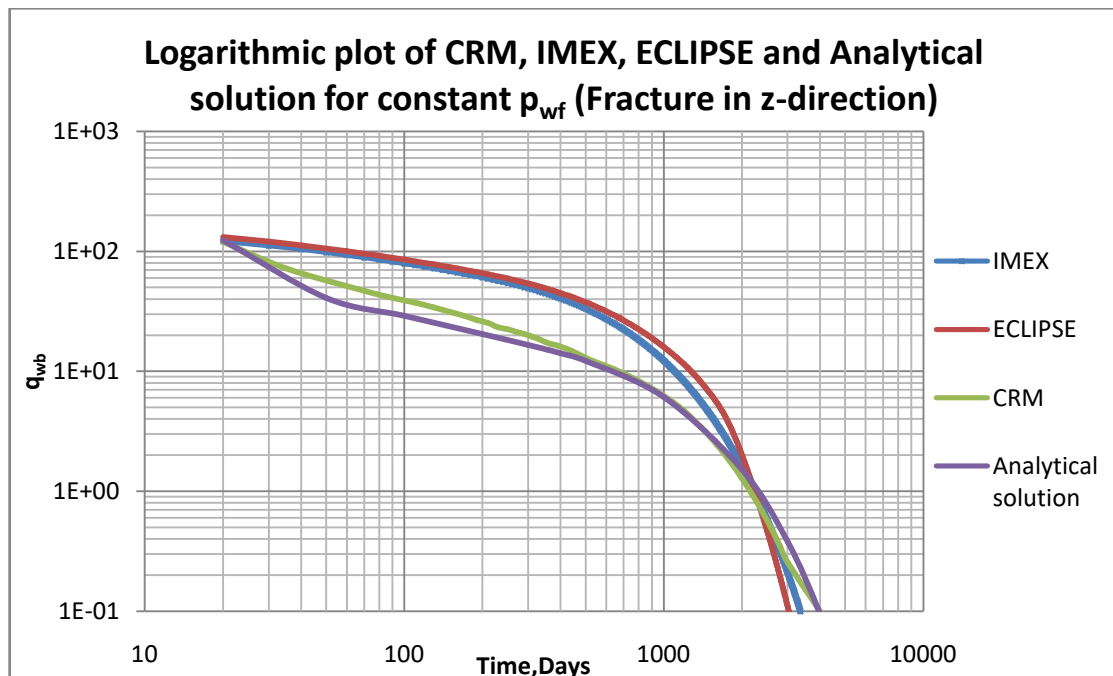


Diagram 6.8: Comparison of the CRM, ECLIPSE, IMEX and the analytical solution for constant p_{wf} production; log-log plot of q versus time.

Diagrams 6.9, 6.10 and 6.11, 6.12 display the wellbore pressure against time for constant rate production and flowrate against time for constant pressure production

for the traverse planar fracture oriented in the vertical direction, respectively, and the change of the curves when permeability is increased.

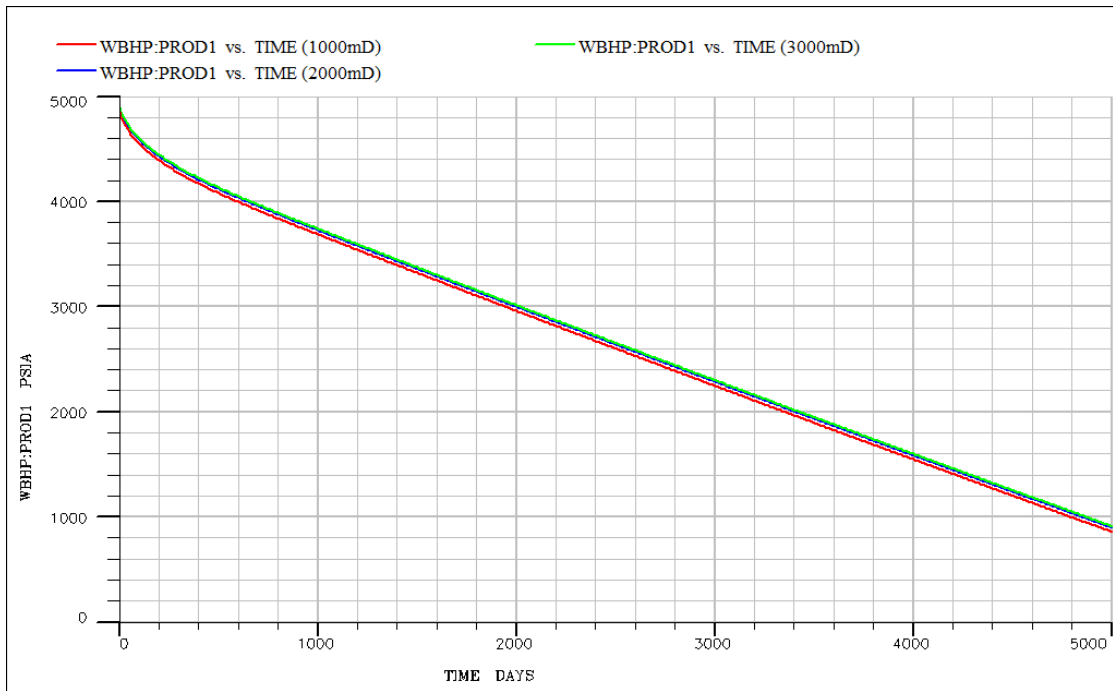


Diagram 6.9: Plot of BHP vs time for constant rate production for different permeabilities and vertical traverse fracture (1000mD, 2000m D, 3000mD).

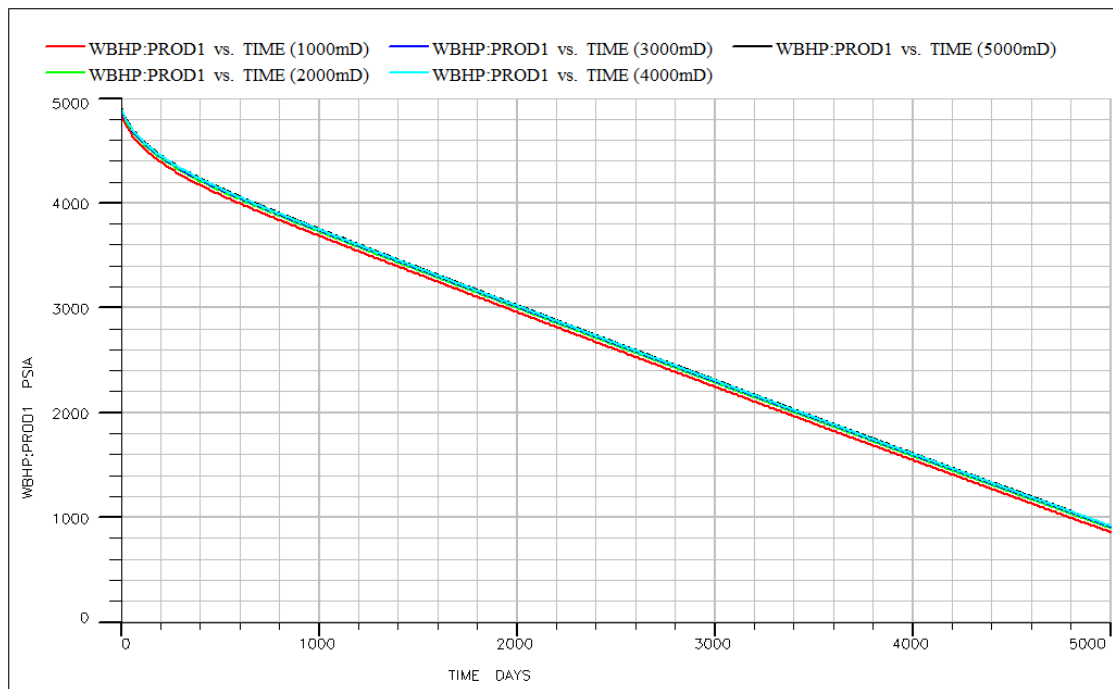


Diagram 6.10: Plot of BHP vs time for constant rate production for different permeabilities and vertical traverse fracture (1000mD-5000mD).

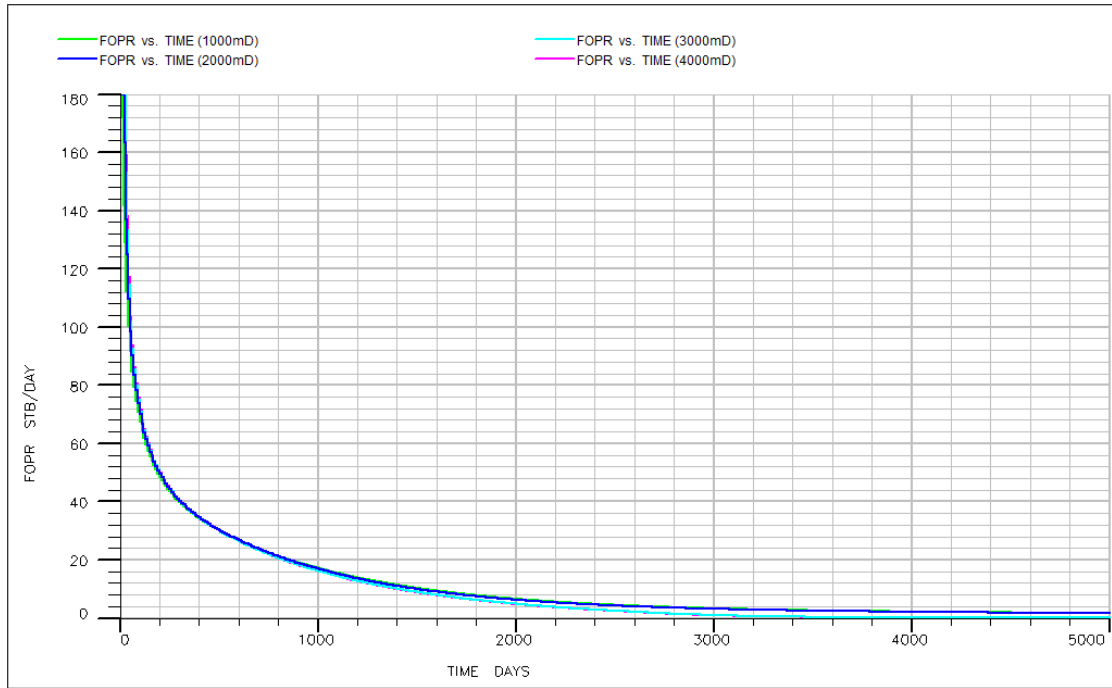


Diagram 6.11: Figure . Plot of oil rate vs time for constant pressure production for different permeabilities and vertical traverse fracture (1000mD-4000mD).

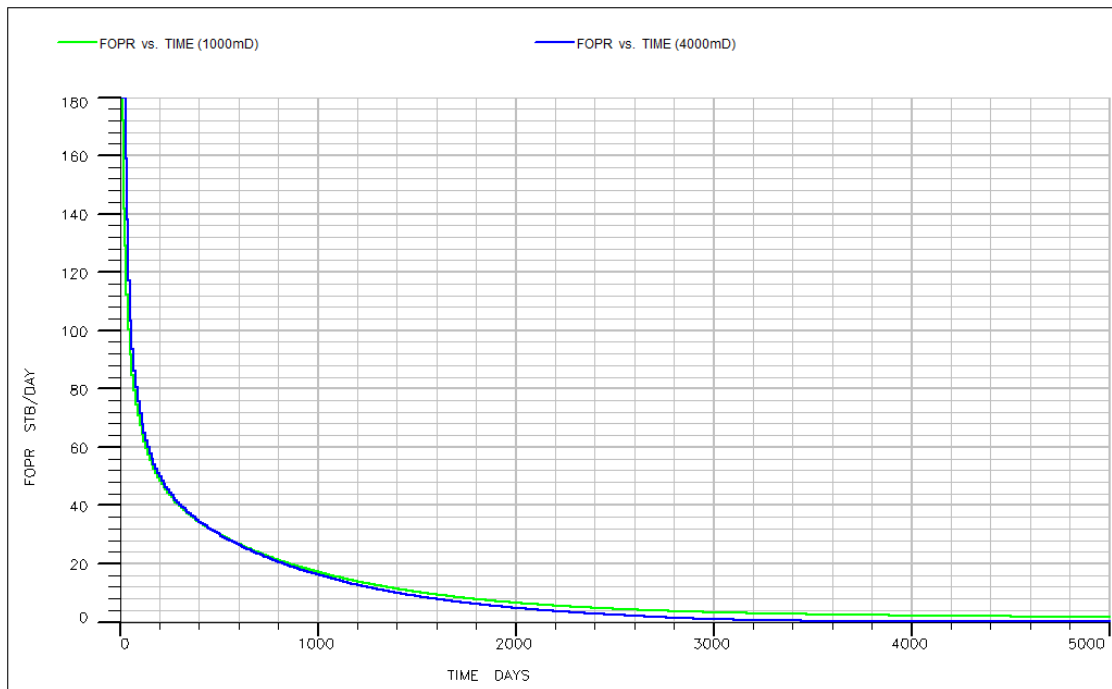


Diagram 6.12: Plot of oil rate vs time for constant pressure production for different permeabilities and vertical traverse fracture (1000mD, 4000mD).

Figures 6.13, 6.14 and 6.15, 6.16 display the wellbore pressure against time for constant rate production and flowrate against time for constant pressure production for the traverse planar fracture oriented in the horizontal direction, respectively, and the change of the curves when permeability is increased.

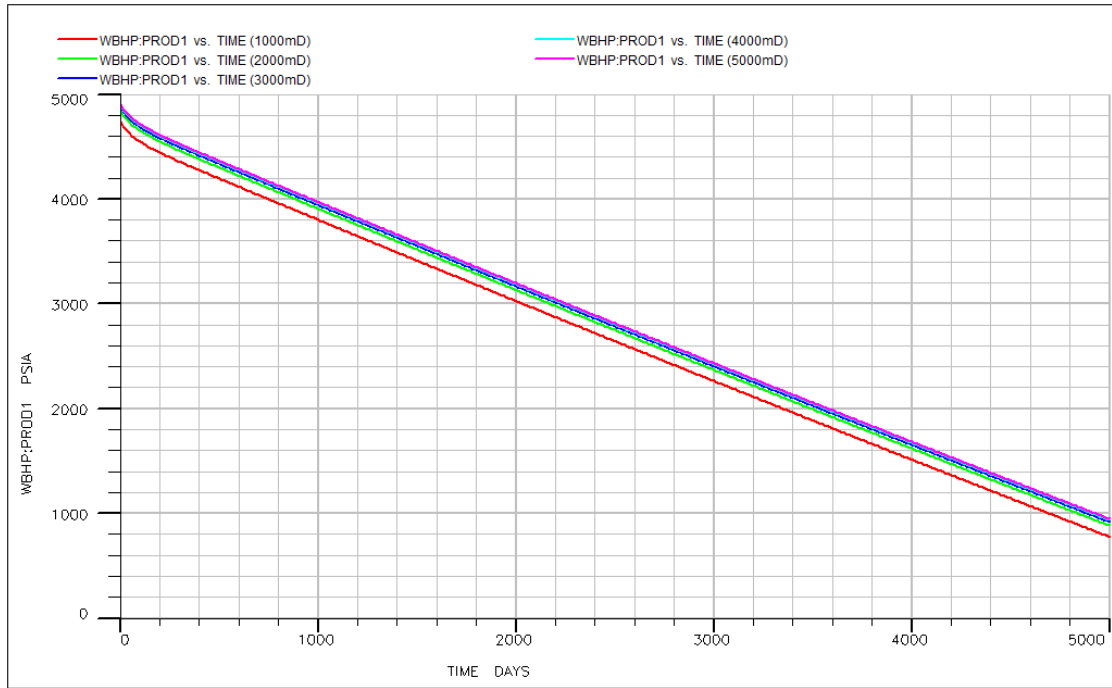


Diagram 6.13: Plot of BHP vs time for constant rate production for different permeabilities and horizontal traverse fracture (1000mD-5000mD).

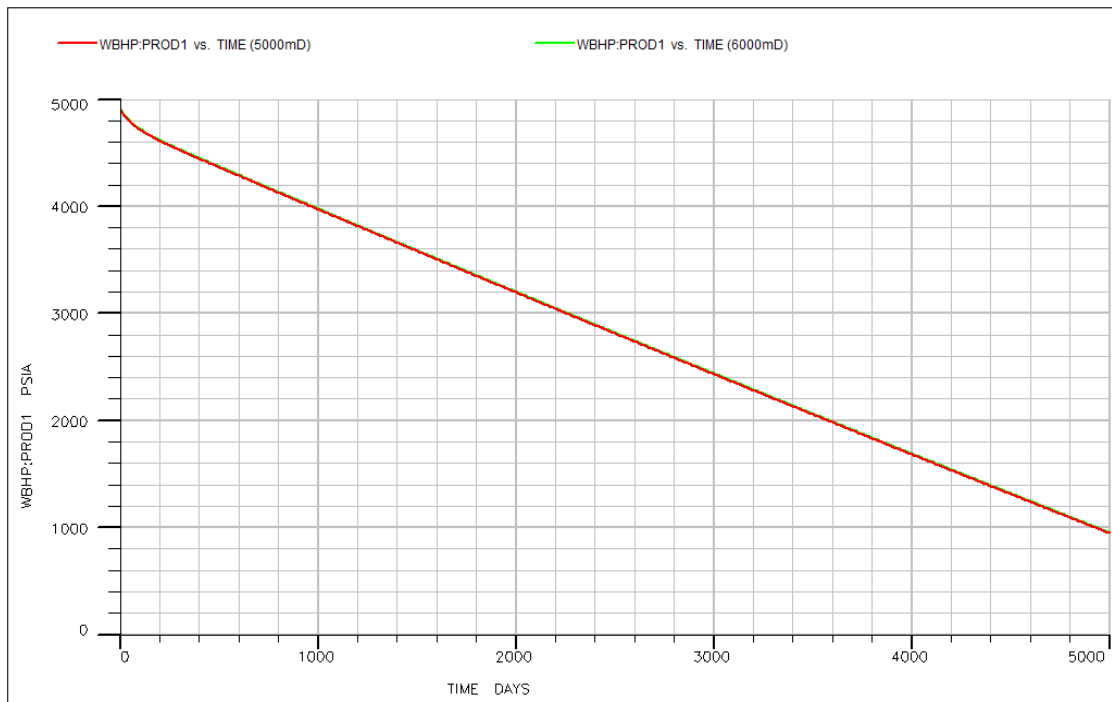


Diagram 6.14: Plot of BHP vs time for constant rate production for different permeabilities and horizontal traverse fracture (5000mD, 6000mD).

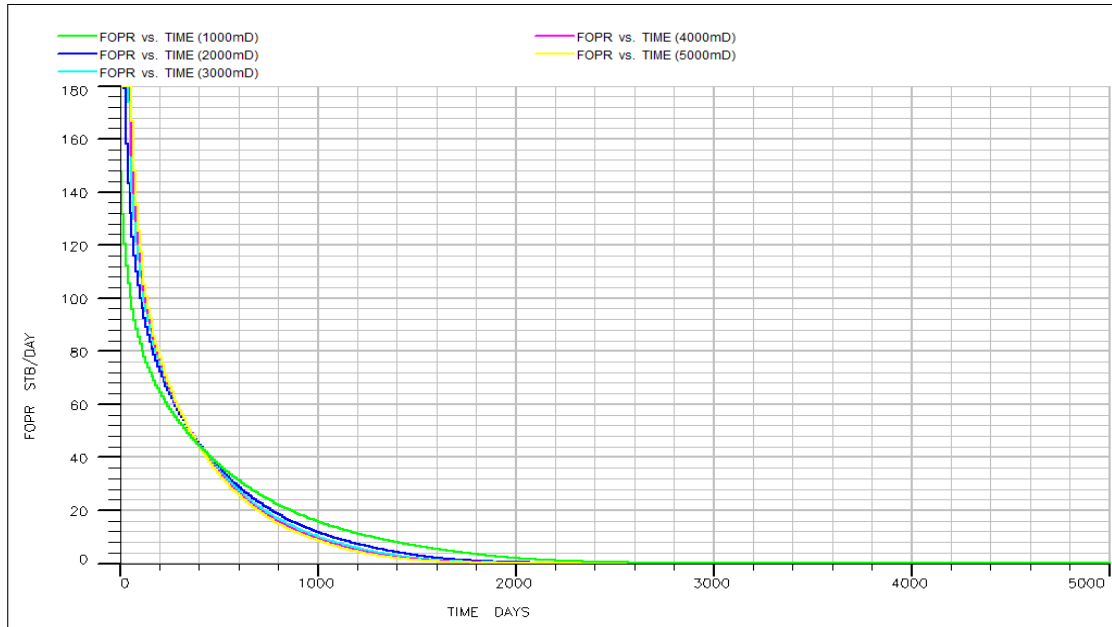


Diagram 6.15: Plot of oil rate vs time for constant pressure production for different permeabilities and horizontal traverse fracture (1000mD - 5000mD).

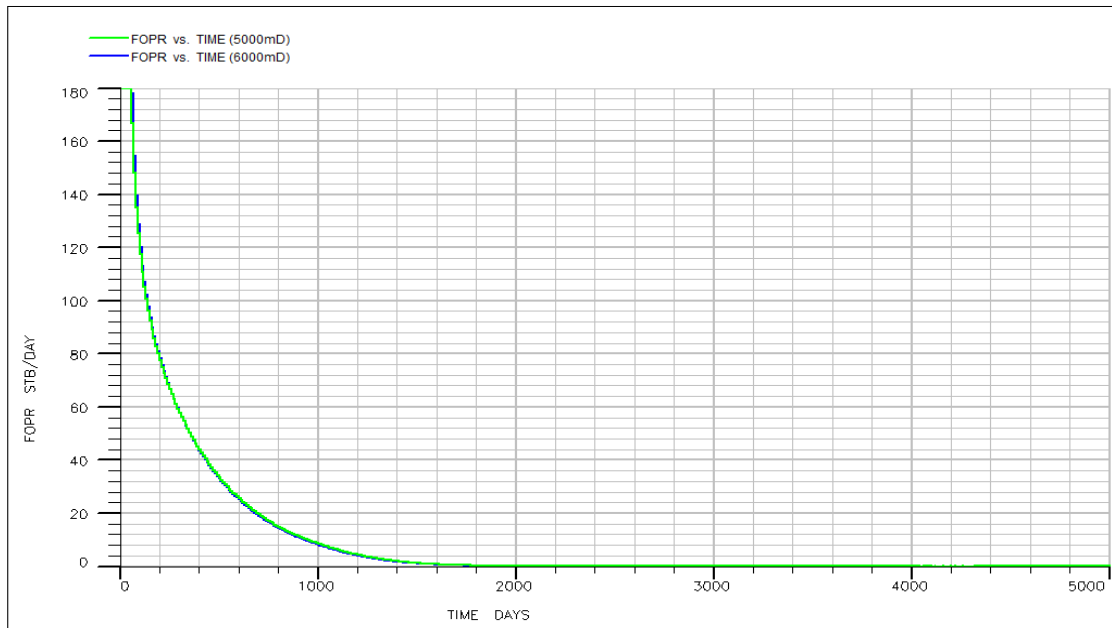


Diagram 6.16: Plot of oil rate vs time for constant pressure production for different permeabilities and horizontal traverse fracture (5000mD, 6000mD).

In diagrams for constant rate production the bottomhole pressure is plotted against time. It is obvious that as permeability gets higher and higher values, the curve is shifted upwards in a parallel way. On the other hand in diagrams for constant wellbore pressure, the oil rate is plotted against time. As permeability gets higher values, the curves of the oil rates change for every permeability value, but they are not moved upwards the way pressure curves did. It should be noted that after a certain value of permeability (close to 5000mD), no change in the diagrams is depicted.

Chapter 7: Grid sensitivity

When trying to produce the model which was proposed by Shahamat (2014) with the numerical simulator ECLIPSE 100, in order to find the appropriate solution, the effect of grid sensitivity was examined. At first I used a very small number of grid blocks (5-5-3) and I continued to increase it until the point I realized there were no differences in the results (or one can stop when there is no memory left to be occupied from the program/computer). Thus, the number of grid blocks in each direction was doubled, tripled etc. Typically, the effective grid size and grid blocks must be defined before carrying on with the simulation. The effective grid size means it is small enough to minimize errors and big enough to save computing source. The grid convergence examination should be executed before analyzing the flow behavior, so as to obtain trustworthy simulation results. The criterion is that the solution should not be thought as reliable except if it is grid independent. In essence the computer run is repeated with finer and finer grids until the results at all points in space do not change anymore.

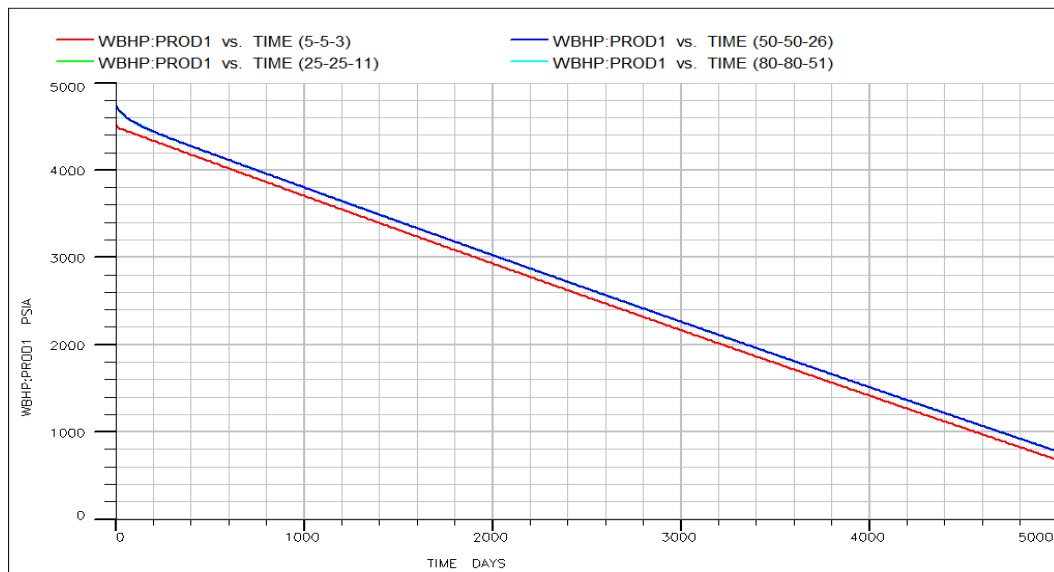


Diagram 7.1: Plot of BHP vs time for constant rate production for traverse fracture oriented in the horizontal direction and different grid sizes.

As it is depicted in diagrams 7.1, 7.2 and 7.3 there are four different grid block situations in each picture. Diagrams 7.1 and 7.2 illustrate the wellbore pressure under constant rate and the flowrate under constant pressure production for the horizontal fracture. Diagrams 7.3 and 7.4 delineate the same graphs but for a vertical fracture. As it is obvious the case with the smaller number of grid blocks has a different curve from the other three cases, while the two cases with the higher

number of grid blocks are identical and we cannot distinguish their curves because they perfectly match. As it is expected the case that was accepted between those two was the one with the finest grids (50-50-26) and (50-51-25).

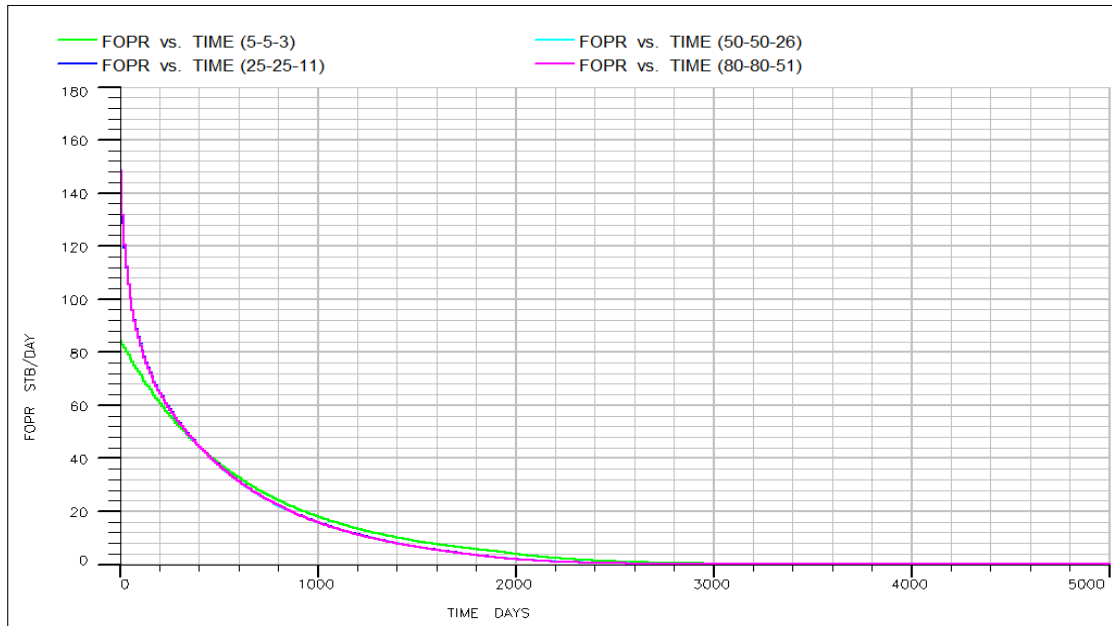


Diagram 7.2: Plot of oil rate vs time for constant pressure production for traverse fracture oriented in the horizontal direction and different grid sizes.

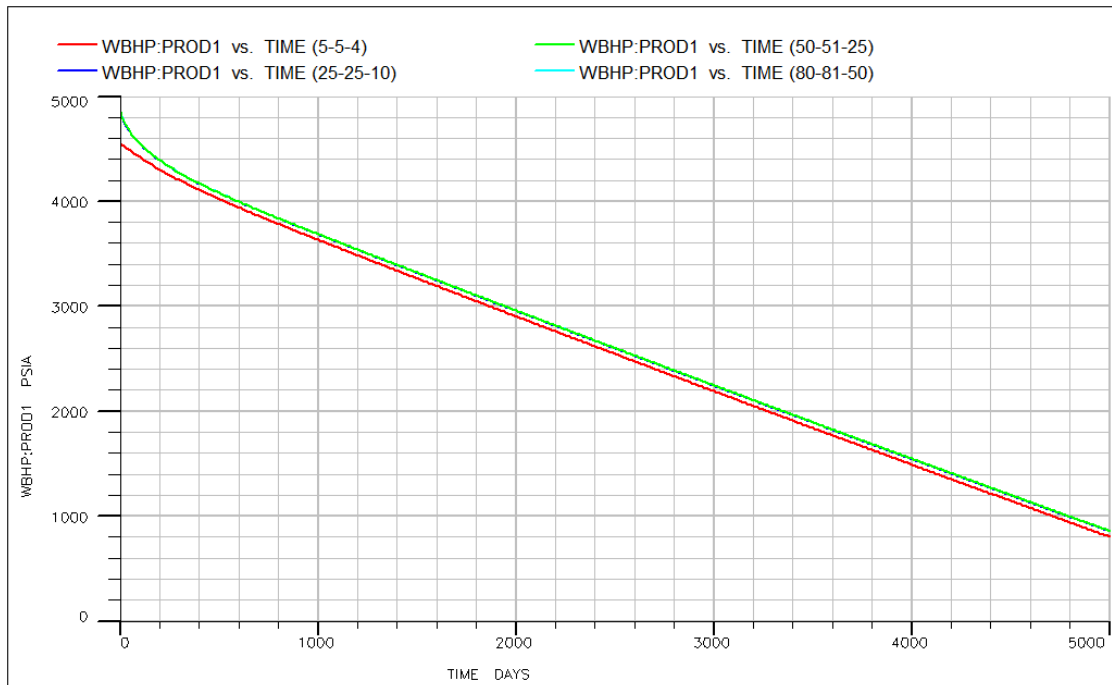


Diagram 7.3: Plot of BHP vs time for constant rate production for traverse fracture oriented in the vertical direction and different grid sizes.

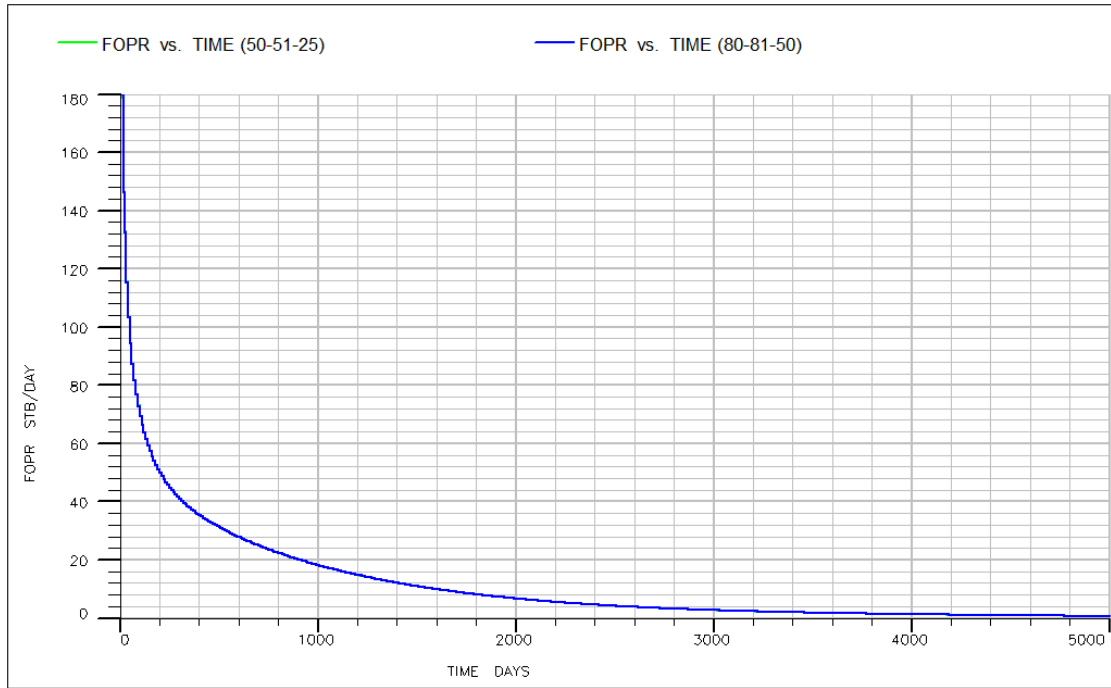


Diagram 7.4: Plot of oil rate vs time for constant pressure production for traverse fracture oriented in the vertical direction and different grid sizes.

The oil rate curves are close to each other, as well as and bottomhole pressure curves, but they are slightly deviated from each other at early times as shown in Diag. 7.1, 7.2 and 7.3. Such difference is due to the grid size as already mentioned. Diagrams 7.1 and 7.3 display the wellbore pressure against time for constant rate production and diagrams 7.2 and 7.4 illustrate the flowrate against time for constant pressure production and a traverse planar fracture, respectively, but also the change of the curves when permeability is increased.

Chapter 8: Conclusions and Summary

The purpose of this dissertation was to formulate simple and easy methods for predicting the future performance of unconventional (tight and shale) oil reservoirs with a linear flow geometry and an extended transient flow. Thus, CRM was proposed, in order to evaluate the reservoir performance fast and easy. Specifically an analogy is described between the electrical and petroleum engineering and two terms are introduced (capacitance and resistance). The procedure was comprised of simple combination of equations for material balance, distance of investigation and boundary dominated flow, utilizing the concept of continuous succession of pseudo-steady states. Afterwards the basic model is discussed, which is a rectangular homogeneous reservoir with a well placed at the center of the reservoir and a hydraulic fracture traversing it, till the boundaries. This process is used during transient and boundary dominated flow of oil reservoirs, when utilizing the distance of investigation equation.

The capacitance-resistance method is similar to the empirical methods because they both utilize minimum amount of data compared to the analytical methods. CRM utilizes the material balance equation, the same way analytical methods do, hence classical concepts are employed to demonstrate a quick, easy and less expensive methodology. This way CRM has a physical basis compared to the empirical solutions and its parameters have a physical meaning. As a result, this new methodology could be placed between the analytical and the empirical methods, utilizing the advantages of each one.

After completing the procedure of developing this new model, the obtained CRM results were compared with the analytical solutions. They were used for the verification of CRM processes for liquid reservoirs which produce under constant flowrate and constant pressure. These solutions utilized the dimensionless diffusivity equation and different initial and boundary conditions for a finite reservoir, in order to acquire analytically the solutions and express them in real time domain. Since the analytical solutions are valid through the whole time of production, they include both transient and boundary-dominated flow.

The obtained results for constant rate and constant wellbore pressure production, between the proposed model and the analytical solutions of the reservoir, were very close to each other without perfectly matching but satisfactory enough. Therefore, the suggested CRM model can be used for the future production prediction of a fractured reservoir. It should be pointed out that by obtaining only four parameters (q , p_{wf} , CRR

and t_{BDF}), and by following the CRM process step-by-step the future production can be computed, at any time step.

Subsequently the CRM and analytical solutions were compared with the results from commercial numerical simulators (ECLIPSE and IMEX) during both transient and BDF but without the assumption that properties are constant, when using the numerical simulation. Before proceeding with the simulation, the grid size had to be determined first. After several attempts with different grid sizes it was easy to conclude that for small grid blocks the error involved was very small, but when blocks were of practical sizes then the problem became significant. Thus, for very small grid blocks, the differences between the solutions were insignificant.

When proceeding with the numerical simulation, from the obtained solutions, it is obvious that the results from ECLIPSE and IMEX are in great agreement and not so close with the other two solutions. Correspondingly, as mentioned before CRM and the analytical model are in greater agreement with each other than with numerical simulation solutions. Taking into account all the aforementioned, numerical simulation can handle more complicated physical behavior of reservoirs, but requires more input data, it is a more expensive and more time-consuming process than the other two procedures. Hence, one should be aware of time, expenses and reliability of the desired results, in order to choose the most suitable model for forecasting production.

References

- Agarwal R.G., 1979. "Real Gas Pseudo-Time" A New Function for Pressure Buildup Analysis of MHF Gas Wells. Paper SPE 8279 presented at the SPE Annual Technical Conference and Exhibition, Las Vegas, Nevada, USA, 23–26 September.
- Ahmed T., Reservoir Engineering Handbook (Fourth Edition), 2010. Chapter 17 - Fractured Reservoirs, p. 1338-1432.
- Albertoni A., Lake L.W., 2003. Inferring Interwell Connectivity Only From Well-Rate Fluctuations in Waterfloods. *SPE Reservoir Evaluation & Engineering* **6** (1): 6–16. SPE-83381-PA.
- Anderson D.M., Mattar L., 2007. An Improved Pseudo-Time for Gas Reservoirs With Significant Transient Flow. *Journal of Canadian Petroleum Technology* **46** (7). PETSOC-07-07-05.
- Anderson D.M., Nobakht, M., Moghadam S., Mattar L., 2010. Analysis of Production Data From Fractured Shale Gas Wells. Paper SPE 131787 presented at the SPE Unconventional Gas Conference, Pittsburgh, Pennsylvania, USA, 23–25 February.
- Bello R.O., Wattenbarger R.A., 2010. Modelling and Analysis of Shale Gas Production With a Skin Effect. *Journal of Canadian Petroleum Technology* **49** (12): 37–48. SPE-143229-PA.
- Blasingame T.A., Lee W.J., 1986. Variable-Rate Reservoir Limits Testing. Paper SPE 15028 presented at the Permian Basin Oil and Gas Recovery Conference, Midland, Texas, USA, 13–15 March.
- Brohi I., Pooladi-Darvish M., Aguilera R., 2011. Modeling Fractured Horizontal Wells As Dual Porosity Composite Reservoirs – Application to Tight Gas, Shale Gas and Tight Oil Cases. Paper SPE 144057 presented at the SPE Western North American Region Meeting, Anchorage, Alaska, USA, 7–11 May.
- Brown M., Ozkan E., Raghavan R., Kazemi H., 2011. Practical Solutions for Pressure-Transient Responses of Fractured Horizontal Wells in Unconventional Shale Reservoirs. *SPE Reservoir Evaluation & Engineering*.
- Bruce W.A., 1943. An Electrical Device for Analyzing Oil-reservoir Behavior. *Transactions of the AIME* **151** (1): 112–124.

Carter R.D., 1985. Type Curves for Finite Radial and Linear Gas-Flow Systems: Constant-Terminal-Pressure Case. *Society of Petroleum Engineers Journal* **25** (5): 719–728. SPE-12917-PA.

Clonts M.D., Ramey H.J., 1986. Pressure Transient Analysis for Wells With Horizontal Drainholes. Paper SPE 15116 presented at the SPE California Regional Meeting, Oakland, California, 2–4 April.

Crain E.R., 2011. UNICORNS IN THE GARDEN OF GOOD AND EVIL: Part 4 - Shale Gas. *Canadian Society of Petroleum Geologists* (2): 19–22.

Dallegge T.A., Barker C.E., Geologic Assessment of Coal in the Colorado Plateau: Arizona, Colorado, New Mexico, and Utah. Chapter L, Coal-Bed Methane Gas-In-Place Resource Estimates Using Sorption Isotherms and Burial History Reconstruction: An Example from the Ferron Sandstone Member of the Mancos Shale, Utah. U.S.G.S. Professional Paper 1625–B*.

Doublet L.E., Pande P.K., McCollum T.J., Blasingame T.A., 1994. Decline Curve Analysis Using Type Curves--Analysis of Oil Well Production Data Using Material Balance Time: Application to Field Cases. Paper SPE 28688 presented at the International Petroleum Conference and Exhibition of Mexico, Veracruz, Mexico, 10–13 October.

Fraim M.L., Wattenbarger R.A., 1987. Gas Reservoir Decline-Curve Analysis Using Type Curves With Real Gas Pseudopressure and Normalized Time. *SPE Formation Evaluation* **2** (4): 671–682. SPE-14238-PA.

Gao C., Lee W.J., Spivey J.P., Semmelbeck M.E., 1994. Modeling Multilayer Gas Reservoirs Including Sorption Effects. Paper SPE 29173 presented at the SPE Eastern Regional Meeting, Charleston, West Virginia, 8–10 November.

Gringarten A.C., Ramey H.J., 1974. Unsteady-State Pressure Distributions Created by a Well With a Single Horizontal Fracture, Partial Penetration, or Restricted Entry. *Society of Petroleum Engineers Journal* **14** (4): 413–426. SPE-3819-PA.

Holditch, S.A. 2006. Tight Gas Sands. *Journal of Petroleum Technology* **58** (6): 86–93. SPE-103356-MS.

Khoshghadam M., Khanal A., Lee J., 2015. Numerical Study of Production Mechanisms and Gas-Oil Ratio Behavior of Liquid-Rich Shale Oil Reservoirs. SPE Annual Technical Conference and Exhibition, September 2015.

King G.E., 2010. Thirty Years of Gas Shale Fracturing: What Have We Learned? Paper SPE 133456 presented at the SPE Annual Technical Conference and Exhibition, Florence, Italy, 19–22 September.

Maugeri L., 2013. The Shale Oil Boom: A U.S. Phenomenon. Report No. 2013-05, Belfer Center for Science and International Affairs, Harvard Kennedy School (June).

Moghadam S., Jeje O., Mattar L., 2011. Advanced Gas Material Balance in Simplified Format. *Journal of Canadian Petroleum Technology* **50** (1): 90–98. SPE-139428-PA.

Muskat, M. 1937. *The Flow of Homogeneous Fluids Through Porous Media*. New York, McGraw-Hill Book Co.

Passey Q.R., Creaney S., Kulla J.B., Moretti F.J., Stroud J.D., 1990. A Practical Model for Organic Richness from Porosity and Resistivity Logs. *AAPG Bulletin* **74** (12): 1777–1794.

Ruppel S.C., Loucks R.G., 2008. Black Mudrocks: Lessons and Questions from the Mississippian Barnett Shale in the Southern Midcontinent. *The Sedimentary Record* **6** (2).

Shahamat M.S., Aguilera R., 2010. A New Method for Production Decline Analysis of Tight Gas Formations. Paper SPE 138149 presented at the Canadian Unconventional Resources and International Petroleum Conference, Calgary, Alberta, Canada, 19–21 October.

Shahamat M.S., Mattar L., Aguilera R., 2014. A Physics-Based Method for Production Data Analysis of Tight and Shale Petroleum Reservoirs Using Succession of Pseudo-Steady States. Paper SPE 167686 presented at the SPE/EAGE European Unconventional Resources Conference and Exhibition, Vienna, Austria, 25–27 February.

Shahamat M.S., 2014. Production Data Analysis of Tight and Shale Reservoirs, May 2014.

Stalgorova E., Mattar L., 2013. Analytical Model for Unconventional Multifractured Composite Systems. *SPE Reservoir Evaluation & Engineering* **16** (3): 246–256. SPE-162516-PA.

Tabatabaie S.H., Pooladi-Darvish M., Mattar L., 2013. Pseudotime Calculation in Low Permeability Gas Reservoirs. Paper SPE 167185 presented at the SPE Unconventional Resources Conference, Calgary, Alberta, Canada, 5–7 November.

Thompson L.G., Manrique J.L., Jelmert T.A., 1991. Efficient Algorithms for Computing the Bounded Reservoir Horizontal Well Pressure Response. Paper SPE 21827 presented at the Low Permeability Reservoirs Symposium, Denver, Colorado, 15–17 April.

Varma A. K., Hazra B., Srivastava A., Estimation of Total Organic Carbon in shales through color manifestations, 2014. *Journal of Natural Gas Science and Engineering*, 53-57.

Wahl W.L., Mullins L.D., Barham R.H., Bartlett W.R., 1962. Matching the Performance of Saudi Arabian Oil Fields With an Electrical Model. *Journal of Petroleum Technology* 14 (11): 1275–1282.

Wattenbarger R.A., El-Banbi A.H., Villegas M.E., Maggard J.B., 1998. Production Analysis of Linear Flow Into Fractured Tight Gas Wells. Paper SPE 39931 presented at the SPE Rocky Mountain Regional/Low-Permeability Reservoirs Symposium, Denver, Colorado, USA, 5–8 April.

Whittle T.M., Gringarten A.C., 2008. The Determination of Minimum Tested Volume From the Deconvolution of Well Test Pressure Transients. Paper SPE 116575 presented at the SPE Annual Technical Conference and Exhibition, Denver, Colorado, USA, 21–24 September.

Yergin D., Ineson R., 2009. America's Natural Gas Revolution. *Wall Street Journal*, November 2, 2009.

Zaitlin B.A., Moslow T.F., 2006. A Review of Deep Basin Gas Reservoirs of the Western Canada Sedimentary Basin. *The Mountain Geologist* **43** (3): 257–262.

APPENDIX

- - CONSTANT RATE - VERTICAL FRACTURE (ECLIPSE)

RUNSPEC

TITLE

Exercise 1

DIMENS

-- NX NY NZ

50 51 25 /

OIL

WATER

FIELD

START

27 FEB 2017 /

WELLDIMS

1 25 1 1 /

GRID

DX

-- Total number of blocks multiplied with the dX of the cell

63750*10 /

DY

-- Total number of blocks multiplied with the dY of the cell

63750*10 /

DZ

-- Total number of blocks multiplied with the dZ of the cell

63750*4 /

TOPS

2550*6000 /

PORO

63750*0.1 /

PERMX

63750*0.01 /

PERMY

63750*0.01 /

PERMZ

63750*0.001 /

```

BOX
1 50 26 26 1 25 /
--
PORO
1250*0.99 /

DY
-- Total number of blocks multiplied with the dY of the cell
1250*0.03 /

PERMX
1250*1000 /

PERMY
1250*1000 /

PERMZ
1250*0.001 /
ENDBOX

EDIT

PROPS
DENSITY
-- oildens waterdens gasdens
 49.0000 63.0000 .0100 /

ROCK
3600 .000004 /

SWOF
--Sw Krw Kro Pcow
 0.25 .00 .90 4.0
 0.50 .20 .30 0.8
 0.70 .40 .10 0.2
 0.80 .55 .00 0.1 /

PVDO
--Pressure Bo oilmiou
 300 1.210 0.6
 800 1.170 0.6
 5000 1.000 0.6 /

PVTW
--Pref Bref Cw Vw (dVw/dp)/Vw
 5000 1.000 0.000003 0.52 0 /

SOLUTION
RPTRST
BASIC=2 NORST=1 /

EQUIL

```

--Datumlevel Pref WOC
6000 5000 6500.03 /

SUMMARY

FOPR
FWPR
WOPR
/
WWPR
/
WBHP
/
WWIR
/
FPR

SCHEDULE

RPTRST
BASIC=2 NORST=1 /

WELSPECS

PROD1 P1 25 26 6000 LIQ 0.333 /
/

--

COMPDAT

PROD1 25 26 1 25 OPEN 2* 0.333 /

/

--

WCONPROD

PROD1 OPEN RESV 4* 10 /

/

--

TSTEP

500*10 /

END

-- CONSTANT PRESSURE - VERTICAL FRACTURE (ECLIPSE)

RUNSPEC

TITLE

Exercise

DIMENS

-- NX NY NZ

50 51 25 /

OIL

WATER

FIELD

START

27 FEB 2017 /

WELLDIMS

1 25 1 1 /

GRID

DX

-- Total number of blocks multiplied with the dX of the cell

63750*10 /

DY

-- Total number of blocks multiplied with the dY of the cell

63750*10 /

DZ

-- Total number of blocks multiplied with the dZ of the cell

63750*4 /

TOPS

2550*6000 /

PORO

63750*0.1 /

PERMX

63750*0.01 /

PERMY

63750*0.01 /

PERMZ

63750*0.001 /

BOX

1 50 26 26 1 25 /

--

PORO
 1250*0.99 /

DY
 -- Total number of blocks multiplied with the dY of the cell
 1250*0.03 /

PERMX
 1250*1000 /

PERMY
 1250*1000 /

PERMZ
 1250*0.001 /

ENDBOX

EDIT

PROPS
 DENSITY
 -- oildens waterdens gasdens
 49.0000 63.0000 .0100 /

ROCK
 3600 .000004 /

SWOF
 --Sw Krw Kro Pcow
 0.25 .00 .90 4.0
 0.50 .20 .30 0.8
 0.70 .40 .10 0.2
 0.80 .55 .00 0.1 /

PVDO
 --Pressure Bo oilmiou
 300 1.230 0.6
 800 1.180 0.6
 5000 1.000 0.6 /

PVTW
 --Pref Bref Cw Vw (dVw/dp)/Vw
 5000 1.000 0.000003 0.52 0 /

SOLUTION
 RPTRST
 BASIC=2 NORST=1 /

EQUIL
 --Datumlevel Pref WOC
 6000 5000 6500.03 /

SUMMARY

FOPR
FWPR
WOPR
/
WWPR
/
WBHP
/
WWIR
/
FPR

SCHEDULE

RPTRST
BASIC=2 NORST=1 /

WELSPECS

PROD1 P1 25 26 6000 LIQ 0.333 /

/

--

COMPDAT

PROD1 25 26 1 25 OPEN 2* 0.333 /

/

--

WCONPROD

PROD1 OPEN BHP 180 4* 500 /

/

--

TSTEP

500*10 /

END

-- CONSTANT RATE - HORIZONTAL FRACTURE (ECLIPSE)

RUNSPEC

TITLE

Exercise 1

DIMENS

-- NX NY NZ

50 50 26 /

OIL

WATER

FIELD

START

27 FEB 2017 /

WELLDIMS

1 3 1 1 /

GRID

DX

-- Total number of blocks multiplied with the dX of the cell

65000*10 /

DY

-- Total number of blocks multiplied with the dY of the cell

65000*10 /

DZ

-- Total number of blocks multiplied with the dZ of the cell

65000*4 /

TOPS

2500*6000 /

PORO

65000*0.1 /

PERMX

65000*0.01 /

PERMY

65000*0.01 /

PERMZ

65000*0.001 /

BOX

1 50 1 50 13 13 /

```

--
PORO
2500*0.99 /

DZ
-- Total number of blocks multiplied with the dZ of the cell
2500*0.03 /

PERMX
2500*1000 /

PERMY
2500*1000 /

PERMZ
2500*0.001 /

ENDBOX

EDIT

PROPS
DENSITY
-- oildens waterdens gasdens
 49.0000 63.0000 .0100 /

ROCK
3600 .000004 /

SWOF
--Sw Krw Kro Pcow
 0.25 .00 .90 4.0
 0.50 .20 .30 0.8
 0.70 .40 .10 0.2
 0.80 .55 .00 0.1 /

PVDO
--Pressure Bo oilmiou
 300 1.160 0.6
 800 1.150 0.6
 5000 1.100 0.6 /

PVTW
--Pref Bref Cw Vw (dVw/dp)/Vw
 5000 1.000 0.000003 0.52 0 /

SOLUTION
RPTRST
BASIC=2 NORST=1 /

EQUIL
--Datumlevel Pref WOC

```

6000 5000 6500.03 /

SUMMARY

FOPR
FWPR
WOPR
/
WWPR
/
WBHP
/
WWIR
/
FPR

SCHEDULE

RPTRST
BASIC=2 NORST=1 /

WELSPECS

PROD1 P1 25 25 6000 LIQ 0.333 /

/

--

COMPDAT

PROD1 25 25 13 13 OPEN 2* 0.333 /

/

--

WCONPROD

PROD1 OPEN RESV 4* 10 /

/

--

TSTEP

500*10 /

END

- - CONSTANT PRESSURE - HORIZONTAL FRACTURE (ECLIPSE)

RUNSPEC

TITLE

Exercise 1

DIMENS

-- NX NY NZ

50 50 26 /

OIL

WATER

FIELD

START

27 FEB 2017 /

WELLDIMS

1 3 1 1 /

GRID

DX

-- Total number of blocks multiplied with the dX of the cell

65000*10 /

DY

-- Total number of blocks multiplied with the dY of the cell

65000*10 /

DZ

-- Total number of blocks multiplied with the dZ of the cell

65000*4 /

TOPS

2500*6000 /

PORO

65000*0.1 /

PERMX

65000*0.01 /

PERMY

65000*0.01 /

PERMZ

65000*0.001 /

BOX

1 50 1 50 13 13 /

--

PORO
 2500*0.99 /

DZ
 -- Total number of blocks multiplied with the dZ of the cell
 2500*0.03 /

PERMX
 2500*1000 /

PERMY
 2500*1000 /

PERMZ
 2500*0.001 /

ENDBOX

EDIT

PROPS
 DENSITY
 -- oildens waterdens gasdens
 49.0000 63.0000 .0100 /

ROCK
 3600 .000004 /

SWOF
 --Sw Krw Kro Pcow
 0.25 .00 .90 4.0
 0.50 .20 .30 0.8
 0.70 .40 .10 0.2
 0.80 .55 .00 0.1 /

PVDO
 --Pressure Bo oilmiou
 300 1.160 0.6
 800 1.150 0.6
 5000 1.000 0.6 /

PVTW
 --Pref Bref Cw Vw (dVw/dp)/Vw
 5000 1.000 0.000003 0.52 0 /

SOLUTION
 RPTRST
 BASIC=2 NORST=1 /

EQUIL
 --Datumlevel Pref WOC
 6000 5000 6500.03 /

SUMMARY

FOPR
FWPR
WOPR
/
WWPR
/
WBHP
/
WWIR
/
FPR

SCHEDULE

RPTRST
BASIC=2 NORST=1 /

WELSPECS

PROD1 P1 25 25 6000 LIQ 0.333 /

/

--

COMPDAT

PROD1 25 25 13 13 OPEN 2* 0.333 /

/

--

WCONPROD

PROD1 OPEN BHP 180 4* 500 /

/

--

TSTEP

500*10 /

END